npj | flexible electronics

Review

Published in partnership with Nanjing Tech University

https://doi.org/10.1038/s41528-025-00465-w

Advances and perspectives in fiber-based electronic devices for next-generation soft systems

Hwajoong Kim[1], Daehyeon Kim[1], Jinho Kim[1], Yukye Lee[1], Minchang Shin[1], Jimin Kim[1], Fransiska M. Bossuyt[2], Gun-Hee Lee[3], Byeongmoon Lee[4], William R. Taylor[2] & Jaehong Lee[1] ✉

Fiber-based electronic devices (FEDs) exhibit high flexibility, low weight, and excellent integrability into wearable, implantable, and robotic systems. Recent advances have enabled applications in sensing, energy harvesting, and storage, and active functions. Despite this progress, challenges such as mechanical fatigue, interfacial delamination, and signal instability remain. This review offers key challenges and perspectives on the future of FEDs as interactive, autonomous platforms for next-generation electronics in healthcare, robotics, and beyond.

Over the past several decades, electronic technologies have advanced significantly across a broad spectrum of applications, such as healthcare[1–5], industrial systems[6–10], defense[11–15], and consumer devices[16–18]. However, conventional rigid and bulky electronic devices reveal inherent limitations in specific real-world environments that require mechanical flexibility, stretchability, and adaptability to target surface[19,20]. In response to these challenges, deformable electronic systems based on soft materials have emerged as promising alternatives, overcoming many of the constraints associated with traditional platforms[21]. Nevertheless, the predominantly planar architecture of soft electronic systems still poses practical difficulties in achieving seamless integration with conformity to dynamic or irregular geometries[22,23].

To address these challenges, fiber-based platforms have emerged as a promising alternative for next-generation soft systems, particularly suited for spatially restricted environments due to their fine diameter and mechanical flexibility[24,25]. These unique features have led to the growing adoption of FEDs across various applications. Wearable applications particularly benefit from the form factor and mechanical compliance of FEDs. By being directly embedded into fabrics, fiber devices enable real-time monitoring of physiological signals and body movements, and can also provide visual feedback through integrated fiber-based displays, while preserving comfort and mobility for the user[26–29]. Compared to conventional patch-type devices, textile-integrated fibers provide higher conformity and reduced motion artifacts, making them advantageous for continuous and long-term use. Additionally, in biomedical contexts, FEDs have shown significant promise for minimally invasive and chronically implantable systems[30–32]. Representative applications include smart sutures integrated with fiber-based electrochemical sensors, mechanical sensors, or electrical stimulators. Depending on the device configuration, these systems can monitor local biochemical markers such as pH levels or analyte concentrations indicative of inflammation, deliver therapeutic electrical stimulation to the sutured site, or detect strain changes in ligaments following surgical repair. These versatile fibers offer both diagnostic functionality and structural support, reducing equipment requirements and simplifying surgical workflows. Furthermore, their tiny volume enables implantation with minimal tissue disruption and immune reactions. Robotic systems also increasingly utilize FEDs to enhance sensory feedback and actuation in soft or articulated components[33–35]. For instance, fiber-based sensors integrated within soft robotic structures can measure actuation-induced deformations without interfering with the motion of soft actuators. Moreover, to realize soft actuators with maximized energy efficiency and lightweight characteristics, various types of fiber-based actuators are being actively developed. In this way, FEDs are evolving beyond simple sensing components into multifunctional platforms capable of detecting various physical and physiological stimuli, harvesting and storing energy, and delivering controlled outputs as needed[36,37].

Despite significant advances in the design, fabrication, and functional integration of FEDs, the transition toward practical deployment and commercial viability remains hindered by several critical challenges. A primary issue is mechanical fatigue under repeated deformation cycles[38–41]. Given the intended use of FEDs in dynamic environments, such as wearable garments, implantable tissues, or robotic systems, the fibers are often subjected to cyclic tensile, compressive, or bending strains. Over time, such mechanical stress can induce microcracks within the fiber devices, ultimately leading to electrical failure or loss of performance. Another major limitation arises from the delamination or detachment of functional materials coated on the fiber surface[42,43]. Conductive polymers or metal nanostructures applied via dip-coating, spray-coating, or electrochemical deposition may not adhere

[1]Department of Robotics and Mechatronics Engineering, DGIST, Daegu, Republic of Korea. [2]Department of Health Sciences and Technology, ETH Zurich, Zurich, Switzerland. [3]Department of Optics and Mechatronics Engineering, Pusan National University, Busan, Republic of Korea. [4]Department of Electrical Engineering and Computer Science, DGIST, Daegu, Republic of Korea. ✉e-mail: jaelee@dgist.ac.kr

reliably under strain or in physiological environments, particularly when exposed to moisture, salts, or enzymatic activity. This can result in a gradual decline in device performance, reduced signal fidelity, or complete delamination of the active layer. Such degradation phenomena are particularly critical in implantable applications, where the devices are chronically exposed to aqueous and chemically active environments within the body. Compromised adhesion or material loss can trigger adverse biological responses, including inflammation or immune rejection, thereby undermining both device performance and biocompatibility. Furthermore, maintaining uniform functionalization along the entire fiber length is a persistent manufacturing challenge, especially when dealing with meter-scale or continuous fibers[44,45]. Variations in coating thickness, surface roughness, or material distribution can cause spatial inconsistencies in electrical conductivity or performance of fiber devices, complicating electrical signal calibration and reducing device reproducibility.

To identify and address these technological bottlenecks, this review provides a comprehensive overview of recent advancements in diverse FEDs, with a particular focus on sensing devices, energy storage and harvesting systems, and various active devices. Moreover, unlike previous reviews that primarily concentrate on single application domains or material systems, this work offers a system-level and integrative perspective on the development of FEDs. To this end, we discuss cross-functional strategies that integrate diverse functionalities and evaluate the technology readiness level (TRL) of each device category, thereby proposing valuable insights for researchers and engineers aiming to implement FEDs in practical applications (Table 1). In the first section, the review begins by introducing various fiber-type sensing devices which can detect mechanical, thermal, chemical, and electrophysiological signals. The discussion encompasses their working principles, material design strategies, performance enhancement approaches, and their applications. In the second section, fiber-based energy harvesters utilizing ambient sources such as human motion and body heat, along with highly stable fiber-shaped energy storage devices, are also discussed. These technologies are reviewed in the context of their potential to enable self-powered fiber systems. The third section provides an in-depth overview of diverse active fiber devices such as light-emitting fibers for displays, fiber-based actuators, and fiber-based electrical stimulator for therapeutic applications. The active-type FEDs extend beyond passive sensing functions and offer capabilities for visual feedback, mechanical actuation, and localized bioelectrical stimulation, thereby expanding the functional scope of fiber-based electronics toward fully interactive systems. Finally, the conclusion outlines current advancements and remaining challenges of FEDs with a specific focus on integrating multiple functional modules, ensuring long-term durability under practical use, mitigating the impact of environmental noise, and maintaining performance reliability. Based on these discussions, we present future directions and strategies for the practical implementation of next-generation soft systems in real-world industrial and medical environments Fig. 1.

Fiber-based sensing technologies

The rapid advancement of smart technologies has accelerated the growth of fields such as the Internet of Things (IoT), artificial intelligence (AI), and autonomous systems[46,47]. Within these fields, accurate and continuous data acquisition through sensors is fundamental to enabling adaptive, data-driven operation, thereby intensifying the demand for high-performance sensing platforms. Similarly, sensing technology is regarded as a critical foundation in the development of fiber-based autonomous smart systems[36,48]. Fiber-based smart sensors offer distinct advantages as wearable or implantable devices, enabling direct signal sensing across diverse environments and supporting real-time data sensing. Fiber-based sensors can be designed to respond to a wide spectrum of physical, chemical, and biological stimuli, depending on the type of signal being targeted (Fig. 2 and Table 2). This versatility allows for precise monitoring across a range of applications. Representative examples include changes in electrical properties caused by mechanical deformation[49–51], thermoelectric or resistive variations induced by temperature fluctuations[52–54], and colorimetric or conductivity shifts resulting from

Table 1 | Technology Readiness Level (TRL) of fiber-based soft systems

Device type	TRL range	Demonstration environment	Mass production readiness	Improvement strategy
Mechanical sensor[118,122–126,130,131]	3–6	Lab-scale prototypes; Wearable, HMI, and soft robotic applications	Partially compatible with textile manufacturing; most remain at research-level scalability	Material encapsulation, hybrid sensing, structural design, Machine learning-based signal correction
Thermal sensor[141–145]	4–6	Lab-scale devices; Wearable and industrial safety demos	Moderate; scalable with thermal drawing process, but further process control needed	Thermal conductivity enhancement, encapsulation of moisture barrier, hybrid composites
Chemical sensor[20,167–169,173]	3–5	Lab-scale devices; Wearable, implantable, and industrial safety applications	Limited; Stability and reproducibility need improvement	Enzyme stabilization, molecularly imprinted polymer optimization, humidity control
Electro-physiological sensor[27,214–216,221]	3–6	Research-grade device; In vivo neural recoding and wearable EMG/ECG/EEG systems, skin electronics	Moderate; Long-term stability and biocompatibility remain challenging	Biocompatible materials and coating, interfacial impedance reduction, Algorithm for real-time signal analysis
Generator[250,253,263,264,268,271,344]	4–6	Early-stage prototype; Wearable applications	Moderate; Mass production demonstrated in select studies	Durable structure for preventing leakage, material optimization, development of complex generation mechanism
Battery[276,278,283]	3–5	Lab-scale prototype; Integrated smart textile system	Limited; Stability and leakage prevention need improvement	Materials optimization, improvement of electrode structure, implementation of thermal runaway mitigation system
Display device[298–300]	4–6	Pre-commercial prototype; Wearable demos and display-integrated system	Good; Ready for industrial adoption	Spectral tunability, enhancement of mechanical durability
Actuator[306,314–317]	4–6	Lab-scale prototype; Soft robotic systems and artificial muscles application	Limited; mass production due to challenges in driven source control	Stable Joule heating design, Machine learning-based feedback control, Improvement of work capacity and accuracy
Stimulator[341–343]	4–6	Lab-scale device; In vivo neural interface and stimulation,	Moderate; Manual or small-scale fabrication processes for most cases, with some studies enabling mass production	Enhancement of charge injection capacity (CIC), Standardization, and systematic establishment of stimulation condition

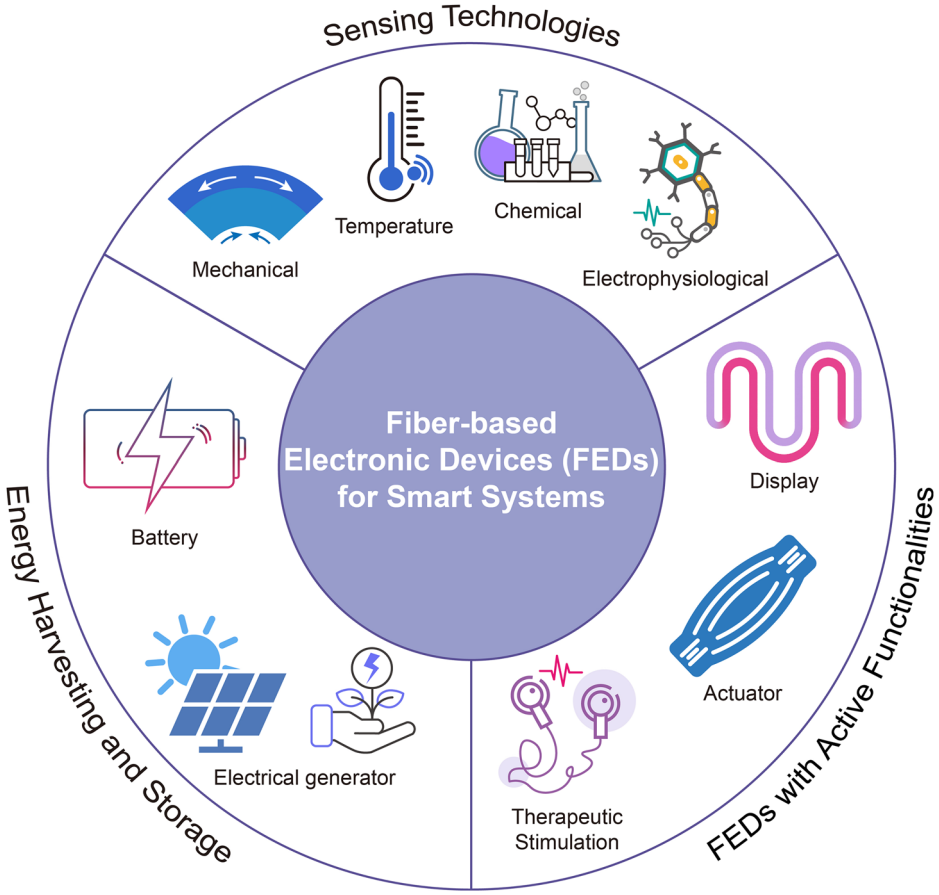

Fig. 1 | Overview of FEDs for smart systems.

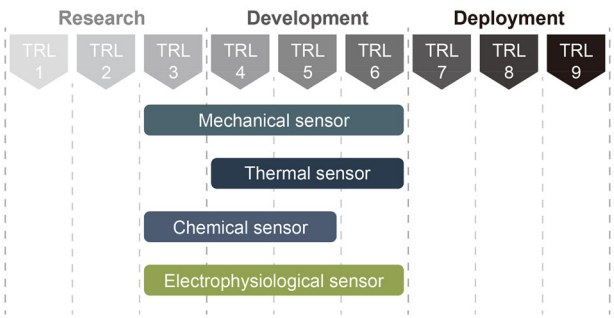

Fig. 2 | Technology readiness level (TRL) of various fiber-based sensors.

specific chemical interactions[55,56]. In addition, fiber sensors are capable of detecting subtle bioelectrical signals generated by muscle contractions and neural activity[57,58].

Fiber-based sensors offer a versatile platform for translating diverse physical and chemical stimuli into measurable electrical signals, enabling their seamless integration into a wide range of smart systems[34]. However, despite their multifunctionality and adaptability, challenges such as material uniformity, mechanical durability under repeated deformation, and signal stability under dynamic conditions continue to pose obstacles to system-level integration. To address these technical limitations, recent research has begun to address these limitations through the integration of advanced materials and machine learning based data processing. Firstly, on the materials side, efforts have focused on enhancing intrinsic properties such as electrical conductivity and mechanical robustness, as well as engineering the sensor microstructure to achieve high selectivity toward specific stimuli. Secondly, in parallel, increasing efforts have been devoted to integrating sensor outputs with AI and machine learning algorithms to construct intelligent sensing platforms with enhanced analytical capabilities and real-time feedback control[59,60]. This integration has taken various forms, employing a range of machine learning models such as linear regression (LR), K nearest neighbors (KNN), random forest, long short-term memory (LSTM), convolutional neural network (CNN), recurrent neural network (RNN), and multilayer perceptron (MLP) among others[61,62]. Moreover, the convergence of advanced materials and machine learning serves as a powerful framework to extract and interpret meaningful patterns and insights from the large-scale datasets generated by fiber type sensors.

Mechanical sensors

Among various types of soft sensors, mechanical sensors that detect physical deformations, such as strain[42,63–66], pressure[67–71], bending[72–76], and twisting[77–79], have been actively developed to enable precise monitoring of mechanical stimuli. These sensors are typically fabricated by combining conductive materials, such as carbon nanotubes (CNTs)[64,66,80–82], graphene[50,78,83–85], MXene[68,86–89], metallic nanofillers[90–92], and conductive polymers[93–96], with soft polymer matrices. To enhance both sensitivity and durability, a variety of fabrication techniques have been employed, including blending & mixing[42,97,98], in-situ formation[69,99,100], dip-coating[101–103], electroplating[104–106], metal deposition[107–109], and melt extrusion[110–112]. Fiber-based mechanical sensors, in particular, can be seamlessly attached to or implanted within the human body due to their intrinsic flexibility and conformability, enabling real-time monitoring of physical and physiological movements. Furthermore, these sensing signals, through interaction with the environment, can be integrated with advanced machine learning technologies, including real-time feedback systems, providing distinct advantages for applications in healthcare, HMI, and soft robotic systems.

Pressure is a key physiological parameter generated in the human body, such as in blood pressure[113,114], pulse[50,115], respiration, and muscle

Table 2 | Comprehensive comparison and overview of fiber-based sensors highlighting their characteristics[24,25,28,29,38–42,45,49–58,345–350]

	Mechanical Sensor	Theral Sensor	Chemical Sensor	Electrophysiological Sensor
Strength	High sensitivity to pressure/strain, fast response	Stable in harsh environments, passive operation, non-contact sensing	High selectivity (e.g., to ions, gases), useful for biochemical monitoring	Directly records physiological signals, high biocompatibility
Weakness	Susceptible to mechanical fatigue, limited selectivity, potential hysteresis	Lower specificity, affected by ambient temperature drift	Easily influenced by humidity/temperature, prone to degradation over time	Susceptible to motion artifacts and noise
Sensing type	Piezoresistive, capacitive, triboelectric, resistive, etc.	Thermoresistive, thermoelectric (e.g., Seebeck effect)	Redox reaction, ion concentration change, pH sensitivity	Bioelectric signal detection (e.g., ECG, EMG, EEG) via electrode-skin, electrode-organ interface
Signal stability & response time	High stability, fast response (ms level)	Moderate stability and response (ms ~ s range)	Often slow response, low SNR, long-term drift	Moderate to high stability, good temporal resolution
Power consumption	Low to moderate (depending on sensing mode)	Low (passive thermal sensing)	Moderate (needs electrochemical reaction or signal amplification)	Moderate (requires amplification, filtering)
Types of fabrication	Simple to complex (depends on material and applications)	Moderate (requires thermal insulation & calibration)	Complex (requires chemical immobilization, selective layers)	Moderate (requires gel interface, conductive coatings)
Cost	Low (due to simple structure, low-cost materials)	Low to moderate (inexpensive materials, moderate fabrication complexity)	Moderate to high (due to reagents, complex functionalization)	Moderate (depends on electrode materials and acquisition system)

activity[116,117], and also serves as a quantifiable signal for interactions with the environment or between robots and objects[70,118,119]. Among pressure sensors, capacitive-type sensors are advantageous due to their fast response and high stability[120,121]. When produced in fiber form, they offer additional benefits such as light weight and miniaturization. Lee et al. developed a fiber-based pressure sensor using highly conductive Ag nanoparticle-based fibers arranged in a crossed-layer structure (Fig. 3a)[122]. The conductive fibers were fabricated via a three-step process: coating Kevlar fibers with Poly(styrene-butadiene-styrene) (SBS), absorbing Ag precursors, and conducting in-situ reduction. These fibers showed excellent electrical conductivity (0.15 Ω/cm) and mechanical robustness. The sensor, made by coating the fibers with Polydimethylsiloxane (PDMS) and assembling them in a cross-point format, exhibited a high response speed (~40 ms), durability, and sensitivity (0.21 /kPa), as shown in Table 3. A 6 × 6 pressure sensor array was fabricated by using weaving techniques capable of detecting ultra-light pressures (as low as 0.25 g), and the fiber-based pressure sensor was successfully applied to human-machine interfaces like wearable gloves for drone or robot control. Despite these merits, capacitive sensors based on flexible materials inherently exhibit a trade-off in sensitivity across pressure ranges. Specifically, they maintain high sensitivity under low pressure (<2 kPa) but show reduced sensitivity at higher pressures (>2 kPa) due to the increased compressive modulus of the constituent materials. To address this, Qu et al. proposed a resistive-capacitive hybrid fiber pressure sensor (HFPS) combining both sensing mechanisms (Fig. 3b)[123]. The HFPS has a three-layer coaxial structure: an elastic electrode layer (Polyurethane (PU) with high CNT content) a piezoresistive layer (PU with low CNT content), and an insulating layer, fabricated via coaxial wet spinning. Under low pressure, reduced insulation gaps increase the capacitance of the sensor. At high pressure, the piezoresistive layer densifies, raising CNT content and dielectric constant. With further pressure, CNTs form conductive paths, increasing effective electrode area and capacitance. The HFPS showed high sensitivity in both low (1.28 /kPa) and high (0.93 /kPa) pressure ranges and could detect 1.6 mg water droplets. This full-range sensitivity enabled stable pulse monitoring under preload, demonstrating its value for wearable medical platforms. A wireless HFPS system further validated its potential in healthcare applications. Nevertheless, such sensors still face challenges: nonlinear signal responses, signal saturation at high pressure, and sensitivity to contact area variations. When implemented in array formats for high-resolution pressure mapping, pressure sensors may face challenges such as crosstalk and reduced spatial resolution. To address these, future work should aim to develop sensors with linear responses across pressure ranges and minimal sensitivity to contact area. In addition, strategies to reduce signal interference in dense arrays will be crucial for enhancing the accuracy and applicability of pressure sensing systems in healthcare, robotics, and other fields.

Joints and soft tissues such as fingers, elbows, and knees undergo continuous bending during daily movements, from subtle displacements to large angular flexions. Accurate detection of these motions is essential for applications in wearable healthcare, rehabilitation monitoring, and advanced HMI technologies. To meet these needs, Wang et al. developed a fully flexible weft-knitted wearable sensor (WTS) using ultrahigh-strength braided smart yarn[124]. This smart yarn, composed of ultra-high molecular weight polyethylene braided around Ag-plated polyamide (PA), provided both rigidity and protection (Fig. 3c). Scalable braiding allowed for mass production, and the smart yarn was integrated into breathable, flexible textile sensors via flat-knitting machines (Fig. 3d). The WTS operates via triboelectricity, generating signals through contact and separation between the smart yarn and PA layer, producing triboelectric charge and inducing alternating voltage and current. The sensor showed high sensitivity (3.00 V/kPa) and strong linearity (R^2 = 0.99). As a smart elbow guard, it accurately detected bending angles and analyzed motion parameters such as range, frequency, and duration (Fig. 3e). It distinguished complex upper-body movements, such as walking, rope skipping, push-ups, and boxing, highlighting its utility in intelligent sports monitoring. The

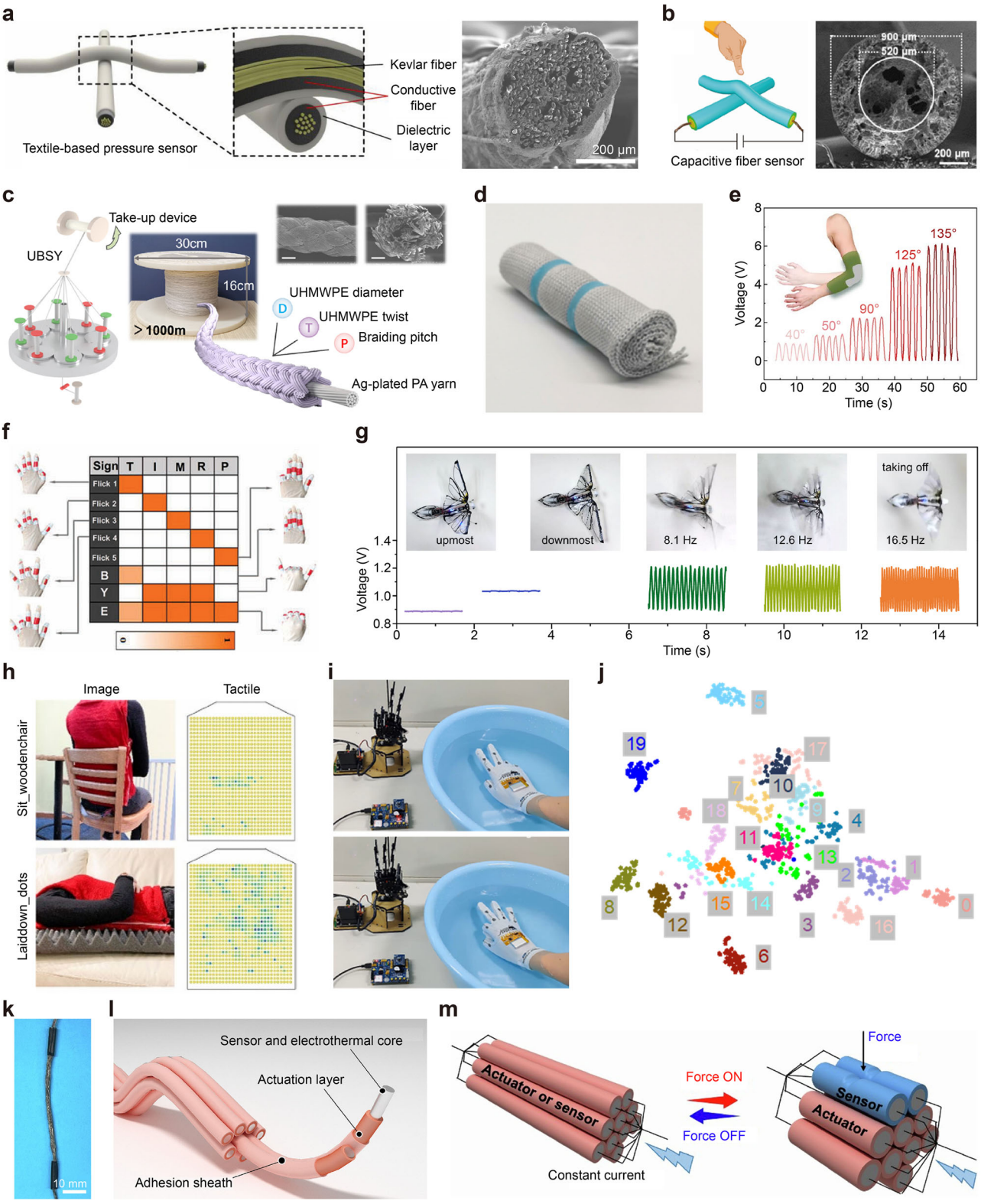

sensor also shows promise for use in extreme sports training, military field monitoring, and hazardous workplace tracking. Despite promising results, challenges persist in accurately quantifying bending angles. Signal drift and material relaxation from repeated deformation and long-term physiological exposure compromise measurement stability. Mechanical interference from sensor placement or skin movement can also cause signal inaccuracies. Future efforts should focus on using durable materials, curvature-insensitive structural designs, and stable attachment strategies to enhance reliability on curved body surfaces.

Measuring strain signals is essential for quantifying and interpreting mechanical deformations in various systems and environments. Strain induced by motion or force reflects structural stability, material behavior, and biomechanical movement. Real-time strain sensing enables early detection of dynamic changes or anomalies. Among various sensing

Fig. 3 | Mechanical sensors. a Schematic illustration of a fiber-based pressure sensor and a cross-sectional SEM image of the conductive fibers. The sensing mechanism is based on measuring the change in capacitance formed at the intersection of two stacked conductive fibers. Reprinted with permission[122]. Copyright 2015, WILEY-VCH Verlag GmbH & Co. KgaA, Weinheim. **b** Schematic diagram of a resistive-capacitive hybrid fiber pressure sensor and corresponding cross-sectional SEM image showing the distinct layers of the fiber electrode. Reprinted with permission[123]. Copyright 2023, American Chemical Society. **c** Schematic of scalable braiding technology and SEM images of the top and cross-sectional morphology of the smart yarn. (UBSY Ultrahigh-strength ultra-high-molecular-weight polyethylene Braided Smart Yarn, UHMWPE Ultra-high-molecular-weight Polyethylene, PA Polyamide) **d** Photographs of the weft-knitted wearable sensor (WTS). **e** Voltage output of the smart elbow guard corresponding to various arm bending angles. **c**–**e** Reprinted with permission[124]. Copyright 2024, Springer Nature. **f** Gesture-based information transmission using a core–shell nanostructured smart fiber. Reprinted with permission[125]. Copyright 2024, WILEY-VCH Verlag GmbH & Co. KgaA, Weinheim. **g** Wirelessly received sensing signals from the ionic hydrogel fiber strain sensor corresponding to different motion states of a robotic bird. Various motions include static wings at different positions, and high-speed wings flapping at different frequencies. Reprinted with permission[126]. Copyright 2022, Springer Nature. **h** Images showing the posture and movement of the user, along with a tactile frame capable of monitoring them. Reprinted with permission[118]. Copyright 2021, Springer Nature. **i** Controlling a robotic hand using a smart glove underwater. **j** t-distributed stochastic neighbor embedding (t-SNE) visualization of 3,000 strain data points (150 samples for each of the 20 gestures). Each point in the figure represents the strain information of one hand gesture projected from 5 dimensions into 2 dimensions. **i**, **j** Reprinted with permission[130]. Copyright 2022, Elsevier Inc. **k** Photograph of the artificial muscles. **l** Schematic illustration of the artificial muscle architecture (i, ii, and iii correspond to the liquid metal-based sensing and electrothermal core, the cured liquid crystal elastomer actuation layer, and the adhesive outer sheath). **m** Schematic of illustration of artificial muscle feedback sensing and actuation by external pressure. **k**–**m** Reprinted with permission[131]. Copyright 2025, Elsevier Inc.

Table 3 | Performance comparison table of mechanical sensors

No.	Fabrication process	Conducting materials	Sensing range	Sensitivity	Durability (Cycles)	Response time	Young's Modulus
1[122]	In-situ formation	Ag particles	0–20 kPa (Pressure)	0.21 /kPa	10,000	40 ms	994 MPa
2[123]	Wet spinning	CNTs	0–50 kPa (Pressure)	1.28 /kPa	2600	20 ms	3.4 GPa
3[124]	Braiding	Ag-plated yarn	0–135° (Bending)	3.00 V/kPa	40,000	~125 ms	1.45 MPa
4[125]	Wet spinning	MXene, AgNWs	0–100% (Strain)	12,383,500 (GF)	500	~380 ms	12.5 MPa
5[126]	Wet spinning	SWCNTs	0–1000% (Strain)	4.41 (GF)	1000	30 ms	240 kPa
6[118]	Dip coating	Graphite/copper nanoparticle	0–140 kPa (Pressure)	~4 kΩ/N	1000	-	12.2 GPa
7[130]	Manual coating	MXene	0–80% (Strain)	10.3 (GF)	500	~110 ms	-
8[131]	Rotational molding	Liquid metal	0–50% (Strain)	1.9 (GF)	500	124 ms	-

mechanisms, such as piezoresistive, piezoelectric, capacitive, and triboelectric, piezoresistive sensors are widely used for their simple design, fast response, and ease of fabrication, relying on changes in electrical resistance. Zhou et al. developed a core-shell nanostructured smart fiber for human motion detection and health monitoring (Fig. 3f)[125]. The fiber consists of a conductive layer formed by coating MXene and silver nanowires (AgNWs) on a wet-spun supramolecular PU fiber, and a shell layer made by electrospinning PU containing silica-modified $SrAl_2O_4:Eu^{2+}$, Dy^{3+} phosphors. This architecture achieved an outstanding gauge factor (12,383,500) and ~100% sensing range. MXene provided strong interfacial bonding for conductive network formation, and AgNWs reinforced conductivity. Integrated into gloves, the fiber enabled encrypted language expression and Morse-code-based signal transmission, showcasing potential for fabric-based interaction systems (Fig. 3f).

Due to their compact and lightweight design, fiber-based strain sensors are also suitable for robotics. Wang et al. fabricated ionic hydrogel fiber strain sensors via wet-spinning of sodium polyacrylate (PANa)-based hydrogel doped with single-walled carbon nanotubes (Fig. 3g)[126]. pH tuning modulated polymer conformation, adjusting modulus, strength, and stretchability through phase separation-induced entangled networks. The ionic hydrogel fiber strain sensor showed a broad sensing range (up to 1000%) and stable function under high-frequency stretching (8.6 Hz). Integrated into a robotic bird, it monitored wing flapping at ~16.5 Hz with a 30 ms response/recovery time, demonstrating utility in both wearable and robotic electronics (Fig. 3g). However, for practical applications in healthcare, rehabilitation, robotics, and virtual reality, key technical challenges remain. Piezoresistive-type fiber strain sensors experience repeated stress during use, which can cause material fatigue and structural deformation, lowering performance over time. They also suffer from signal drift due to stress relaxation under static strain, limiting long-term accuracy. To address these issues, future work should focus on integrating fatigue-resistant elastic materials and developing components with minimal time-dependent behavior.

In recent research, various intelligent applications have been realized by integrating fiber-based mechanical sensors with machine learning technologies. This integration enables a transition from simple signal acquisition to system-level perceptive platforms capable of interpreting complex physical interactions[127–129]. A notable example is presented by Luo et al., who developed a tactile textile system for posture and activity recognition using a piezoresistive fiber-based sensing network (Fig. 3h)[118]. The core of the sensing fiber consists of stainless steel, which provides mechanical robustness and electrical conductivity, while the sheath layer is composed of a piezoresistive composite of graphite nanoparticles, copper nanoparticles, and PDMS elastomer. This coaxial structure is fabricated through a drawing-based coating process, yielding highly flexible fibers with a diameter of approximately 600 μm. The resulting fibers can be seamlessly integrated into garments such as vests using digital knitting, enabling body-scale tactile sensing. To interpret the large-volume, high-dimensional pressure data produced by the knitted vest, Luo et al. employed a convolutional neural network (CNN) for posture recognition. CNNs are particularly advantageous for spatially structured data such as tactile maps, as they utilize convolutional filters to extract local and translation-invariant features. The parameter-sharing mechanism of CNNs further improves computational efficiency and generalization, which is especially beneficial for wearable systems. In this study, the CNN model achieved 99.66% classification accuracy across ten different seated and reclining postures, demonstrating its robustness in dealing with sensor-level noise and inter-subject variability. Notably, the use of the vest configuration enabled the system to comprehensively map pressure distributions across the torso, allowing for fine-grained recognition of body orientation. This result not only highlights the effectiveness of CNN-based tactile learning for posture classification but also reveals its transformative potential in healthcare applications. By embedding such sensor-textile systems into garments, it becomes feasible to continuously monitor and assess a patient's posture in real time. This capability could be extended to posture correction, rehabilitation monitoring, and early detection of mobility disorders, offering a

non-invasive, comfortable, and data-driven solution for personalized health care interventions.

Another representative example of an intelligent system based on fiber-mechanical sensors is the HMI platform. In such systems, sensor-generated data is not merely collected but actively utilized to interpret user intent and to enable interaction with external devices such as machines or robotic systems (Fig. 3i, j)[130]. This potential of integrating fiber-mechanical sensing with machine learning technologies is exhibited in the research of Duan et al. In their study, MXene-based fiber sensors were integrated into a glove using textile-compatible sewing techniques. These sensors captured finger deformation signals, which were then wirelessly transmitted through a flexible circuit module embedded in the glove. Their dense connectivity structure allows for capturing complex dependencies among input channels, and their nonlinear activation functions enable them to model fluctuations and variability in sensor signals caused by different users or dynamic hand motions. Moreover, multilayer perceptron, machine learning algorithm, offers the advantage of relatively low computational cost, making them well-suited for embedded and real-time wearable platforms. Through this approach, the system achieved a classification accuracy of 98.1% across 20 distinct hand gestures, including numbers and symbolic signs such as "OK" and "I love you." Following classification, the decoded gesture was used to remotely actuate a robotic hand in real time, demonstrating the full sensing-to-control capability of the integrated system. This example clearly illustrates that the role of machine learning extends beyond passive data analysis; it enables real-time decision-making and actuation, highlighting its essential contribution to intelligent, feedback-driven HMI applications.

Data acquired from sensors can be utilized through two primary strategies: machine learning and feedback control. Machine learning algorithms are well suited for extracting patterns and making inferences from large datasets, enabling predictive modeling and complex behavior recognition. In contrast, feedback control leverages real-time sensor input to dynamically regulate actuator responses. This approach is particularly effective when sensing and actuation are physically integrated within the same system, allowing for direct, low-latency interactions without the need for external computation. Such sensor–actuator integrated architectures have been extensively explored in the development of artificial muscles, a key class of soft robotic systems that demand responsive and adaptive actuation. In the study by Chen et al., an example of an artificial muscle, which is an integration system of sensor and actuation, can be confirmed (Fig. 3k)[131]. The sensor introduced in this study is constructed using a coaxial fiber structure that consists of a liquid metal core fully enclosed by a liquid crystal elastomer shell (Fig. 3l). When external mechanical stimuli such as bending, compression, or tensile force are applied, the cross-sectional area of the liquid metal core decreases, resulting in a measurable change in electrical resistance (Fig. 3m). This resistive change serves as the fundamental sensing mechanism of the fiber. Based on this sensing principle, the authors developed an artificial muscle system in which the sensing and actuation functions are intrinsically coupled through a material-driven feedback control process. When mechanical deformation is applied to one fiber within a parallel fiber bundle, the resistance of the deformed fiber increases due to the reduction in its internal cross section. As a result, electrical current is redistributed toward adjacent fibers that experience less deformation. This redirection of current causes localized heating through resistive change. The generated heat increases the temperature of the liquid crystal elastomer above its transition point, leading to thermal contraction of the neighboring fiber. When the external force is removed, the system passively returns to its original shape through the elastic recovery of the elastomer matrix. This configuration enables autonomous actuation in response to external mechanical inputs without requiring external controllers. Because sensing and actuation occur within the same physical structure, the fiber system functions as a self-regulating artificial muscle capable of real-time feedback response. Rather than replacing machine learning, the embedded feedback control mechanism introduced in this study offers complementary advantages, particularly in applications that demand fast and localized decision-making without depending on large volumes of data or intensive computational resources.

Fiber-based mechanical sensors are attracting growing interest due to their ability to detect various mechanical stimuli such as pressure, bending, and strain with high spatial resolution and mechanical flexibility. These features make them suitable for applications in health monitoring, human machine interfaces, rehabilitation systems, and soft robotics. However, for reliable operation in real-world environments, several challenges must be overcome. Sensor outputs can be influenced not only by the intended stimulus but also by unintended mechanical disturbances such as off axis deformation or vibration. In addition, environmental factors like humidity and temperature fluctuations may alter the mechanical and electrical properties of soft polymer materials, resulting in signal drift and reduced durability. To address these limitations, a combination of materials design and adaptive signal processing is essential. Encapsulation can improve environmental stability and long-term reliability, while structural tuning of fiber geometry and electrode configuration enhances sensitivity and selectivity. The integration of advanced materials such as conductive composites or nanomaterials can further improve resilience, stretchability, and signal quality under complex loading conditions. Furthermore, fiber-based sensors are increasingly being used not only for passive sensing but also as active elements in intelligent control systems. When coupled with computational techniques such as machine learning, sensor outputs can support pattern recognition, prediction, and adaptive responses. These algorithms help correct nonlinearities and external noise in real time. In parallel, feedback control enables systems to monitor their own behavior and adjust parameters dynamically, improving linearity and stability. Together, these approaches expand the role of fiber-based sensors from simple signal detectors to multifunctional elements that support autonomous and adaptive operation in diverse environments.

Temperature sensors

Thermal sensing technologies have been widely adopted in applications ranging from body temperature monitoring to industrial safety management[132,133]. These sensors detect thermal energy or temperature fluctuations from objects or environments and convert them into electrical signals. Representative thermal sensors include temperature sensors, heat flux sensors, and thermal imaging cameras. Among these, temperature sensors are the most commonly used due to their simplicity and compatibility with a variety of smart systems. Temperature sensors are generally classified as either contact-based or non-contact types[134,135]. Contact-based sensors, such as thermistors, resistance temperature detectors (RTDs), thermocouples, and mercury thermometers, measure temperature through direct thermal conduction and typically offer high accuracy[136,137]. In contrast, non-contact sensors, such as infrared (IR) sensors and thermal cameras, detect emitted thermal radiation from surfaces, making them suitable for applications where direct contact is difficult or undesirable[138,139]. Temperature sensors have evolved from early rigid and fragile equipment such as mercury thermometers into portable and wearable forms like digital thermometers and smart watches[32,140]. Recently, wearable-type temperature sensors that can conform to the skin and respond to body movements have been actively investigated. This section reviews recent developments in fiber-based temperature sensors, focusing on their device architectures, sensing mechanisms, and applications, along with a discussion on their technical challenges and potential (Table 4).

Figure 4a, b show a stretchable fiber-based temperature sensor fabricated using the inorganic thermoelectric material copper(I) iodide (CuI)[141]. The temperature sensor was fabricated by absorbing a high concentration of copper ions into a polyurethane (PU)-based fiber, followed by in-situ synthesis of CuI nanoparticles using an iodization agent. In addition, to enhance insulation and durability, an encapsulation layer was added to the fiber. The densely embedded CuI nanoparticle network enabled the sensor to achieve a high Seebeck coefficient of 203.6 μV/K under strains of up to 835%. Temperature sensing is based on the Seebeck effect, in which a voltage

Table 4 | Comparison of various parameters for thermal sensors

No.	Fabrication process	Conductive Materials	Temperature range	Temperature resolution	Sensitivity	Linearity
1[141]	chemical synthesis	CuINPs	-	-	~0.225 mV/°C	~0.999
2[142]	Wet spinning	PEDOT:PSS	30–50 °C	0.1 °C	−1.72%/°C	0.98
3[143]	Thermal drawing	rGO/PLA	25–45 °C	0.5 °C	−0.285%/°C	0.999
4[144]	Thermal drawing	-	25–600 °C	-	0.5 pm/°C	0.999
5[145]	Thermal drawing	$Ge_5As_{55}Te_{40}$	25–115 °C	0.1 °C	1 mV/°C	~0.999

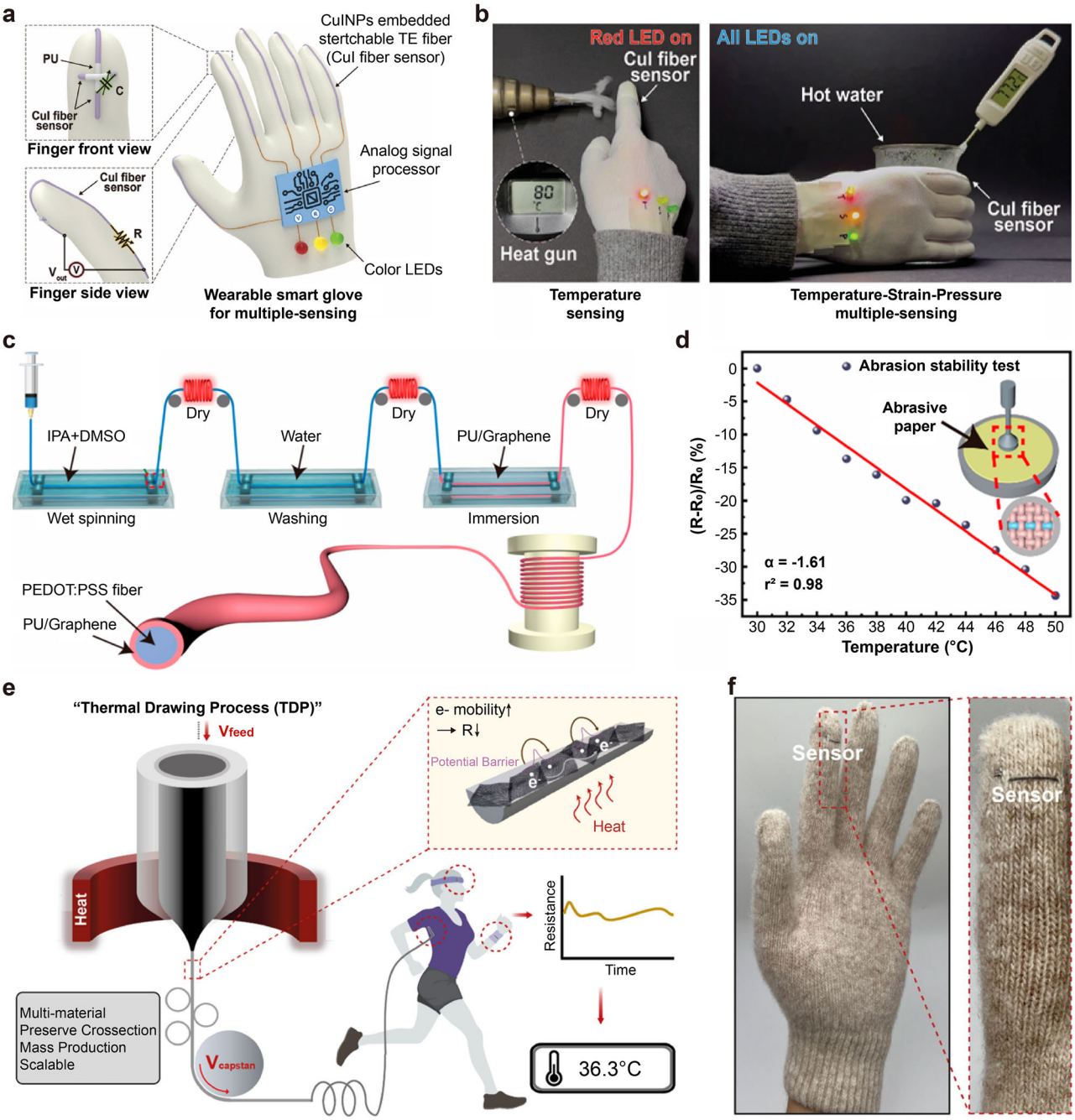

Fig. 4 | Temperature sensors for healthcare applications. a Schematic illustration of a wearable smart glove for temperature, strain, and pressure sensing. (PU: Polyurethane; CuINPs: Copper(I) iodide nanoparticles). **b** Photographic images demonstrating of temperature sensing capability. The diode is operating in response to the elevated temperature. **a**, **b** Reprinted with permission[141]. Copyright 2024, WILEY-VCH Verlag GmbH & Co. KgaA, Weinheim. **c** Schematic illustration of the fabrication process for a poly(3,4-ethylenedioxythiophene)-poly(styrenesulfonate) (PEDOT:PSS)-based temperature sensor. (IPA: Isopropanol; DMSO: Dimethyl sulfoxide). **d** Sensing performance of the PEDOT:PSS-based temperature sensor. (α: Temperature coefficient of resistance; r^2: Linearity) **c**, **d** Reprinted with permission[142]. Copyright 2023, American Chemical Society. **e** Schematic illustration of the fiber drawing process and the temperature sensing mechanism of the sensor. **f** Photographic images showing a fiber-based temperature sensor sewn onto the fingertip of a glove. **e**, **f** Reprinted with permission[143]. Copyright 2023, Springer Nature.

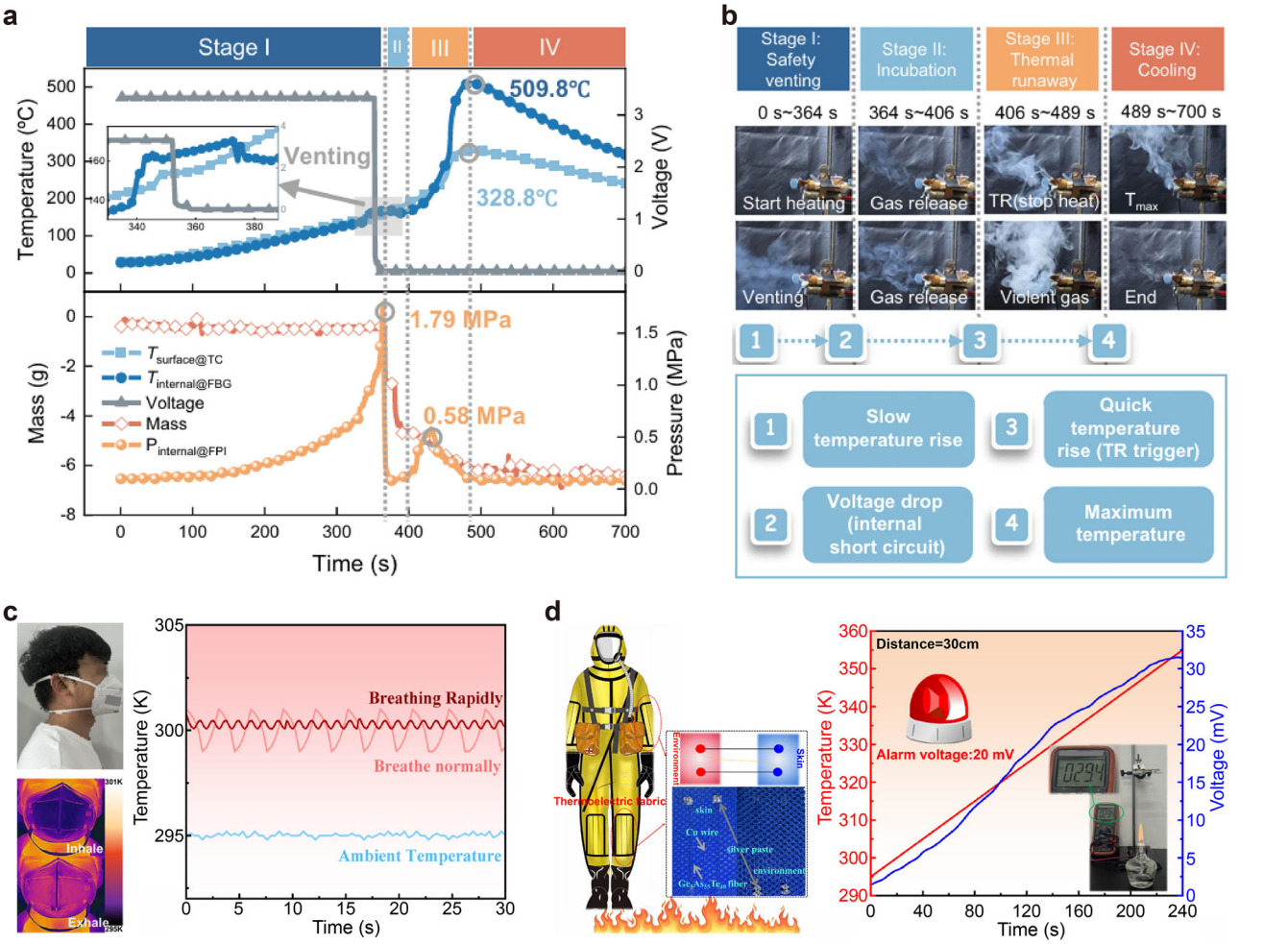

Fig. 5 | Temperature sensors for thermal protection. a Thermal runaway characteristics of 18650 cells with 100% state of charge (SOC). **b** Photographs captured at key moments of the critical reactions of the cells during thermal runaway, including safety venting (I), incubation period (II), thermal runaway (III), and cooling down (IV). **a**, **b** Reprinted with permission[144]. Copyright 2023, Springer Nature. **c** Photographic and infrared images of the mask, along with temperature responses during normal and rapid breathing. **d** Schematic illustration of a thermoelectric temperature sensor demonstrated for combustion detection, and corresponding temperature response. **c**, **d** Reprinted with permission[145]. Copyright 2024, American Chemical Society.

is generated between the two ends of the fiber in response to a thermal gradient. Demonstrated in a glove-mounted configuration, the sensor enabled localized temperature monitoring at the fingertip. Furthermore, the system also featured multi-modal sensing capabilities, including pressure and strain detection, allowing for real-time tracking of finger movement, contact force, and skin temperature. Despite these advantages, the CuI material remains vulnerable to moisture and oxygen, leading to potential chemical degradation over time. To ensure long-term stability, further optimization of the encapsulation layer is necessary to improve environmental resistance and mechanical resilience.

Fan et al. developed a core-shell fiber temperature sensor comprising a PEDOT:PSS-based sensing core and a PU/graphene composite coating layer (Fig. 4c)[142]. The fabrication process involved wet-spinning PEDOT:PSS, followed by dip-coating with the PU/graphene composite. In this core-shell structure, PEDOT:PSS served as the thermoresistive sensing element, while the outer layer enhanced thermal conductivity and overall sensitivity. Additionally, the fiber temperature sensor exhibited high sensitivity (−1.72%/°C), high resolution (0.1 °C), and a linear resistance-temperature relationship ($R^2 = 0.98$) (Fig. 4d). The sensor was attached to the underarm area to enable real-time monitoring of body temperature, demonstrating its effectiveness for non-invasive health tracking in individuals who are sensitive to temperature changes, such as infants, elderly people, and patients with Alzheimer's disease. The inherent flexibility of the fiber allowed seamless integration into wearable textiles, verifying potential for use in garment-embedded healthcare systems. However, factors such as response and recovery speed, washability, and long-term electrochemical stability must be carefully considered to ensure reliable practical deployment. Future research directions include the development of doping strategies or hybrid material systems to further enhance the conductivity and stability of PEDOT:PSS.

Figure 4e presents a fiber-based temperature sensor fabricated using the thermal drawing process[143]. This method involves heating and drawing a multilayer preform into micro-scale fibers, allowing for the scalable production of continuous and high-uniformity functional fibers over hundreds of meters. The fabricated fiber sensor exhibits a well-defined multi-layer structure consisting of an rGO/PLA composite core, a polyethylene cladding for mechanical protection, and a sacrificial polystyrene layer that is removed post-drawing. This design ensures both mechanical durability and stable temperature sensing performance, retaining functionality under typical textile fabrication processes such as sewing, embroidering, and washing. Furthermore, the rGO/PLA sensing layer features a negative temperature coefficient, where rising temperature enhances charge carrier mobility, resulting in decreased resistance. Based on this mechanism, the fiber-based temperature sensor was integrated into gloves to detect skin temperature changes and touch interaction, demonstrating its potential as a functional textile for interactive human–machine interfaces (Fig. 4f).

Unlike conventional temperature sensors primarily intended for body temperature monitoring, the fiber-based temperature sensors discussed in Fig. 5 are designed to detect environmental temperature variations and

Table 5 | Performance comparison across multiple parameters of chemical sensors

No.	Fabrication process	Target analyte	Limit of Detection	Selectivity	Sensitivity	Response time
1[30]	Dip coating	Homovanillic acid	4.58 nM	Excellent	83.7 pA/nM	2–5 s
2[167]	Dip coating	pH	~0.02 pH	Excellent	58.9 mV/pH	-
3[168]	Dry spinning	glucose	6 μM	Good	11.7 μA/mM cm^2	<4 s
4[169]	Electrospinning	Ammonia gas	1 ppm	Good	0.36 ΔE/ppm[a]	≤20 s
5[173]	Electrospinning	Formaldehyde gas	0.05 ppm	Excellent	-	4 s

[a]ΔE indicates the difference in color perception.

provide early fire warning capabilities, thereby enhancing safety. Mei et al. developed a compact optical fiber sensor capable of simultaneously monitoring temperature and pressure for real-time detection of thermal runaway in lithium-ion batteries[144]. A Fiber Bragg Grating (FBG) for temperature sensing and a Fabry-Perot Interferometer (FPI) for pressure sensing are integrated within a single fiber structure. Moreover, it was fabricated with a diameter of 125 μm and a length of 12 mm, allowing for direct insertion into commercial 18650-format cells. As shown in Fig. 5a, the sensor captured dynamic changes in temperature, pressure, voltage, and mass loss during induced thermal runaway events. The rapid response to both temperature and pressure variations highlights the potential of the fiber-based optical sensor as an effective early warning system. Operating over a temperature range of 25–600 °C and a pressure range of 0– 2 MPa, the sensor exhibited excellent linearity ($R^2 > 0.999$) and repeatability. Figure 5b summarizes the thermal runaway process into four well-defined stages (Stage I to IV), highlighting the ability of the fiber sensor to provide advanced diagnostic for combustion and predictive safety systems. This sensing approach is particularly relevant for safety-critical environments such as electric vehicles (EVs), energy storage systems (ESS), and unmanned aerial vehicles (UAVs), where the integration of bulky sensors is often limited by space constraints. The fine and flexible fiber geometry allows for minimally invasive integration and cell-level thermal condition tracking while maintaining system simplicity.

The final example highlights a fiber-based temperature sensing system developed for respiratory monitoring and proximity fire warning-addressing personal health along with environmental safety[145]. To overcome the limitations of conventional thermoelectric materials with low Seebeck coefficients, the authors synthesized an amorphous inorganic material, $Ge_5As_{55}Te_{40}$, and successfully processed it into a thermoelectric fiber. This material exhibits a high Seebeck coefficient of approximately 1050 μV/K and excellent thermal stability, maintaining its amorphous phase even during high-temperature thermal drawing. The fabricated thermoelectric fiber demonstrated high temperature resolution of 0.1 K, rapid response time (<5 s), and stable operation across a broad temperature range (25–115 °C), with reliable output under repeated thermal cycling. These properties enabled long-term durability and signal stability in practical applications. Finally, the fiber-based temperature sensor was integrated into textiles, and the textiles were used to construct wearable systems for respiratory sensing in face masks and heat proximity alerts in protective garments (Fig. 5c, d). These applications leverage temperature changes from breath or ambient sources.

Fiber-based temperature sensors have demonstrated their capability to move beyond conventional temperature measurement by enabling real-time, durable, and textile-compatible sensing in complex environments. However, for more refined environmental perception, future systems must evolve toward multimodal sensing platforms that can capture temperature variations in conjunction with other physical or chemical stimuli. Moreover, improving the response time, resolution, and long-term environmental durability remains essential to ensure stable operation in real-world applications.

Chemical sensors

Chemical sensors have been widely employed in diverse applications, including physiological monitoring, disease diagnosis, environmental monitoring, and industrial safety, by detecting various chemical species and their concentrations in biological and environmental systems[146,147]. In the biomedical field, early diagnostic approaches largely depended on large-scale, stationary analytical systems designed for single-use applications, and participants needed to go hospitals frequently for diagnostic purposes[148,149]. With the advancement of thin-film and flexible sensor technologies, these systems have transitioned into miniaturized platforms, enabling point-of-care diagnostics[150,151]. Recently, increasing demands for user convenience and real-time physiological monitoring have increasingly focused on the development of wearable and implantable sensing technologies. In industrial applications, chemical sensors have been widely employed to detect hazardous gases, toxic chemicals, and heavy metal ions[152,153]. These sensors typically monitor the concentration of specific analytes at fixed locations. However, such a stationary sensing approach often fails to accurately reflect the actual exposure conditions of workers, due to spatial limitations in sensor placement and the lack of user-centered data collection. To overcome these limitations, recent efforts have focused on the development of fiber-form-factor chemical sensors that can be conformally integrated with the human body for real-time detection of surrounding chemical species. Fiber-based chemical sensors offer lightweight and flexible characteristics, enabling seamless integration into garments or protective equipment[154,155]. These features allow for stable and continuous detection even in dynamically changing environments induced by user movement. In addition, their applicability in structurally constrained environments, where conventional sensors often face limitations, represents a significant advantage[73,156]. In this context, fiber-type chemical sensors, characterized by high mechanical flexibility, stretchability, and breathability, have emerged as promising next-generation platforms for biomedical and industrial applications. Here, we highlight the broad range of applications enabled by fiber-based chemical sensing systems (Table 5).

Central nervous system (CNS) diseases are often difficult to diagnose at early stages and to monitor during treatment, underscoring the critical need for biomarker-based sensing technologies capable of tracking disease progression. Among various biomarkers, blood homovanillic acid (HVA), a major dopamine metabolite, reflects CNS dopamine fluctuations and is closely associated with the onset and therapeutic response of psychiatric and neurodegenerative diseases[157,158]. Accordingly, real-time tracking of blood HVA, a major dopamine metabolite, provides a practical means of evaluating disease progression and therapeutic efficacy in dopamine-associated CNS diseases[159,160]. Zou et al. developed an implantable electrochemical fiber sensor capable of monitoring HVA, a major dopamine metabolite, in peripheral blood rather than cerebrospinal fluid[30]. This sensor features a dual-fiber configuration, in which the working electrode (WE) and reference electrode (RE) are co-twisted to prevent current crosstalk, and is encapsulated with polydimethylsiloxane (PDMS) to ensure stable electrochemical performance (Fig. 6a). The working electrode was fabricated using highly flexible Carbon Nanotube (CNT) fibers with high conductivity and low bending stiffness, coating it with a molecularly imprinted polymer layer to maximize selective detection of HVA. Additionally, the fabricated CNT sensor exhibits an electrocatalytic effect toward HVA, achieving a low limit of detection (LOD) of 4.58 nM. Ultimately, the HVA fiber sensor was implanted in the rat caudal vein for monitoring HVA, demonstrating an accuracy of 97.8%, thus verifying the sensor's high reliability (Fig. 6b). Moreover, it effectively detected trace-level changes in HVA concentration,

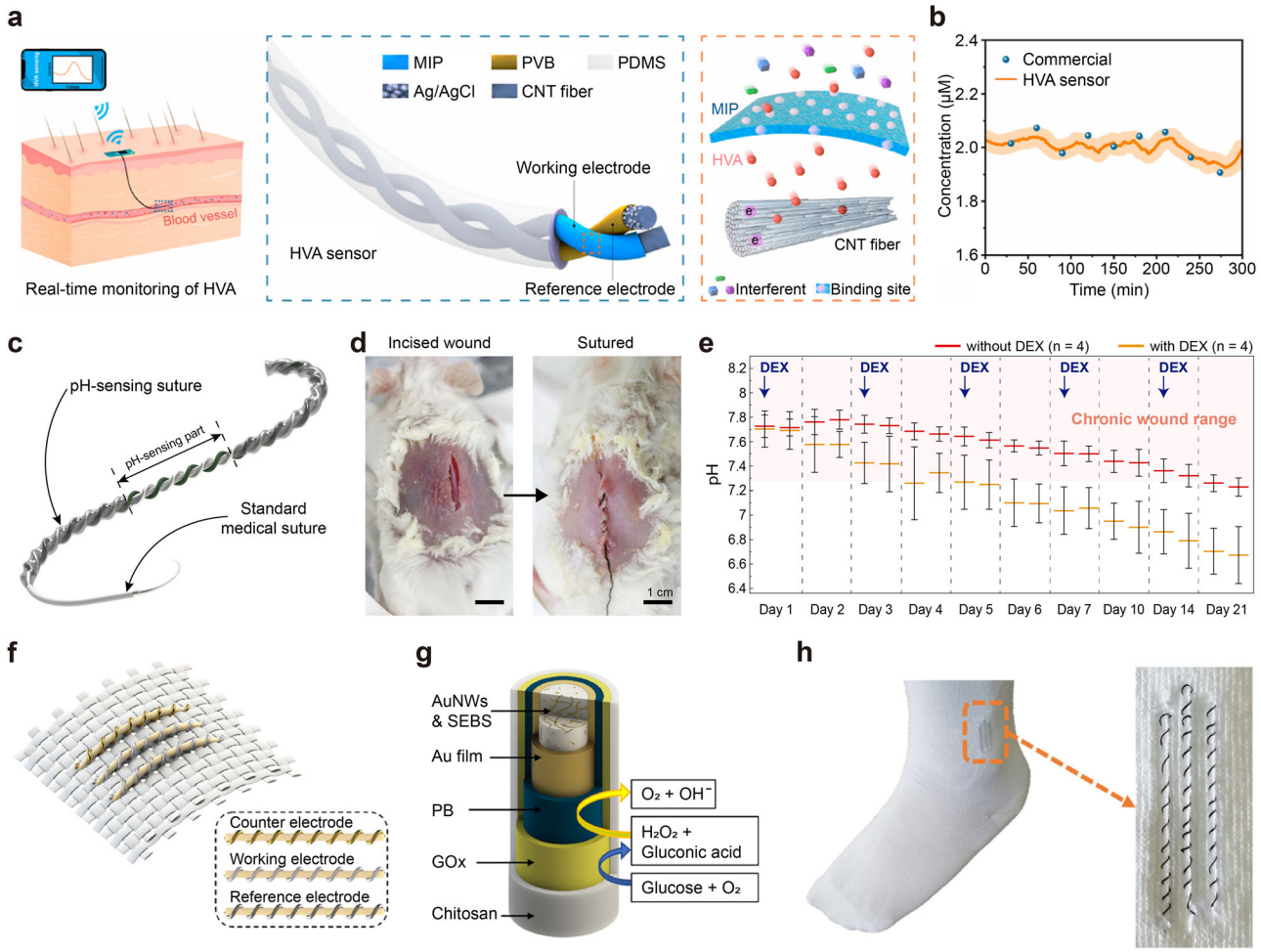

Fig. 6 | Chemical sensors in biomedical applications. **a** Schematic of the wireless sensing platform employing an implantable fiber sensor for real-time monitoring of Homovanillic (HVA) levels in blood. (MIP: Molecularly imprinted polymer; PVB: Polyvinyl butyral; PDMS: Polydimethylsiloxane; CNT: Carbon nanotube) **b** Comparison of calibration data for HVA from collected blood samples with on-body readings from the HVA fiber sensor. The data obtained from the HVA fiber sensor matched well with ex situ measurements of blood samples by a commercial ELISA kit with an accuracy of up to 97.8%. **a**, **b** Reprinted with permission[30]. Copyright 2024, American Chemical Society. **c** Design of the pH-sensing suture, featuring a core supporting suture thread, a PANI-coated working fiber electrode, and an Ag/AgCl-coated reference fiber electrode. **d** Photograph before (left) and after (right) the application of the pH-sensing suture to the dorsal wound. **e** pH monitoring depending on the presence or absence of dexamethasone (DEX) treatment. Over 3weeks of observation, the pH level in the AD models without dexamethasone treatment gradually decreased, but this decline was further accelerated with dexamethasone treatment. **c**–**e** Reprinted with permission[167]. Copyright 2024, WILEY-VCH Verlag GmbH & Co. KgaA, Weinheim. **f** Schematic illustration of the three-electrode glucose sensor integrated into an elastic textile. **g** Schematic illustration of the fiber working electrode, with Prussian blue (PB) and glucose oxidase (Gox) for selective glucose detection. (SEBS: styrene-ethylene/butylene-styrene) **h** Photographs of the stretchable glucose sensor sutured into an elastic sock. **f**–**h** Reprinted with permission[168]. Copyright 2019, American Chemical Society.

confirming its potential for precise dopamine activity monitoring. The HVA fiber sensor developed in this study offers a significant advantage by enabling tracking of CNS status in a simpler and safer manner, without the need for risky procedures such as cerebrospinal fluid sampling. In particular, it is expected to reduce the burden on patients with neuropsychiatric disorders, such as Parkinson's disease and schizophrenia, who require frequent monitoring, and could be a valuable tool for early diagnosis and drug response evaluation.

Real-time detection of biomarkers related not only to neurotransmitters like dopamine but also to the wound environment and tissue homeostasis is also important[161,162]. Local pH changes accompany various biological processes, such as the wound environment, tissue homeostasis, and cellular metabolism, and serve as key biomarkers for assessing disease progression, wound healing, and infection status[163,164]. In particular, the pH level at the wound site is closely related to inflammation and the healing rate, making it one of the critical factors that require precise and continuous monitoring[165,166]. However, conventional pH measurements rely on intermittent methods using external equipment, which have limitations in terms of real-time detection and minimizing wound irritation. To address these issues, recent advancements have led to the development of fiber-based pH sensing sensors in the form of sutures, which can be directly applied to the wound site[167]. The pH-sensing suture shown in Fig. 6c is designed with a structure that integrates the WE and RE into the core fiber, maintaining the functionality of conventional sutures while enabling continuous monitoring of pH changes at the wound site. The WE was coated with polyaniline (PANI) on a polyurethane (PU) fiber dispersed with gold nanoparticles (AuNPs), allowing for the measurement of pH changes based on potential variations. The RE was coated with Ag/AgCl and further covered with polyvinyl butyral to ensure long-term electrochemical stability. The pH-sensing suture exhibits a sensitivity of 58.9 mV/pH within the pH range of 4.0–8.0, closely aligning with the theoretical value of 59.16 mV/pH, making it ideal for accurate pH monitoring in physiological conditions. To validate the performance of this sensor, an in vivo experiment was conducted by suturing an incision site with the pH-sensing suture to continuously monitor the pH of the wound in real time. This demonstrated that the suture could function as a medical suture while simultaneously detecting pH

changes at the wound site continuously (Fig. 6d, e). This research presents a fiber-based pH sensing sensor that functions like a conventional suture and enable real-time monitoring of the inflammation status at the wound site. It offers the potential to enhance the efficiency of wound management in existing medical environments.

Researchers have conducted studies not only for temporary disease prevention and healing monitoring but also for chronic disease monitoring using chemical sensors. Conventional glucose measurement technologies typically involve blood sampling from the fingertip. However, this method is invasive, leading to disadvantages such as discomfort from blood collection and pain during measurement. Zhao et al. developed a highly stretchable fiber-based glucose sensor and successfully integrated it into a wearable system by suturing it into a sock, enabling glucose monitoring in sweat[168]. This glucose sensor is based on an Au fiber three-electrode system, consisting of the working, reference, and counter electrode (Fig. 6f). The WE is designed to selectively detect glucose by coating the surface with Prussian Blue (PB) and Glucose Oxidase (GOx), while the RE is fabricated by depositing Ag/AgCl (Fig. 6g). Due to the selective oxidation of GOx and the electron transfer facilitation by PB, the sensor exhibits high detection performance (13.9 μA/mM cm^2) and a LOD of 6 μM. Additionally, to maximize the sensor's stretchability, a helical structure in this study demonstrated that this structure maintain stable detection performance without signal distortion even under a strain of up to 200%. Based on these high mechanical properties and stable detection performance, the wearable integration potential of the sensor was evaluated by suturing the fiber sensor into a sock and conducting an on-body test (Fig. 6h). The subject's sweat was measured before and 2 h after a meal, and the results demonstrated that the sensor functioned properly during wear, successfully detecting changes in glucose concentration in real time. In view of these findings, the system demonstrates high practicality in enabling non-invasive and continuous glucose monitoring, providing a more convenient health monitoring solution for diabetic patients and individuals requiring blood glucose management, in addition to showing potential for integration with wearable smart healthcare systems.

Fiber-based chemical sensors are also applicable to a wide range of industrial settings, including industrial safety, environmental monitoring, and the detection of compositional and reaction-state changes in precision chemical processes. Despite their widespread use in industrial settings, most metal oxide-based sensors suffer from low selectivity toward target analytes and typically exhibit detectable responses only at concentrations exceeding 5 ppm[169,170]. Such limitations are particularly critical given that even trace-level leakage of toxic gases may result in severe hazards for workers, highlighting the need for sensing systems capable of reliable detection at low concentrations. In addition, many conventional systems installed as stationary or facility-integrated units make it difficult for individual workers to achieve real-time safety perception and active response[171,172]. Kim et al. developed a colorimetric gas sensor, which enables simple and prompt detection of low-concentration toxic gases down to 1 ppm and can be seamlessly integrated into wearable textile systems[169]. This sensor was fabricated based on densely electrospun nanofibers and employs colorimetric dyes and ionic liquids to induce selective responses to specific gases. In particular, lead acetate ($Pb(Ac)_2$) and lead iodide (PbI_2) were applied for the detection of hydrogen sulfide (H_2S) and ammonia (NH_3), respectively (Fig. 7a). By uniformly dip-coating the dye onto the fiber matrix, the sensor achieves high sensitivity for gas detection even at low concentrations down to 1 ppm, representing a substantial enhancement compared to commercial H_2S sensors, which typically respond only above 5 ppm (Fig. 7b). To evaluate the practical applicability of the sensor, the nanofiber-based gas sensor was sewn into textile fabrics to construct a smart textile sensing platform. When the sensor-integrated fabric was attached to the subject's garment and exposed to H_2S or NH_3 gas, a clear color change was observed, white to brown upon H_2S exposure and yellow to transparent as the NH_3 concentration increased, thereby enabling real-time visual monitoring of the surrounding gas environment by the subject (Fig. 7c). This sensing platform enables the detection of toxic gases at concentrations as low as 1 ppm, overcoming the limitation of conventional gas sensors that require higher concentrations for activation, and thus demonstrating its effectiveness in trace amount gas monitoring. This gas sensing platform enables the detection of toxic gases at concentrations as low as 1 ppm, overcoming the limitation of conventional gas sensors that require higher concentrations for activation, and thus demonstrating its effectiveness in monitoring trace amounts of gases.

In addition, in working environments where exposure to hazardous gases may occur, real-time detection and immediate safety response by workers are critically important. Accordingly, gas sensors need to maintain high sensitivity under high-temperature and long-term operating conditions, which remains a challenge as conventional metal oxide-based sensors often suffer from sensitivity degradation and poor long-term stability due to catalyst agglomeration and surface deterioration at elevated temperatures. To address this issue, a gas sensor incorporating a heterojunction structure of carbon nitride nanosheets (MCN) and SnO_2 was proposed to enhance sensitivity and thermal stability by providing a stable support for atomically dispersed Pt catalysts[173]. The sensor was fabricated via an electrospinning process by mixing Pt atoms with a Sn precursor ($SnCl_2$), where the Pt atoms function as electron transfer mediators, amplifying the gas sensing signals (Fig. 7d). To evaluate the applicability of the sensor in real-world industrial environments, sensing experiments were conducted using 10 representative hazardous gases that are frequently encountered in industrial settings, including formaldehyde (HCHO), NH_3, and H_2S (Fig. 7e). Gas sensing performance tests demonstrated that the sensor is capable of detecting multiple gases, exhibiting particularly high sensitivity toward HCHO. Compared to conventional SnO_2-based sensors, its response was ~5 times higher. It also exhibited excellent thermal stability, showing only a 7.1% decrease in sensitivity after continuous operation for over 170 h at high temperatures. Compared to conventional catalyst-based sensors, which suffer from performance degradation due to the agglomeration and oxidation of metal nanoparticles at high temperatures, the proposed sensor demonstrates long-term operational stability. This sensor is expected to overcome key limitations of conventional metal oxide-based sensors, such as thermal instability and catalyst agglomeration, and contribute to the development of gas sensing technologies with high sensitivity and long-term operational stability. In particular, the sensor's ability to detect hazardous gases such as HCHO in real time highlights its strong potential for applications in industrial safety and environmental monitoring. Although it currently exhibits high sensitivity primarily toward specific target gases, future studies may expand its capabilities toward multi-gas detection and improved selectivity through the integration of diverse metal oxides and catalytic combinations.

The various fiber-based chemical sensors discussed thus far have emerged as essential technologies for biomedical and industrial applications, offering considerable potential for deployment across a wide range of fields, including healthcare, environmental monitoring, and industrial safety management. While conventional chemical sensors have exhibited limitations in sensitivity, selectivity, durability, and real-time monitoring, recent studies have demonstrated progressive performance enhancements through the use of fiber-based platforms, enabling garment-integrated sensing, precise biomarker detection from biofluids, and reliable gas sensing under harsh conditions, to meet the diverse demands of emerging applications, with active research efforts continuing to advance this field. In future studies, the integration of multimodal sensing capabilities into a single fiber-based system is expected to emerge as a key research direction.

Electrophysiological sensors

Electrophysiological sensors are designed to detect voltage variations or electric currents across multiple biological scales, ranging from individual ion channel proteins to entire organs such as the heart, by utilizing the intrinsic electrical properties of biological cells and tissues[174,175]. With the rapid advancement of medical and healthcare technologies in modern society, electrophysiological sensors have emerged as essential tools for the precise assessment and effective management of human physiological

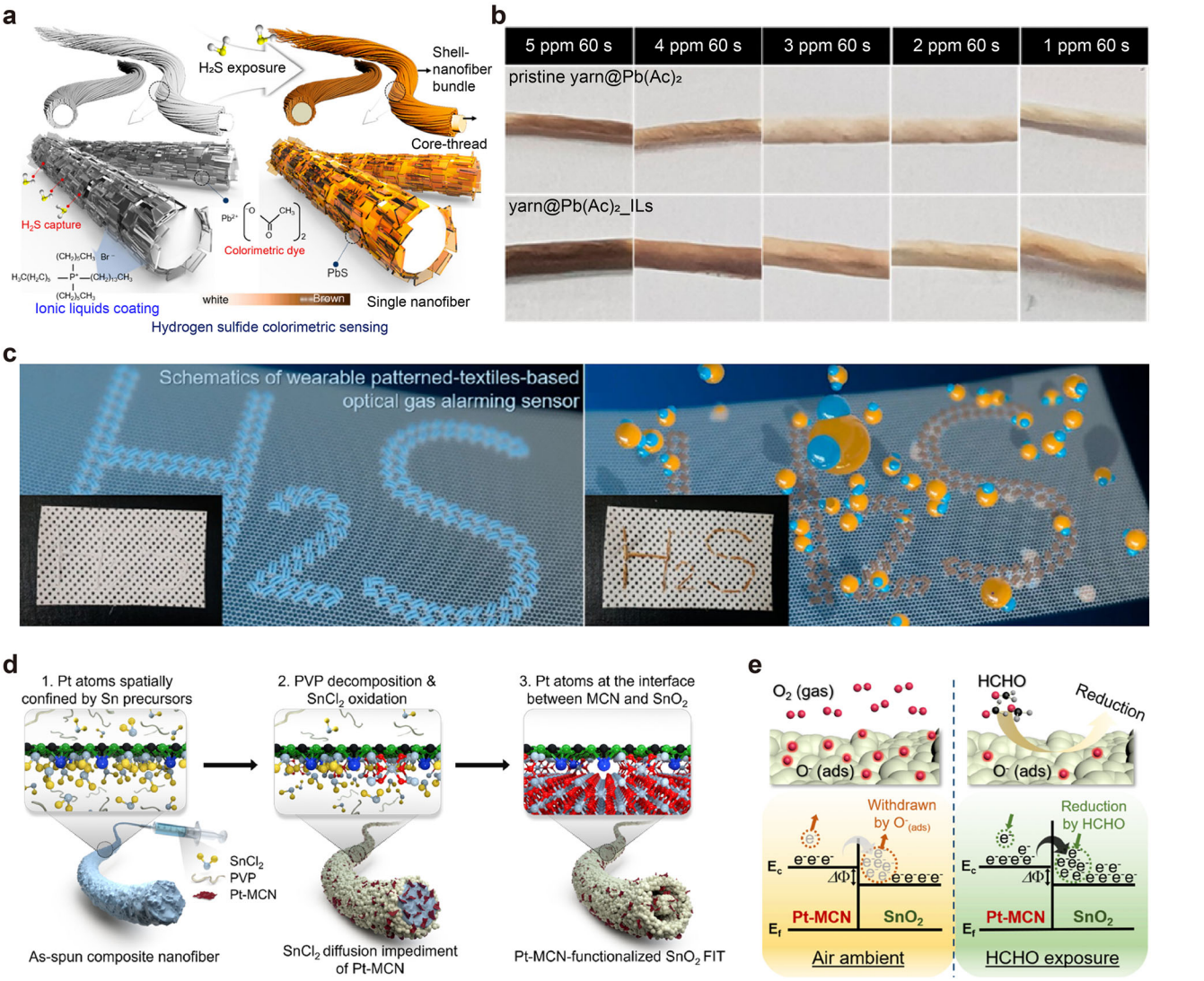

Fig. 7 | Chemical sensors for toxic gas detection. a Schematic illustrations of H_2S-induced colorimetric transitions in yarn. **b** Photographs of yarn exposed to different H_2S concentrations under controlled time. **c** Photographs of the patterned textile-based optical gas sensor showing color change before (left) and after (right) exposure to H_2S gas. **a**–**c** Reprinted with permission[169]. Copyright 2020, American Chemical Society. **d** Schematic of the Pt single-atom anchoring process and the formation of the nanofiber structure. (PVP: Polyvinylpyrrolidone; MCN: SA-anchored shredded melamine-derived carbon nitride nanosheets) **e** Schematic illustration of the HCHO-sensing mechanism and band diagram of the MCN/SnO_2 heterojunction. **d**, **e** Reprinted with permission[173]. Copyright 2020, American Chemical Society.

conditions[176,177]. Adoption of electrophysiological sensing technologies is expanding from clinical diagnostics by medical professionals to applications in fitness tracking and personal health management. Electrophysiological sensors offer precise detection of diverse low-amplitude biosignals, including electrocardiography (ECG)[178–182], electromyography (EMG)[183–187], electrocorticography (ECoG)[188–192], electrooculography (EOG)[193–197], and electroretinography (ERG)[198–202], while enabling continuous real-time monitoring. Owing to these capabilities, they hold significant potential for early disease diagnosis and prevention, effective chronic disease management, and real-time surveillance of high-risk patients. In addition, electrophysiological sensors allow real-time analysis of physiological responses, including heart rate, muscle fatigue, and respiratory patterns, thereby enabling diverse applications such as personalized fitness optimization, fatigue regulation, and sleep pattern monitoring.

Electrophysiological sensors can be broadly categorized based on their mode of application into wearable types, which are attached to or worn on the skin surface, and implantable types, which are directly inserted into the body for internal monitoring[203,204]. Wearable sensors enable non-invasive acquisition of biosignals, offering advantages in user comfort and suitability for prolonged monitoring owing to their user-friendly design[32,205]. Among conventional wearable biosensors that interface with the skin, hydrogel-based electrodes have been widely utilized; however, they present several drawbacks, including skin irritation, allergic reactions, signal degradation due to dehydration, limited lifespan, and the need for frequent replacement[206,207]. To address these limitations, dry sensors have emerged as a promising alternative; however, their inherently high skin-electrode contact impedance often leads to compromised signal quality[208,209]. In response, recent studies have increasingly focused on developing sensor technologies that employ novel materials, such as liquid metals (LM) and liquid metal-based composites (LMP), capable of simultaneously achieving high mechanical flexibility and superior electrical conductivity[210,211]. These emerging materials integrate the respective advantages of conventional wet and dry sensors and are being actively developed to enhance both skin conformability and signal fidelity. Implantable sensors are directly integrated into biological tissues, enabling high signal accuracy and long-term stability in in vivo environments. Owing to these advantages, they are particularly suitable for applications requiring the detection of subtle biosignals, such as those in the nervous system. However, implantable sensors

pose several critical challenges due to their direct insertion into biological tissues. Conventional implantable electrodes, typically fabricated from rigid materials such as silicon or metal, have been associated with stiffness mismatch against soft neural tissues, leading to acute and chronic neural injuries, neuronal loss, and reactive gliosis[212,213]. To overcome these limitations, implantable sensors must satisfy essential criteria, such as long-term biostability, high biocompatibility, and mechanical robustness, to ensure safe and reliable long-term monitoring in vivo. In particular, the reliable acquisition of biosignals and continuous monitoring via advanced signal processing techniques are essential. Addressing these requirements involves several key challenges, including the development of novel materials that concurrently offer flexibility and durability, structural innovations to mitigate neural damage, and improvements in mechanical performance. These research efforts aim to overcome the intrinsic limitations of conventional electrophysiological sensors and advance toward safer and more efficient platforms for long-term monitoring.

Taylor et al. integrated carbon nanotube thread (CNTT) into stretchable textiles using standard sewing techniques, thereby creating soft, wearable dry sensors capable of non-invasive and continuous EKG monitoring (Fig. 8a and Table 6)[214]. CNTT is a fiber-based material fabricated by twisting 21 strands of monofilament carbon nanotube fibers (CNTF), which are synthesized via solution spinning. The resulting fiber exhibits outstanding electrical conductivity, superior mechanical strength, and a unique combination of stretchability and flexibility. These properties make CNTT highly promising for applications in electronic textiles and wearable sensor systems. Specifically, CNTT exhibits low skin-electrode contact resistance, enabling stable and reliable acquisition of biosignals. In addition, it is significantly lighter and softer than conventional metal-based electrodes, offering enhanced comfort during extended periods of wear. CNTT can serve dual functions as both sewable electrodes and signal transmission wires. Notably, CNTT-based electrodes demonstrate excellent durability, maintaining their performance even after repeated machine washing, while their intrinsic biocompatibility ensures safe and long-term use. In addition, the CNTT fabrication process is scalable, rendering it well-suited for the practical development of electronic textiles. CNTT-based electrodes were sewn into the inner rib area of a shirt to maintain direct contact with the skin, enabling continuous EKG monitoring during walking and running. Experimental results confirmed that the CNTT electrodes delivered signal quality comparable to that of commercial Holter monitor electrodes (Fig. 8a).

One of the key requirements for developing advanced smart sensing systems is the incorporation of multimodal sensing capability. While electrophysiological sensors are highly effective in monitoring human bio-signals, the complexity of physiological states often cannot be fully captured by a single type of signal. Therefore, for more accurate and comprehensive diagnosis and analysis, it is essential to develop systems capable of simultaneously collecting and interpreting various physiological and environmental cues. In this context, Wang et al. proposed an organic bioelectronic fiber that can be seamlessly integrated with biological tissues without interfering with native biological functions of the host, while simultaneously enabling multimodal sensing functionalities (Fig. 8b)[215]. Unlike conventional sensing technologies that primarily focus on electrophysiological signal acquisition, this bioelectronic fiber platform integrates multiple sensing modalities into a single, flexible architecture, enabling responsive detection of diverse environmental stimuli. For instance, when a fiber array is attached to the thumb muscle area, it can effectively collect electromyography (EMG) signals and detect real-time amplitude variations corresponding to increased muscle activity under external loading. Beyond EMG monitoring, the fiber array functions as a humidity sensor, exhibiting changes in electrical characteristics in response to environmental moisture or mist exposure. Furthermore, by incorporating pH-responsive components, the system can distinguish varying concentrations of pH mist sprays. Additionally, upon exposure to hazardous gases such as ammonia, the dedoping reaction of PEDOT:PSS allows the system to function as a gas sensor. This fiber-based multimodal sensor thus acts as an integrated platform capable of capturing a wide range of physiological and environmental stimuli. Moreover, by precisely tuning the orientation and density of the fiber network during fabrication, the electrical resistance and functional properties can be engineered to meet specific application requirements. These bioelectronic fibers are fabricated via a solution-based orbital spinning process at ambient conditions. The resulting fibers maintain a diameter below 10 μm and form an open, mesh-like structure with microscale porosity, enabling conformal integration with highly curved or complex biological surfaces. Thanks to this structure of the bioelectronic fiber, it facilitates an imperceptible wearing experience, minimizing tactile interference and ensuring long-term user comfort. Collectively, the organic bioelectronic fiber platform. meets critical design criteria-biocompatibility, multifunctionality, imperceptibility, mechanical flexibility, and reusability-positioning it as a promising solution for the next generation of wearable biosensing technologies.

To accurately measure biosignals such as EMG during dynamic movements, it is essential to achieve seamless and stable integration between electrophysiological sensors and biological tissues. This requires the sensor to possess biocompatible mechanical properties, including high flexibility and stretchability. Various studies have explored coating soft and stretchable fiber substrates with solid conductive fillers such as carbon nanotubes (CNTs), graphene, and silver nanowires or nanoparticles. However, these solid-filler-coated fibers often suffer from a significant increase in electrical resistance under strain, resulting in a marked decrease in overall conductivity. To address this limitation, Lee et al. developed a bi-layered liquid metal-polymer composite (BiLMP) that combines outstanding durability, electrical conductivity, stretchability, and biocompatibility (Fig. 8c)[216]. The BiLMP was fabricated through a two-step process: first, fibers were coated with polymer-attached LMPs (PaLMPs) using a suspension shearing technique to impart stretchability; then, CNT-attached LMPs (CaLMPs) were applied to enhance initial conductivity and mechanical robustness. As a result, the fabricated BiLMP exhibited high conductivity (2.24×10^6 S/m) and maintained stable electrical performance even under mechanical deformation. Moreover, BiLMP-based stimulation thread devices (BiLMP-S-threads) demonstrated excellent structural adaptability, enabling reliable operation even under suturing and knotting conditions (Fig. 8d). This characteristic makes them well-suited for applications in invasive one-dimensional bioelectronic systems, such as electrodes for recording brain activity. The BiLMP-S-thread (200 μm in diameter) was implanted into the sciatic nerve of wild-type mice. Upon detecting hindlimb movement, the BiLMP-S-thread was able to measure EMG signals from the tibialis anterior muscle (Fig. 8e).

In neural interface technologies such as ECoG and intracortical recording systems, implantable sensors are essential for achieving high-precision signal acquisition. While prior studies have focused on neural recording under static or mildly active conditions, vigorous movement poses a major challenge. Relative motion between the implanted device and surrounding tissue often leads to mechanical mismatch, resulting in neural tissue damage and signal degradation. To address this issue, Tang et al. developed a soft fiber-based neural device (FND), inspired by the structural architecture of axons (Fig. 8f)[57]. The FND utilizes PEDOT:PSS, a highly conductive and biocompatible polymer, as the primary building block of a conductive nanofiber network. Using a glycerol, water mixture as a liquid matrix, the FND was fabricated to exhibit low elastic modulus, high conductivity, and low interfacial impedance. As a result, the FND demonstrates approximately 100 times greater flexibility than conventional platinum–iridium (PtIr) wires, thereby enabling stable and reliable neural recordings in vivo. Notably, the FND maintains mechanical compliance with neural tissue even during vigorous body movements, ensuring robust and undistorted signal acquisition. In this study, a 16-channel array was constructed by bundling 16 individual FNDs with a 100 μm inter-channel spacing. The array was implanted into the dorsal lateral geniculate nucleus (dLGN) and connected to a wireless head-mounted recording system. Compared to conventional metal-based electrodes, the FND-based neural recording system exhibited low specific impedance (579 kΩ·μm^2) and more

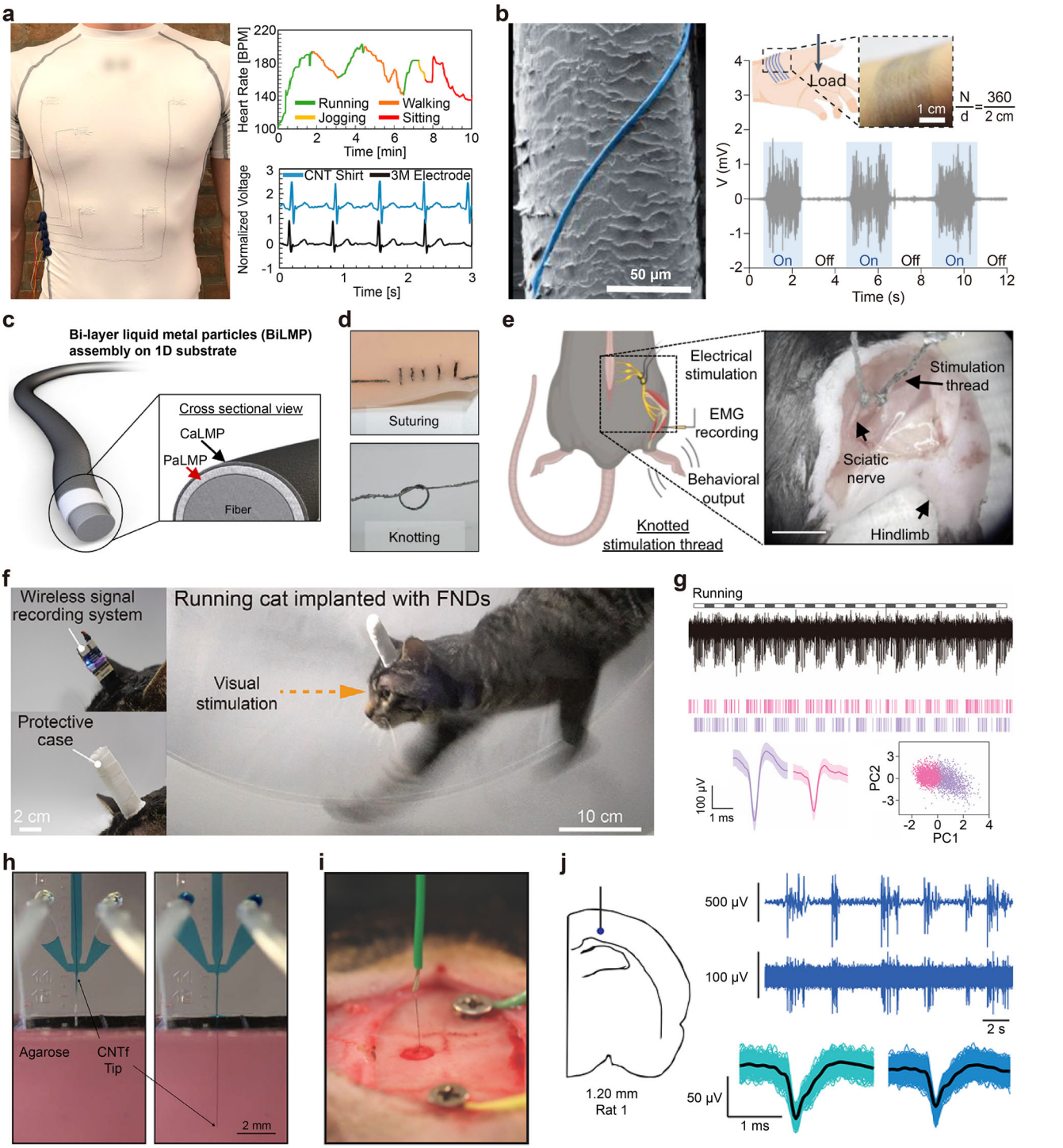

Fig. 8 | Electrophysiological sensors. a An athletic shirt integrated with CNTT electrodes is capable of monitoring the wearer's heart rate during various activities such as running, jogging, walking, and sitting. In addition, it enables reliable electrocardiogram (EKG) signal acquisition. Reprinted with permission[214]. Copyright 2021, American Chemical Society. **b** SEM image of a fiber exhibiting morphing morphology on a human hair, highlighted with blue color (left) and fiber array on thumb muscle for ON/OFF EMG signal detection (right). N/d indicates the number of fibers (N) across a distance (**d**). Reprinted with permission[215]. Copyright 2024, Springer Nature. **c** Schematic illustration of the BiLMP structure, consisting of two distinct layers: PaLMP and CaLMP. (LMP: Liquid metal particle) **d** Various mechanical interactions in one-dimensional bioelectronic devices based on BiLMP-coated fibers. **e** EMG signals are recorded from the tibialis anterior muscle in response to leg movement using a BiLMP-S-thread sutured to the hindlimb of a mouse. **c**–**e** Reprinted with permission[216]. Copyright 2023, Springer Nature. **f** Photographic images showing a cat running with fiber neural devices (FNDs). **g** Neural spike signals recorded from a running cat using a wireless signal acquisition system. (PC: Principal component) **f**, **g** Reprinted with permission[57]. Copyright 2024, WILEY-VCH Verlag GmbH & Co. KgaA, Weinheim. **h** A 12 μm CNTF electrode was stably inserted 4.5 mm into a brain phantom without bending using a microfluidic-assisted method. **i** Insertion of a CNTF electrode into the cortical depth of an anesthetized rat using a fluidic microdrive. **j** EEG signals (top) and neural spikes (bottom) recorded from a CNTF electrode inserted 1.20 mm below the cortical surface of a rat. **h**–**j** Reprinted with permission[221]. Copyright 2018, American Chemical Society.

Table 6 | Comparative overview of parameters for electrophysiological sensors

No.	Fabrication process	Materials	Target signal type	SNR	Impedance @ 1 kHz	Biocompatibility & Contact stability
1[214]	Solution spinning	CNT	EKG	30	20 kΩ	The fiber sensor is fabricated using a nontoxic material, CNT, and integrated into sportswear, where it exhibits relatively limited contact stability.
2[215]	Orbital spinning	PEDOT:PSS	EMG	-	20 kΩ	PEDOT:PSS is a biocompatible mixed ionic and hyaluronic acid, as a skin extracellular matrix analogue, enhances fibre spinnability and skin adhesion.
3[216]	Suspension shearing-based coating	LMP	EMG	-	-	The BiLMP-coated fiber is biocompatibility and contact stability, as demonstrated by in vivo experiments, and can be securely sutured to biological tissue.
4[57]	Wet spinning	PEDOT:PSS	Neural spike	-	579 kΩ·μm^2	The FND, made of biocompatible PEDOT:PSS and fluorine rubber, enables stable neural recordings even in dynamic in vivo conditions by maintaining reliable tissue contact.
5[221]	Wet spinning	CNT	EEG & Neural spike	-	17.44 MΩ·μm^2	Biocompatible CNTf microelectrodes enable stable signal acquisition even under dynamic in vivo conditions by minimizing tissue damage and maintaining reliable contact during mechanical deformation.

than threefold higher SNR, while maintaining long-term signal stability with minimal attenuation. Neural signals were recorded in response to light-induced visual stimuli while the subject cat freely moved and ran, simulating real-world dynamic conditions (Fig. 8f). The results confirmed that the FND maintained stable neural signal fidelity even under strong physical activity (Fig. 8g). Furthermore, compared to conventional rigid electrodes, it was demonstrated that the FND results in reduced neural tissue damage and minimized glial response even after long-term implantation. These findings suggest that the FND's ability to maximize mechanical compatibility with neural tissue can significantly enhance neural signal recording in vivo.

Most existing implantable electrodes are fabricated from metals or micromachined silicon, resulting in a stiffness mismatch with brain tissue of up to approximately 10^8 times[217,218]. This pronounced mechanical mismatch can induce both acute and chronic neural damage, including neuronal death and gliotic responses[219,220]. Accordingly, the development of electrodes made from highly flexible materials has emerged as a key research direction. However, the high softness of ultra-flexible electrodes poses significant challenges for insertion, often hindering smooth implantation. As a result, methods have been developed that involve using temporary stiffeners to reinforce the electrodes before insertion or inserting the electrodes with a rigid probe and removing the probe afterward. However, both stiffeners and probes can cause neural tissue damage during the implantation process, and even after removal or dissolution, they continue to induce cell loss and neuronal activation. This poses a risk of both acute and chronic neural damage, as well as an increased likelihood of surrounding neuronal injury and disruption of the blood-brain barrier (BBB). To overcome these limitations, Vitale et al. developed a microfluidic device employing fluidic microactuation technology (Fig. 8h)[221]. By regulating the fluid flow within microchannels, controlled tensile forces are applied to the electrode, preventing bending and enabling precise micron-scale insertion into brain tissue, without the need for external stiffeners. Moreover, the device incorporates localized fluid diversion at the injection site to prevent increases in intracranial pressure. They successfully inserted CNTf electrodes (12 μm in diameter) into an agarose-based brain phantom to a depth of 4.5 mm using the Fluidic Microdrive (Fig. 8h). Subsequently, CNTf electrodes were precisely implanted into the cortical depth of the rat brain using the Fluidic Microdrive, allowing for continuous neural signal recording (Fig. 8i, j). These results demonstrate that the Fluidic Microdrive facilitates accurate and minimally invasive insertion of ultra-flexible electrodes, thereby minimizing tissue damage and offering a refined approach to neural interfacing.

These studies have enhanced the performance of neural interfaces and demonstrated high applicability in clinical and daily-life applications that require long-term monitoring. Notably, these technologies are evolving beyond basic biosignal monitoring to function as neural signal transducers. Such functionality can support rehabilitation for amputees using prosthetic limbs or patients with neuromuscular impairments, while also contributing to the development of assistive devices that utilize neural control signals. Despite these promising developments, there are still challenges that need to be addressed for these technologies to advance into practical applications. First, electrophysiological sensors handle large volumes of data, requiring the development of advanced data processing techniques. Algorithms for noise suppression, signal stability enhancement, and real-time signal analysis will be essential. Second, continued innovation in materials and device architectures is necessary to improve SNR. Wearable and implantable sensors require continued technological improvements to ensure high-quality electrical signal sensing and recording. Third, thermal management remains a critical issue, especially for implanted devices, where heat generation must be minimized to avoid adverse effects on surrounding biological tissues. Lastly, research aimed at improving biocompatibility and durability is essential, and systematic research and clinical evaluations must continue to ensure the long-term reliability and safety of the sensors. In conclusion, the various electrophysiological sensors and neural interface technologies discussed in this study hold the potential for advancements in biosignal monitoring and neural interface applications. Future research

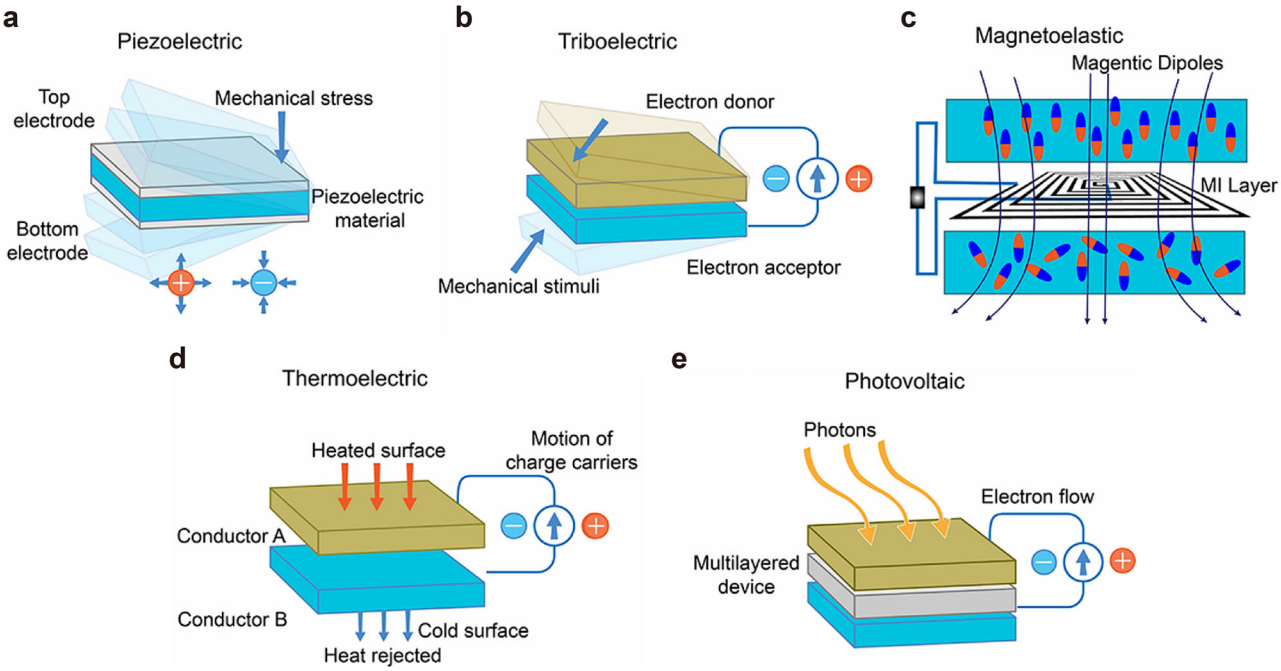

Fig. 9 | Classification and mechanism of electric generation. **a** Piezoelectric, **b** Triboelectric, **c** Magnetoelastic, **d** Thermoelectric, **e** Photovoltaic effects. **a**–**e** Reprinted with permission[222]. Copyright 2024, American Chemical Society.

should focus on further enhancing electrode material performance, advancing data processing technologies, and increasing the practical applicability of these technologies in clinical settings. Furthermore, electrical sensors based on neural interface technologies are expected to play a critical role not only in rehabilitation therapy but also in a wide range of areas such as neural prosthetics, smart medical systems, and brain-computer interfaces (BCI). As these studies accumulate, electrophysiological sensors will be expected to play an important role in fields such as healthcare, rehabilitation, neuroscience, and BCI.

Fiber-based energy harvesting and storage

To enable the practical deployment of fiber-based smart systems, equal attention must be given to both high-performance sensing technologies and stable energy supply systems capable of sustaining long-term operation. With the rapid advancement of fiber-based sensing technologies, their integration into diverse textile platforms has accelerated, giving rise to a wide range of multifunctional smart systems. However, in most of the smart systems developed to date, while the sensing components have been successfully implemented in fiber form, essential energy supply elements, such as batteries and interconnects, still rely on conventional components with limited mechanical flexibility[40]. This mechanical mismatch, arising from the disparity in flexibility between fiber-based sensors and conventional power components, can compromise the overall deformability of the system and ultimately limit the long-term stability and continuous operation of the sensors. Therefore, to address mechanical mismatches and ensure system-wide flexibility, the integration of fiber-based energy harvesting and storage technologies is essential for establishing fully compliant and unified smart textile platforms. Researchers are actively developing energy harvesting technologies such as piezoelectric, triboelectric, and magnetoelastic principles[222], leveraging reusable environmental energy sources to produce usable levels of electrical power suitable for operating wearable or low-power electronics[223,224]. The energy sources utilized in these energy harvesting technologies include mechanical deformations, such as human motion or repetitive movements of machinery, as well as sustainable energy forms like solar radiation, thermal gradients, and ambient radiofrequency (RF) waves. These mechanisms enable the capture of underutilized ambient energy and its conversion into usable electrical power for low-power electronics. Moreover, their inherent compatibility with textiles enables seamless integration into garments, making them highly promising for continuous and autonomous energy harvesting in daily life. Both advanced energy harvesting strategies and the integration of efficient and reliable energy storage technologies are required to achieve the development of autonomous smart systems. Recent research has explored various storage platforms, including supercapacitors that offer high power density and rapid charge-discharge performance, and highly safe aqueous batteries based on Zn-ion and Na-ion chemistries[225–227]. To further improve safety, alternative electrolytes with enhanced thermal and chemical stability, such as solid-state and gel-based formulations, are being investigated to replace conventional liquid electrolytes. Additionally, flexible fiber-shaped batteries are being developed to meet the mechanical requirements of wearable systems, facilitating seamless integration into textile-based platforms. By integrating energy harvesting and storage technologies into textile platforms, it becomes possible to enable multifunctional capabilities such as biosignal monitoring, environmental sensing, and wireless communication. Importantly, such technologies pave the way for fully autonomous systems that can operate independently of external power supplies, enabling continuous and self-sustained functionalities. This energy autonomy forms a foundational requirement not only for sensing and communication but also for driving active functionalities, such as actuation and therapeutic stimulation, which are discussed in the following chapter.

Fiber-based energy generators

In the perspective of energy generating sources, active and passive energy sources are utilized. First, active energy sources are induced by human motions or machine actuation. Those sources are reliable sources that can be effectively exploited by fiber-based energy harvesters. These devices convert external mechanical stimuli, such as contact-separation[228–230], compression[231–233], and bending[234,235], into electrical energy through triboelectric[236–240], piezoelectric[241–244], and magnetoelastic conversion mechanisms[245–247]. The triboelectric mechanism involves charge separation induced by contact and subsequent separation between two dissimilar materials (Fig. 9a). Due to the difference in their electron affinities, electrons are transferred during contact, resulting in an electrostatic potential difference across the surface. When applied to highly flexible fiber-based devices, the triboelectric effect can be maximized due to the large surface

area, which results in more friction between fiber devices, under mechanical deformability of the substrate[248,249]. In addition, triboelectric nanogenerators (TENGs) inherently generate high voltage with low current output[250]. This characteristic makes TENGs particularly advantageous for electronic systems that require high-voltage input. However, repeated contact-separation cycles may lead to material abrasion and gradual degradation in electrical output, posing challenges to long-term durability and stability[236,251]. The other weakness is that this mechanism relies on surface friction, and its energy conversion efficiency tends to decrease under low-friction conditions. The piezoelectric mechanism generates electrical voltage through dipole reorientation and induced polarization within the piezoelectric layer under applied mechanical pressure (Fig. 9b). Owing to this principle, piezoelectric devices, where the output is proportionally correlated with the magnitude and frequency of the applied mechanical force. This enables reliable and predictable performance, particularly advantageous for consistent energy harvesting under cyclic loading conditions[244,252]. However, this effect is only triggered by dynamic deformation, as piezoelectric materials do not respond to static pressure[252,253]. Therefore, continuous energy generation requires cyclic mechanical loading and unloading, and the transient nature of the response imposes inherent limitations on sustained power delivery. Moreover, mechanical stimuli can induce an indirect energy generation process. The magnetoelastic mechanism operates based on variations in the magnetic field that occur when a magnetostrictive material is subjected to mechanical stimuli. These changes in magnetization induce an electric current through electromagnetic induction (Fig. 9c). This mechanism enables non-contact power generation, offering unique advantages. The magnetoelastic mechanism operates without direct mechanical contact, which helps prevent surface abrasion and enhances long-term durability. This operating principle also enables wireless energy harvesting, and magnetoelastic devices enable to utilize efficient performance even over long distances. They can also function in constrained environments or through obstacles, making them suitable for enclosed or in vivo applications. However, the stability of the electrical output can be influenced by the content and spatial distribution of magnetic particles within the active layer[246,247]. Furthermore, the generation procedure can be interrupted by external magnetic field, which may lead to energy generation efficiency degradation.

In addition to active energy sources, passive energy sources have also garnered increasing attention in the field of energy harvesting. In line with this trend, researchers have been expanding the scope of energy sources to include passive inputs. Such sources, including heat and light, can operate under static conditions, unlike mechanically driven energy harvesting devices that rely on user motion[254–256]. The strength possibly makes a stable energy supply. Among the energy harvesting strategies using passive energy sources, thermoelectric harvesting[222,257,258], which utilizes thermal energy, is based on the Seebeck effect, wherein a temperature gradient induces electron movement and generates an electric potential (Fig. 9d). In wearable devices, this principle allows electricity generation without physical motion by exploiting the temperature difference between the skin and the surrounding air[133,256,259,260]. However, a constant heat supply is necessary to maintain the temperature gradient, which directly influences the output performance of thermal energy harvesters. Furthermore, the absence of a continuous thermal gradient significantly hinders the energy harvesting efficiency of these systems. Therefore, recent research has focused on enhancing electron mobility through the doping of conductive materials, as well as improving energy conversion efficiency by employing structural designs that increase the effective cross-sectional area for heat transfer. Alongside thermal energy, light represents another major energy source that is readily available in everyday environments. Photovoltaic harvesting, based on the photovoltaic effect, generates electricity through the movement of electrons at the junction of p-type and n-type semiconductors upon light exposure (Fig. 9e). This mechanism enables the use of both natural and artificial light sources[261]. Photovoltaic energy harvesting offers a relatively high energy density output[262]. Another key advantage is its use of an eco-friendly and virtually limitless energy source. On the other hand, since energy generation in photovoltaic systems relies entirely on light absorption, the output inevitably drops in the absence of light, such as during nighttime or in dark indoor environments. To address this limitation, recent research has focused on enhancing energy conversion efficiency and developing strategies to improve performance under low-light conditions.

Figure 10a illustrates the structural configuration of a textile-based TENG weaved using a single-electrode triboelectric yarn (SETY)[263]. The SETY adopts a core–shell architecture, in which a conductive silver yarn serves as the central core, while two distinct electrospun nanofibers, composed of polyvinylidene fluoride (PVDF) and polyacrylonitrile (PAN), are uniformly deposited around the core. Within the triboelectric layer, PVDF and PAN function synergistically to enhance device performance: PVDF, with its high dielectric constant, primarily contributes to triboelectric charge generation, while PAN improves the overall structural flexibility of the fiber, owing to its excellent inherent softness. By combining tailored material properties with architectural optimization, this approach effectively enhances the triboelectric performance and energy conversion efficiency. The SETY fabricated via electrospinning exhibits a diameter of approximately 350 μm and a weight of 0.33 mg/cm. Owing to its lightweight, flexible nature and scalability in production, it holds strong potential for practical applications. Building on the advantages of lightweight design and scalability, Ahn et al. systematically evaluated the energy harvesting performance of the TENG constructed by weaving SETYs. Under an operating frequency of 2.5 Hz and an applied contact force of 5 N, the device demonstrated a maximum output voltage of 40.8 V, a current density of 0.705 $\mu A/cm^2$, and a charge density of 9.513 nC/cm^2. Furthermore, the generated current exhibited a proportional increase with expanding contact area, indicating excellent output stability and strong potential for scalability (Fig. 10b).

In addition to energy conversion efficiency, energy harvesting devices are also expected to maintain mechanical stability under long-term deformation while allowing ease of maintenance. To fulfill these requirements, Zhou et al. designed a TENG with integrated self-healing functionality and enhanced durability (Fig. 10c)[250]. The self-healing functionality of the device is enabled by the integration of an electrically heated wire (EHW) and a low-melting-point alloy (LMPA) as a key structural component. The self-healing process is thermally induced by Joule heating, which raises the temperature of the EHW, leading to the melting of the LMPA at approximately 47 °C. Upon cooling, the resolidified alloy restores the structural integrity. Under a mechanical load of 25 N and frequency of 3 Hz, the TENG exhibited a maximum output power density of 348.5 $\mu W/m^2$, demonstrating its capability to maintain stable energy generation even under higher external loads compared to conventional triboelectric devices (Table 7). In addition, the device demonstrated broad applicability through two applications. First, it was integrated with cotton yarn and woven into a wearable, finger-mounted format, validating its potential as a touch-interfaced wearable electronic device (Fig. 10d). Second, the TENG was applied to a gear within a rotary mechanical system, where it exhibited stable operation under high-load conditions, suggesting its potential for energy harvesting applications in industrial infrastructures (Fig. 10e).

Parallel to triboelectric-based energy harvesting strategies, piezoelectric devices have also been actively explored for mechanical-to-electrical energy conversion. Since the electrical output of piezoelectric systems depends on the extent of mechanical deformation, developing materials with both high flexibility and mechanical integrity is essential for optimizing performance. To address this challenge, Wu et al. developed a fiber-shaped piezoelectric nanogenerators (PENGs) with a core-shell architecture, using a combination of perovskite precursor and a PVDF–polyethylene oxide (PEO) composite[253]. Among the three components, the perovskite and PVDF enhance piezoelectric performance, while PEO contributes to mechanical flexibility. Perovskite crystals that enhance piezoelectric performance are formed inside the matrix through in situ crystallization. In the subsequent thermal treatment step, β-phase formation in PVDF further improves the piezoelectric properties. Meanwhile, PEO contributes to mechanical durability through its intrinsic material flexibility, allowing the fiber to maintain stable electrical output under structural deformation conditions such as

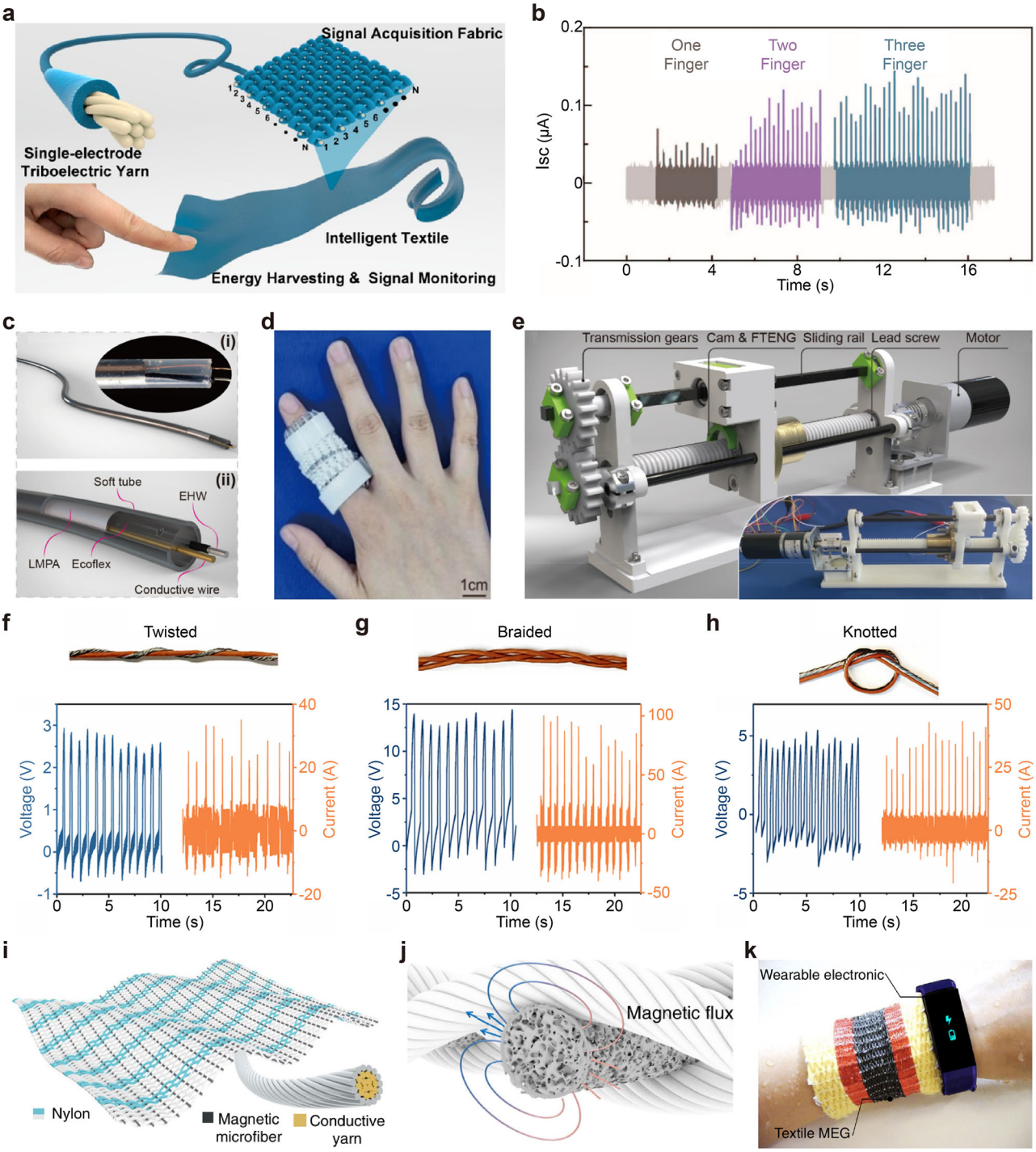

Fig. 10 | Magnetoelectric, triboelectric, and piezoelectric fiber generators. **a** Schematic of triboelectric nanogenerator (TENG) woven with single-electrode triboelectric yarns (SETY). **b** Differentiated signal outputs based on the number of touching fingertips and their contact areas. (I_{sc}: Short circuit current). **a**, **b** Reprinted with permission[263]. Copyright 2020, American Chemical Society. **c** Schematic illustrations showing the structure of the fiber TENG, which is composed of a soft tube, low-melting-point-alloy (LMPA), Ecoflex rubber, conductive wire, and electrically heated wire (EHW) with an insulating layer. **d** TENG on a finger. **e** Schematic and working principle of the TENG for lead screw crack detection. **c**–**e** Reprinted with permission[250]. Copyright 2022, American Chemical Society. **f** a twisted piezoelectric nanogenerator (PENG) yarn in response to finger touching. **g** braided PENG yarns in response to hand pressing. **h** 1 knotted PENG yarn and stainless steel yarn in response to hand pressing. **f**–**h** Reprinted with permission[253]. Copyright 2023, American Chemical Society. **i** Schematic design of the textile magnetoelastic generator (MEG). **j** schematic of the working mechanism of the textile MEG. **k** Schematic of the textile MEG mixed with wool fibers driving a wearable electronic. **i**–**k** Reprinted with permission[264]. Copyright 2021, Springer Nature.

twisting, knotting, and braiding (Fig. 10f–h). Under a vertical pressure of approximately 3.1 kPa, the device achieved a maximum power density of 281 μW/cm^3 and an average power density of 10.6 μW/cm^3. These results indicate both high output performance and operational stability, demonstrating the device's potential as a fiber-based piezoelectric energy harvester for practical applications.

A porous and flexible magnetic fiber was introduced by Zhao et al. through extrusion of a silicone matrix containing uniformly distributed

Table 7 | Comparison of various parameters for fiber-based energy generators

No.	Energy conversion mechanism	Power density	Output voltage	Durability (cycles)	Flexibility
1[263]	Triboelectric	336.2 μW/m	40.8 V	-	0–40% (Strain)
2[250]	Triboelectric	348.5 μW/m	~50 V	28,800	-
3[253]	Piezoelectric	281.0 μW/cm^3	~7.4 V	19,200	0–2 /cm (curvature)
4[264]	Magnetoelastic	6.67 W/m^2	~2.3 V	20,000	0–180% (Strain)
5[268]	Thermoelectric	70 mW/m^2	~3 V	-	0–91° (Bending)
6[344]	Thermoelectric	40 mW/cm^2	~5 V	-	434% (Strain)
7[271]	Photovoltaic	7.63 mW/cm^2	~4.4 V	1000	∞ ~ 1.6 mm (Bending radius)

NdFeB nanoparticles (Fig. 10i, j)[264]. The magnetic fiber was woven with Ag-coated nylon fibers into a wearable format, enabling electricity generation from variations in the magnetic field induced by the user's movements. To demonstrate its functional reliability in humid environments, the device stably detected arterial pulse waveforms even in the presence of sweat or water between the skin and the fiber surface. The mechanical deformation induced by the pulse generated magnetic field variations, which were successfully converted into electrical signals, thereby enabling self-powered cardiovascular sensing. Moreover, the device exhibited excellent moisture resistance, maintaining its output performance even after 168 h of continuous water immersion. In addition, the device exhibited a short-circuit current density of 0.63 mA/cm^2 and maintained stable voltage output even when worn in water during swimming. The textile magnetoelastic generator (MEG), woven into a wristband format, demonstrated its applicability in powering electronic devices by successfully driving a wearable electronic device under such humid and dynamic conditions (Fig. 10k).

In actual human motion, human body movements are not limited to single motions but rather appear as complex combinations of multiple dynamic actions[265]. However, most current energy harvesting devices are designed based on principles optimized for specific types of motion and are therefore tailored to achieve high efficiency and selectivity only under constrained or repetitive motion conditions. Although such structures exhibit excellent performance under specific conditions, they may lead to energy loss in practical environments where multiple types of motion occur simultaneously[230,266]. Therefore, the development of energy harvesting systems capable of simultaneously collecting and converting multiple forms of mechanical stimuli is essential. Such parallel-operating platforms enable stable energy harvesting even under complex and unpredictable usage conditions, offering the potential to evolve beyond merely powering low-power sensors toward serving as a reliable power source for a wide range of wearable electronic devices and autonomous smart systems.

Wearable thermoelectric generators (TEGs) require body heat as their energy source, allowing them to be applied to any location on the human body[230,254]. However, since thermoelectric harvesting relies on the temperature difference between the human body and the surrounding environment, its energy conversion efficiency significantly decreases when the temperature difference between the body and the environment is small[143,267]. To address the low energy conversion efficiency of conventional planar thermoelectric devices under limited temperature differentials, Sun et al. developed a three-dimensional fiber-based architecture that enhances both thermal collection and electrical output[268]. Carbon nanotube fibers (CNTFs) were first doped with complementary p-type and n-type materials, PEDOT:PSS and oleamine, respectively, to establish the fundamental p–n thermoelectric junctions required for effective Seebeck generation. These doped fibers were subsequently assembled into a vertically aligned π-loop configuration through an interlocking process (Fig. 11a). This spatial arrangement effectively aligned the thermoelectric legs with the out-of-plane thermal gradient and significantly increased the cross-sectional contact area for heat transfer, thereby improving thermal flux and maximizing the temperature differential across the thermoelectric elements (Fig. 11b). As a result of this structural transformation, the three-dimensional TEG demonstrated a 24-fold increase in output voltage compared to its planar counterpart. In addition, it achieved a peak power density of 70 mW/m^2 and maintained stable operation with less than 3% output degradation under mechanical deformation, confirming both its electrical robustness and mechanical durability in wearable applications.

In addition to weaving-based architectures, recent approaches to enhancing thermoelectric performance have focused on structural modifications within single fibers. A stretchable and porous thermoelectric fiber featuring a three-dimensional interconnected porous network was developed by Li et al (Fig. 11c)[236]. to improve power generation efficiency, utilizing a conductive polymer matrix composed of Ti_3C_2Tx MXene and polyurethane (PU). To maintain a stable temperature gradient and enhance power generation efficiency, a porous architecture with abundant internal air gaps was introduced, resulting in a reduced thermal conductivity of 0.19 W/mK. This structure was fabricated by first preparing a uniformly dispersed ink composed of Ti_3C_2Tx MXene nanoflakes and a PU solution, followed by wet spinning and subsequent drying. A textile thermoelectric generator composed of 24 the thermoelectric fibers connected in series generated an output voltage of approximately 3.6 mV under a typical skin temperature of ~32 °C and air temperature of ~24 °C (Fig. 11d, e). This voltage is sufficient to enable self-powered operation of low-power wearable electronic devices. This fiber-level structural design not only reduces unwanted heat loss commonly observed in densely packed thermoelectric fibers but also takes advantage of the porous network to reduce material weight-both of which are critical for wearable energy harvesting applications.

Energy harvesting devices utilizing the photovoltaic effect have also drawn considerable attention for powering wearable electronics. Photovoltaic systems are particularly advantageous in sunlight-rich environments during the daytime, where they can provide high power output and thus serve as an effective complementary energy source to thermoelectric devices that rely on ambient thermal gradients. However, despite these advantages, the application of photovoltaic technologies in fiber-based platforms remains limited. This limitation arises primarily from the inherently curved geometry of fiber structures, where the cylindrical surface restricts the optimization of light-harvesting area compared to planar configurations[269,270]. To address this limitation, Song et al. developed a fiber-based dye-sensitized solar cell (FDSSC) with enhanced light-harvesting efficiency by integrating a light diffusion layer and a light conversion layer (Fig. 11f, g)[271]. The two layers, designed to enhance light-harvesting efficiency, serve two distinct yet complementary optical functions. First, the light diffusion layer, composed of PU embedded with Al_2O_3 microparticles, scatters incident sunlight omnidirectionally. This scattering mechanism redistributes light uniformly across the entire surface of the cylindrical fiber, regardless of the angle of incidence, thereby enhancing the interaction between light and the photoanode. Second, the light conversion layer, consisting of phosphor-dispersed PVDF-HFP, addresses the spectral mismatch between the solar spectrum and the dye's absorption characteristics. Although incident sunlight spans a broad wavelength range, from ultraviolet (UV) to near-infrared (NIR), the N719 dye used in this study exhibits peak photoresponsivity in the visible range. To better align with this absorption window, the conversion layer incorporates two types of phosphors that down-convert UV photons and up-

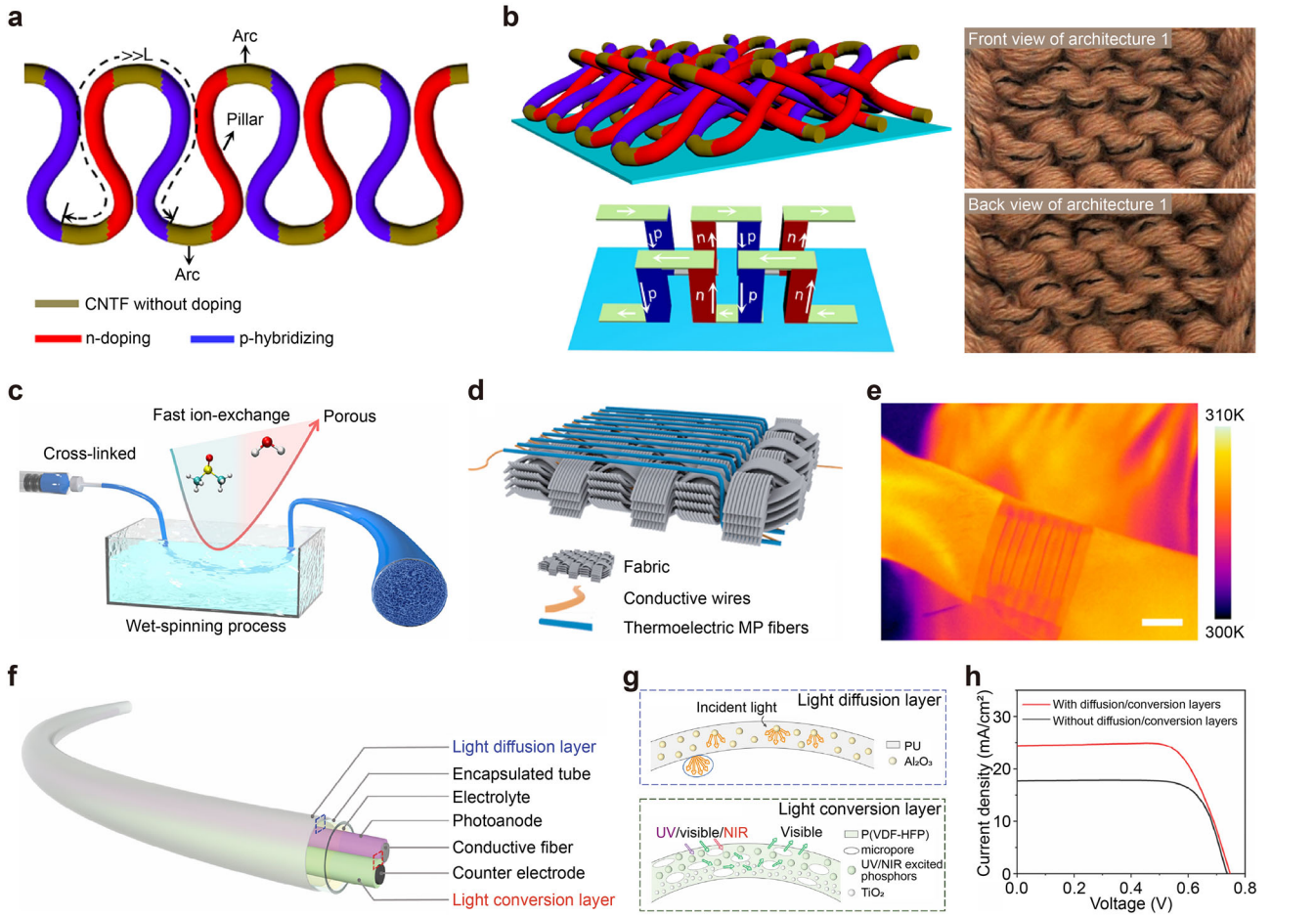

Fig. 11 | Thermoelectric fibers for heat energy conversion. a n-p type doped triboelectric loops. **b** 3D architecture with triboelectric loops. **a**, **b** Reprinted with permission[268]. Copyright 2020, Springer Nature. **c** Schematic diagram of the preparation process for a porous fiber. **d** Illustration for construction of wearable thermoelectric fabric. (MP: Mxene-polyurethane) **e** infrared image of the thermoelectric fabric on a wrist. **c**–**e** Reprinted with permission[344]. Copyright 2023, American Chemical Society. **f** Configuration of fiber-dye-sensitized solar cell (FDSSC) and inner structure. **g** Illustration of working mechanism in a diffusion layer (top) and a conversion layer (bottom). (P(VDF-HFP): poly(vinylidene fluoride-co-hexafluoropropylene)) **h** Comparison of electrical performance with and without the two-layer structure. J–V curves of FDSSCs show that the power conversion efficiency increased from 9.84% to 13.11% with the introduction of diffusion/conversion layers. **f**–**h** Reprinted with permission[271]. Copyright 2024, WILEY-VCH Verlag GmbH & Co. KgaA, Weinheim.

convert NIR photons into visible light. These converted photons are subsequently reflected back toward the photoanode, enhancing the effective photon absorption and thereby improving the overall photovoltaic performance. As a result, the proposed FDSSC exhibited a 33% enhancement in power conversion efficiency compared to the control device lacking the optical management layers (Fig. 11h). The dual-layer structure broadens spectral utilization, which leads to the observed improvement. Notably, the device achieved a short-circuit current density J_{SC} of 24.43 mA/cm^2, validating its superior light-harvesting capability and overall photovoltaic performance.

Such energy harvesting systems remain inherently limited by fluctuations in the surrounding environment, such as changes in absorbance of light and temperature, making it difficult for them to serve as fully independent power platforms. To address this limitation, hybrid approaches that incorporate energy harvesting modalities less affected by environmental variability may offer a viable solution. For instance, integrating triboelectric nanogenerator (TENG) or piezoelectric nanogenerator (PENG) could enable the construction of complementary power systems, where the strengths of each mechanism compensate for the limitation of the others.

Energy storage devices

A wide range of research has been actively conducted to maximize the energy conversion efficiency of fiber-based energy harvesting devices. To improve device performance, recent efforts have focused on incorporating advanced materials and applying microscale structural engineering techniques. However, without parallel advancements in energy storage technologies, the energy generated from such devices cannot be retained or utilized effectively. The absence of a reliable storage system limits the continuous and autonomous operation of wearable electronics, rendering even highly efficient energy harvesters functionally inadequate at the system level[272,273]. As a result, increasing attention has been directed toward the development of highly stable, fiber-shaped batteries that can be seamlessly integrated with textile-based energy harvesting platforms. In particular, various strategies have been proposed to improve the cycle life of lithium-ion fiber batteries, which offer high energy density[274,275]. These include precision packaging techniques employing ultrahigh-barrier polymeric tubing to minimize environmental degradation[276,277], as well as interfacial stabilization of gel electrolytes using aligned internal channel structures[278–280]. In parallel, alternative systems are being actively investigated to address the flammability concerns associated with organic electrolytes[281,282]. These efforts include the development of aqueous zinc-ion batteries and gel polymer electrolyte-based configurations, both of which offer enhanced safety for wearable applications.

To address this challenge, Gong et al. incorporated a high-barrier encapsulation layer into a fiber-shaped lithium-ion battery to mitigate moisture-induced degradation and enhance long-term operational stability

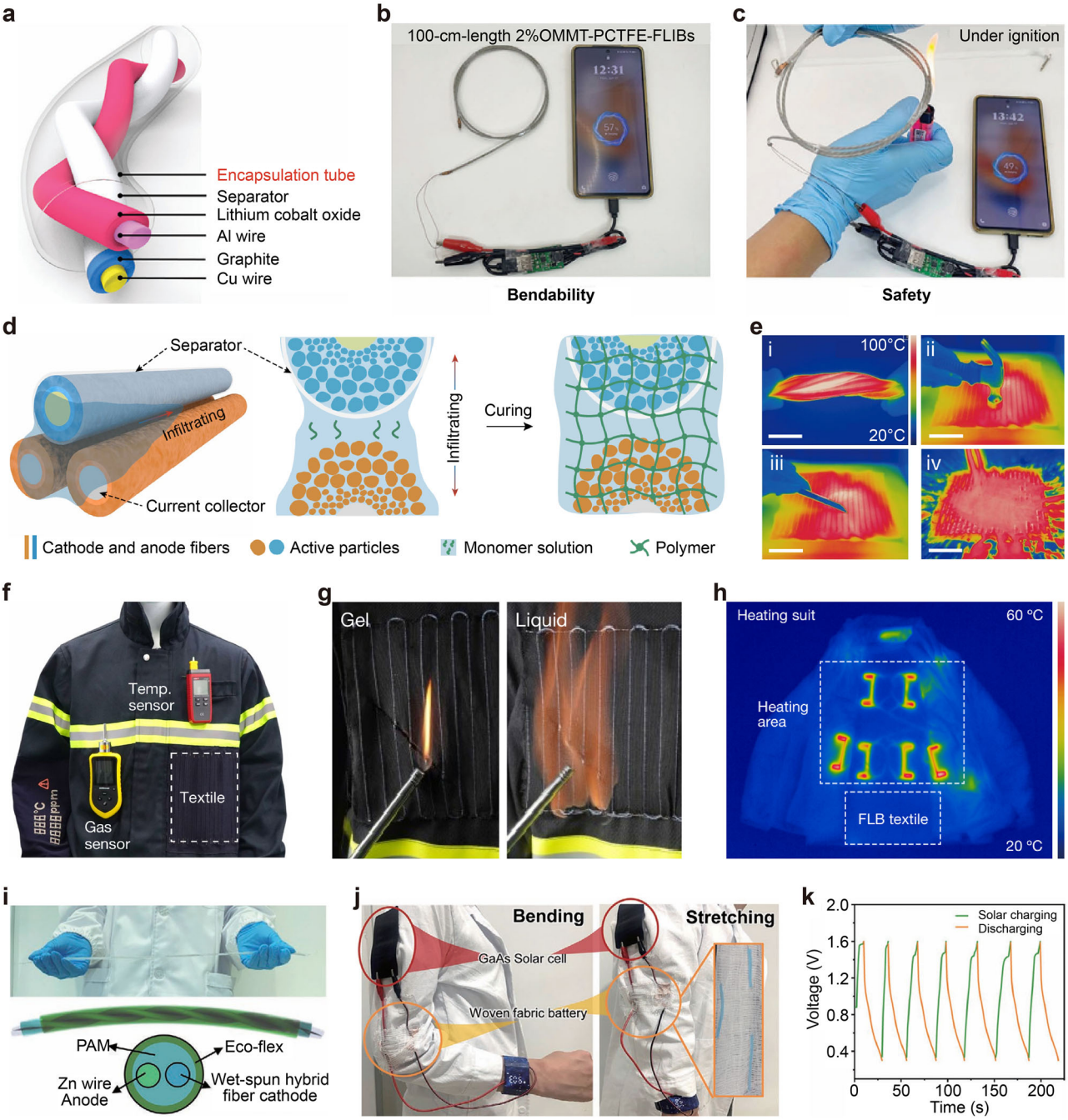

Fig. 12 | Energy storage devices. a Structure schematic of lithium ion battery with a high density tube encapsulation. **b** Photograph of stable energy supply under bending situation. (OMMT: Organically modified montmorillonite; PCTFE: Polytrifluorochloroethylene; FLIBs: Fiber lithium-ion batteries) **c** Photograph of stable energy supply when exposed to ignition. **a**–**c** Reprinted with permission[276]. Copyright 2024, WILEY-VCH Verlag GmbH & Co. KgaA, Weinheim. **d** Schematic of gel electrolyte formation process. **e** Infrared thermal images for the fiber lithium-ion battery (FLB) discharging under various harsh conditions. **f** Photograph of a multifunctional fire fighter suit with a gel type lithium battery. **g** Photographs of ignition of textiles with gel and liquid electrolyte. **h** Infrared thermal imaging of the FLB textile supplying power for the heating suit. **d**–**h** Reprinted with permission[278]. Copyright 2024, Springer Nature. **i** Photograph of a Zinc based fiber battery. (PAM: Polyacrylamide). **j** Integration of the Zinc battery into a self-powered wearable system. **k** Cycling profiles of solar charging and discharging for the integrated system at a current density of 1 A/g. **i**–**k** Reprinted with permission[283]. Copyright 2022, WILEY-VCH Verlag GmbH & Co. KgaA, Weinheim.

(Fig. 12a)[276]. While conventional fiber battery casings composed of tetrafluoroethylene-hexafluoropropylene (FEP) and perfluoroalkoxy (PFA) copolymers exhibit relatively high water vapor permeability, this work utilized polytrifluorochloroethylene (PCTFE), whose barrier performance is mainly attributed to its higher crystallinity, fewer free volume pores, and smaller pore size. The PCTFE tubes were fabricated via melt extrusion, enabling continuous production of moisture-resistant encapsulation layers. Furthermore, by incorporating 2 wt% of organically modified montmorillonite (OMMT) into the PCTFE matrix, the authors extended the water vapor diffusion path and reduced the internal free volume of the polymer, resulting in a significantly reduced water vapor transmission rate of approximately 0.006 mg/day·pkg. Compared to batteries encapsulated with conventional FEP or PFA tubes, which retained 80% of their initial capacitance after 27 days, the PCTFE/OMMT composite tubes enabled the device to maintain over 80% of its capacitance even after 200 days of ambient storage, and supported up to 870 charge-discharge cycles (Table 8).

Table 8 | Comparison of functional metrics in energy storage devices

No.	Storage mechanism	Energy density	Power density	Cycle life (cycles)	Charging rate/discharging rate	Stability
1[276]	Electrochemical	-	-	870	0.3 C/0.5 C	Good
2[278]	Electrochemical	128 Wh/kg	1.48 mW/cm^2	1000	0.2 C/0.1–0.5 C	Excellent
3[283]	Electrochemical	53.8 mWh/cm^3	100 mW/cm^2	150	-	Excellent

The fiber-shaped battery employing this composite encapsulation tube retained 85.31% of its capacity even after 10,000 repeated bending cycles, demonstrating excellent mechanical durability (Fig. 12b). Remarkably, it also maintained stable power output even under direct ignition exposure (Fig. 12c). While such an insulating layer offers a straightforward fabrication approach for physical protection, recent efforts have also focused on replacing flammable organic liquid electrolytes with solid or gel-state alternatives to enhance system-level safety while preserving the high energy density of lithium-based chemistries.

To address interfacial instability, one of the primary challenges to ensuring the reliability and safety of fiber-shaped lithium-ion batteries, Lu et al. introduced a dual-channel electrode structure composed of internal network channels and inter-fiber alignment channels[278]. This architecture was designed to mitigate performance degradation commonly observed in gel electrolyte systems. The aligned channel network enables rapid infiltration of low-viscosity monomer solutions into the electrode matrix, and subsequent in situ polymerization forms a polymer gel electrolyte with significantly improved electrode–electrolyte interfacial adhesion and uniform gel distribution (Fig. 12d). The developed fiber lithium-ion battery (FLB) demonstrated an energy density of approximately 128 Wh/kg and a specific capacity near 170 mAh/g, along with excellent flexibility. Even after 100,000 cycles of repeated mechanical deformations, including bending, twisting, and stretching, the resistance variation remained below 10%, confirming high mechanical durability. Moreover, the FLB retained 87.7% of its capacity and achieved 99.6% Coulombic efficiency after 1000 charge-discharge cycles, validating its long-term electrochemical stability under operational stress. The fiber-shaped battery exhibited exceptional environmental and mechanical durability, maintaining stable operation even under boiling water splash conditions, repeated knife scratching, and hammer impact (Fig. 12e). To demonstrate the practical utility of the FLB in harsh environments, the device was integrated into a multifunctional firefighting suit equipped with various electronic modules. While the textile battery using liquid electrolyte caught fire during ignition testing, the FLB with the gel electrolyte exhibited no ignition, even under direct flame exposure (Fig. 12f, g). Furthermore, the FLB successfully powered a heating suit, elevating its temperature to ~80 °C (Fig. 12h). These results validate the FLB's capability to safely operate under extreme thermal and mechanical stresses, offering great potential for powering high-output wearable electronics such as smart garments, fire-protective clothing, space suits, and bionic systems.

Zinc-based aqueous batteries have recently gained significant attention as a more stable alternative to lithium-based systems, particularly for wearable and fiber-shaped electronics where mechanical stability and environmental tolerance are critical. Zhou et al. developed a fiber-shaped Zn-ion battery system that maintains the intrinsic safety of aqueous electrolytes while substantially improving energy density, mechanical flexibility, and integration capability[283]. By combining high-capacity vanadium pentoxide (V_2O_5) nanowires with mechanically and electrically robust reduced graphene oxide (rGO), the team fabricated highly aligned hybrid fibers via rheologically engineered wet-spinning. These hybrid fibers were used as cathodes, paired with a zinc wire anode, and the full battery was assembled using a polyacrylamide (PAM)-based $ZnSO_4$ gel electrolyte (Fig. 12i). To ensure environmental robustness and mechanical resilience, the entire device was encapsulated in a soft, biocompatible Ecoflex matrix. The resulting fiber battery achieved a high volumetric energy density of 492.17 mAh/cm^3 and an electrical conductivity of 448 S/cm, while maintaining 88.37% of its capacity after 1500 charge–discharge cycles. To demonstrate its practical viability, the battery was integrated with a GaAs-based solar cell and used to form a closed-loop charging system. Under 180 min of light exposure, the system successfully stored 5.28 mAh of charge, corresponding to a solar-to-storage energy conversion efficiency of 9.80%, thus validating its applicability for self-powered wearable electronics (Fig. 12j, k).

To enable the practical implementation of fiber-based energy systems, high-performance energy harvesting technologies have been advanced in parallel with the development of fiber-based batteries designed to provide robust energy storage stability and long-term reliability across a range of environmental conditions. Recent studies have significantly advanced the stability and performance of fiber-based batteries through innovations in electrolyte packaging, the development of novel electrolyte materials, and the engineering of cathode, anode, and separator components. Advancements in battery technology are paving the way for energy-autonomous fiber-based smart systems, enabling their deployment as versatile power platforms in applications.

FEDs with active functionalities

FEDs with active functionalities are increasingly utilized across diverse fields, offering both sensing functionality and the ability to provide signal outputs and control physical motion. Electroluminescent fiber technologies offer new opportunities in wearable displays and electronic garments, and show potential in industrial signaling, visualization of robotic interfaces, safety alert systems, and creative fields such as art and performance[284,285]. In addition, fiber-based actuators, utilizing materials such as shape memory alloys (SMAs), shape memory polymers (SMPs), and stimuli-responsive polymers (e.g., thermo-, photo-, pH-, and magneto-), are attracting attention as promising alternative components in wearable robotic systems and rescue robots. In particular, fiber-type soft actuators with high flexibility and low weight are considered emerging candidates for applications such as prosthetics and artificial muscles[286,287]. Furthermore, fiber-based electrical stimulation technologies are being explored for rehabilitation and chronic disease management and have also been applied to the development of soft neural prosthetic systems. These devices can provide localized, controllable, and consistent stimulation to neural and muscular tissues, contributing to improved therapeutic outcomes and patient quality of life. They are also expected to play a role in the advancement of robot-assisted medical technologies[288–290]. However, FEDs with active functionalities still face challenges related to reliability, long-term durability, and output accuracy. In response to these challenges, extensive efforts are being made to develop new materials, optimize device structures, and improve control systems. In the future, these devices are expected to evolve into smart systems that enable closer interaction between humans and machines.

Fiber-based display systems

Light-emitting fibers for display are advanced optoelectronic components developed to extend conventional planar display technologies into flexible and stretchable fiber platforms. These light-emitting fibers have been developed by applying electroluminescent materials, organic light-emitting diodes (OLEDs)[291–294], or electrochromic materials[295–297], enabling the provision of visual information while preserving the inherent lightness and flexibility of textiles. Unlike conventional LED or OLED panels that are built on rigid substrates and are prone to mechanical failure or deformation under motion, fiber-type light-emitting devices are fabricated by coating emissive materials onto the fiber surface or embedding them inside the fiber structure,

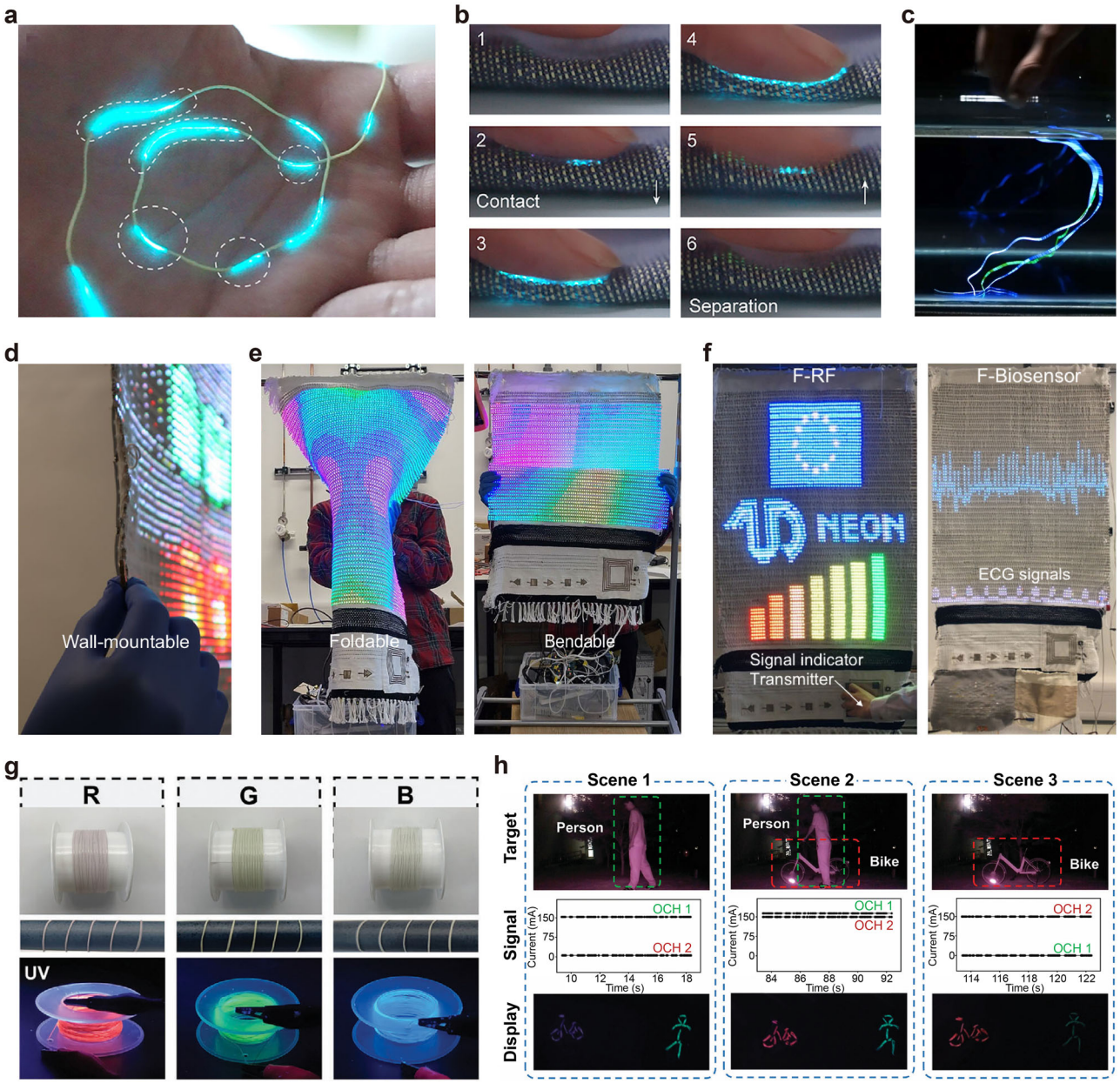

Fig. 13 | Fiber-based display systems. a Wireless visual sensing fibers (WISE) fiber placed on the hand enables multi-node visual touch sensing. Transmitter parameter (30 dBm, 20 kHz, 5 cm). **b** Digital images of ambient electromagnetic energy driving WISE fiber visual touch sensing. **c** Photographic image showing WISE fibers that capture electromagnetic energy and emit light underwater. **a**–**c** Reprinted with permission[298]. Copyright 2024, Elsevier Inc. **d** A photograph showing the side view of a textile display system. **e** Mechanical stability of the textile display system under folding and bending conditions. **f** A textile-based display system capable of receiving various input signals and providing real-time visual feedback. (F-RF: Fiber-radio frequency antenna; F-Biosensor: Fiber-biosensor) **d**–**f** Reprinted with permission[299]. Copyright 2021, Springer Nature. **g** Optical and fluorescent photographs of the prepared RGB fibers. **h** Real-time displaying of two dynamic target objects of a person and bike to smart textile. (OCH: Optical channel) **g**, **h** Reprinted with permission[300]. Copyright 2025, WILEY-VCH Verlag GmbH & Co. KgaA, Weinheim.

allowing stable light emission under bending and stretching conditions. These technologies have demonstrated potential in applications such as smart garments, wearable displays, activity and health data visualization in sportswear, safety indication for industrial workers, and interactive or performance costumes that provide real-time visual interfaces.

Recent studies have further advanced the functionality of such fiber displays. Yang et al. proposed a wireless visual sensing electronic (WISE) fiber that can operate without external circuits or power sources, suggesting new possibilities for wireless fiber-based display systems (Fig. 13a)[298]. This system utilizes ambient electromagnetic energy coupled via the dielectric properties of human body to activate the internal electroluminescent layer of the fiber. The core emission mechanism is based on ZnS:Cu^{2+} electroluminescence, where electrons trapped in defect states are excited to the conduction band under an electric field and subsequently return to the ground state, emitting light in the 400–550 nm visible range (Table 9). Moreover, the WISE fiber adopts a single-electrode configuration, offering a simpler structure compared to conventional dual-electrode electroluminescent fibers, and enables a sensitive response to changes in surface impedance caused by moisture, touch, or polar liquids (Fig. 13b, c). The fiber is fabricated through a layer-by-layer dip-coating process to form the core electrode, dielectric layer, and emission layer, resulting in a monofilament

Table 9 | Performance comparison table of fiber-based display systems

No.	Operating mechanism	Luminance	Driving voltage	Display resolution	Flexibility	Lifetime
1[298]	Electroluminescent	250 cd/m^2	-	-	0–360° (Twisting)	5000 @touch
2[299]	Electromagnetic	1000 ± 10 cd/m^2	3 V	5 mm @120 × 65 pixels	∞ ~ 10 mm (Bending radius)	Over a year
3[300]	Electro-thermochromic	-	-	-	-	50cycles @Switching

fiber with ~350 μm diameter and ~75 μm emission layer thickness. In addition, its compatibility with modern rapier looms also supports scalable textile integration while maintaining emission functionality. This system eliminates the need for wired connections or external power, enabling simplified architectures and supporting multiple sensing nodes within a single fiber. The main advantage of this technology is that it eliminates the need for a power supply or external circuits, minimizing the complexity of the device system. It also enables multi-node visual sensing within a single fiber, allowing real-time interfaces without complex electronics. Furthermore, its structural flexibility makes it suitable for wearable or on-skin interfaces, providing intuitive visual feedback. However, challenges remain, including stability under fluctuating electromagnetic environments, sensitivity variations due to surface contamination or humidity, and reduced brightness in low-coupling conditions. Future work is needed to improve optimize electromagnetic coupling and enhance interface stability for practical deployment.

Choi et al. demonstrated a textile-based full-color display system with multifunctionality and large-area scalability (Fig. 13d–f)[299]. This system includes various components, including RGB LEDs, radio frequency antennas, touch sensors, photodetectors, temperature sensors, biosensor modules, and energy storage units, and is realized as a multifunctional display system integrated into a fabric-based platform. One notable feature is its Lego-like modularity, where each device can be independently embedded, replaced, or upgraded. This design extends beyond simple display applications to support real-time signal visualization, health and environmental monitoring, and IoT-based control. For instance, biosensor modules can amplify and display electrocardiogram (ECG) signals, and capacitive touch sensing enables user interaction. However, this system still faces several technical limitations. The implementation of a full-color textile display consumes up to 35 W of power during operation. This suggests that low-power integration strategies and energy-efficient circuit architectures are required for practical applications. Signal interference between devices within the woven network is another issue. Therefore, high-energy-density power sources, signal integration algorithms, and electromagnetic shielding structures should be considered to address this challenge. This work is regarded as a representative example of multimodal sensing-display integration, demonstrating feasibility for large-area smart home displays, wearable interfaces, and next-generation e-textile platforms.

Another example of the fiber-based display system is the self-adaptive intelligent textile display system using electro-thermochromic fluorescent fibers[300]. This platform combines real-time target recognition via a deep convolutional neural network (DCNN) with corresponding visual output using thermally triggered emissive fibers. The fibers, fabricated via coaxial wet spinning, have a core-shell structure with a conductive core for heating and an outer hydrogel shell incorporating thermo-responsive fluorophores. At ambient temperature, the fluorophores remain aggregated in a non-emissive solid state. Upon Joule heating, the core raises the local temperature, causing a phase transition to an amorphous liquid, triggering light emission based on aggregation-induced emission. When the fiber cools, recrystallization suppresses emission. In addition, Förster resonance energy transfer (FRET) mechanisms enable multicolor emission by modulating the distance between the energy donor and acceptor depending on the temperature (Fig. 13g). Based on these mechanisms, light-emitting fibers exhibit fast response (≤1 s), flexible color modulation, and high mechanical flexibility. In the final demonstration, the light-emitting fiber was linked with a DCNN-based image recognition system, which detected external targets such as a person or bicycle in front of the user, and visualized the results in real time on the fiber-based textile display (Fig. 13h). This work represents a step forward in interactive visual interfaces, laying the foundation for applications such as emotion-aware clothing, AI-integrated wearable displays, and next-generation smart textiles.

As these examples show, fiber-based displays are evolving beyond light emission to become integrated platforms incorporating sensors, power sources, and feedback systems. Key factors for future development include improving emission efficiency, reducing driving voltage, and enhancing stretchability and durability under repeated mechanical deformation. The ultimate goal is to realize fully autonomous fiber-based display systems that operate without external power sources by integrating fiber-based energy storage and driving circuits. These advancements are expected to broaden the applications of fiber-based displays in wearable electronics, smart garments, and biocompatible interfaces.

Fiber-based actuators

Unlike conventional rigid actuators, their inherent flexibility and lightweight nature make them promise for use in bioinspired robots, wearable systems, and artificial muscle applications[301,302]. These fiber-type soft actuators are categorized according to their driven source, including light-[303–305], magnetic-[306,307], electric-[308–310], and thermal-driven mechanisms[311–313]. Light-responsive fiber actuators offer advantages such as remote control and fast response, but their applicability is limited in biological tissues or opaque environments due to light penetration constraints, and issues such as material degradation and energy inefficiency under continuous illumination must be addressed. Magnetically driven fiber actuators also enable contactless control and fast response as well as complex motions. However, the need for external magnetic field generators increases the system complexity. In contrast, electrostatic- and thermal-driven actuators provide relatively simple system integration. This section introduces various fiber-based actuators driven by different mechanisms.

In the first study, a self-recoverable coiled artificial muscle fiber was developed using an elastic carbon nanotube (CNT) core and a thin liquid crystal elastomer (LCE) sheath to enhance recovery performance[314]. The electrothermal-driven fiber-type actuator operates through reversible switching between nematic and isotropic phases, triggered by Joule heating (Fig. 14a). It achieves a maximum contractile stroke of 56.9%, power density of 7.03 kW/kg, contraction rate of 1522%/s, and over 32,000 stable actuation cycles, with full shape recovery even under zero shear stress (Table 10). The LCE is synthesized via thiol-Michael addition, coated on CNT fibers, crosslinked under UV irradiation, and twisted precisely to form a coiled structure. This process allows continuous production of fibers over tens of meters, making it suitable for scalable manufacturing. In addition to actuation performance, isometric stress testing revealed a peak stress of 17.7 MPa (119.6 mN), over 50 times higher than that of human skeletal muscle (~0.35 MPa). Based on its outstanding mechanical properties, demonstrations include multi-directional bending of endoscopic medical robot arms and antagonistic joint motion using biceps-triceps interaction in bionic arms (Fig. 14b). Finally, the ability of the fiber-based actuators to maintain deformation under low power suggests strong potential for medical and wearable robotics.

Another study introduced a proprioceptive twisted and coiled fiber actuator (TCFA) capable of simultaneous actuation and sensing (Fig. 14c)[315]. Although the developed TCFA demonstrated a relatively modest contraction ratio (~36%), stress output (up to 450 kPa), and strain rate (6.6%/s), it operated stably at a low temperature of 83 °C, enabling continuous

Fig. 14 | Fiber-based actuators. a Actuation modes and mechanisms of the coiled artificial muscle, driven by electrothermal energy. (RM 82: 1,4-Bis-[4-(6-acryloyloxyhexyloxy) benzoyloxy]-2 methylbenzene; EDDT: 2,2′-(ethylenedioxy) diethanethiol; PETMP: Pentaerythritol tetrakis (3-mercaptopropionate); CNT: Carbon nanotube) **b** Demonstration of the endoscope-like robot arm and biceps-triceps interaction. This actuator exhibits a 56.9% strain at 14 V. **a**, **b** Reprinted with permission[314]. Copyright 2023, American Chemical Society. **c** Photographic image of the artificial arm system upon adding the payload from 0.3 to 0.4 N. Twisted and coiled polymer actuator (TCA) is driven electrothermally and achieves 35% contraction with a low power input of only 0.2 W/cm. Reprinted with permission[315]. Copyright 2024, WILEY-VCH Verlag GmbH & Co. KgaA, Weinheim. **d** Actuating process of the magnet-driven fiber actuators. Reprinted with permission[306]. Copyright 2023, WILEY-VCH Verlag GmbH & Co. KgaA, Weinheim. **e** Snapshots showing the shape change of self-winding fiber actuator (SWFA) from a straight structure to a helically coiled structure upon near infrared (NIR) irradiation. The actuation mechanism is based on the contraction and relaxation of the liquid crystal polymer induced by light. In addition, the SWFA can operate for an extended period without noticeable fatigue, even after 24 h of continuous self-oscillation (1,270,000 cycles). Reprinted with permission[316]. Copyright 2021, Springer Nature. **f** Time-lapse snapshots exhibited the salt accumulation during the desalination process of the original RGO@HHF and **g** double-twisted RGO@HHF. This is attributed to the dual driving responsiveness of the fiber actuator to water and light. (RGO@HHF: Hollow hydrogel fiber loaded with reduced graphene oxide). **f**, **g** Reprinted with permission[317]. Copyright 2023, WILEY-VCH Verlag GmbH & Co. KgaA, Weinheim.

operation without external cooling. The actuator is composed of a polyethylene (PE) core fiber coated with an elastomeric sheath containing silver nanoparticles (AgNPs). Therefore, electrothermal-driven method is induced by Joule heating, while resistance changes in the fiber during operation enable self-sensing of deformation. Specifically, when current is applied into the sheath layer, the AgNP layer generates heat, raising the internal temperature of the fiber. This thermal source causes radial expansion of the twisted and coiled structure, leading to contraction of the whole fiber actuator system. Simultaneously, nonlinear resistance changes allow real-time tracking of deformation levels. Based on this self-sensing capability, a robotic arm with closed-loop control was demonstrated, achieving precise control of bending angles in response to external loads.

Table 10 | Comparison of various parameters for fiber-based actuators

No.	Driven source	Mechanism	Contraction range	Physical output	Power density	Durability (cycles)
1[314]	Electrothermal-driven	Phase/structural transition of materials	~56.9%	2110 J/kg (Work capacity)	7.03 kW/kg	32,000
2[315]	Electrothermal-driven	Phase/structural transition of materials	~35%	650.4 J/kg (Work capacity)	-	100
3[306]	Magnet-driven	Magnetic dipole alignment	~70%	2.5 mm/s (Working velocity)	-	-
4[316]	Light-driven	Asymmetric internal stress	~66%	62 mg (Output force)	5 W/cm^2	1,270,000
5[317]	Water & light dual driven	Volumetric change	~83%	3.8%/s (Contraction rate)	-	-

Lee et al. developed fiber-based soft actuators that can be wirelessly controlled via external magnetic fields (Fig. 14d)[306]. The system features a bimorph structure with a hollow core composed of styrene-ethylene-butylene-styrene (SEBS) and cyclic olefin copolymer elastomer (COCe), allowing asymmetric motion under stress. To assist this asymmetric motion, the hollow core is filled with ferromagnetic composites responsive to magnetic fields. Additionally, these magnet-driven fiber actuators can be continuously fabricated using a thermal drawing process and programmed for various motions through magnetization. Specifically, when exposed to a uniaxial magnetic field, programmed magnetization and structural deformation enable the fiber actuator to perform bending, twisting, and walking motions. This implies the feasibility of multifunctional locomotion without complex electronics or multiple motors, with potential applications in in vivo biomedical drug delivery, manipulation in confined spaces, and targeted therapy systems.

Inspired by the coiling behavior of plant tendrils, another system based on self-winding fiber actuators (SWFAs) utilizing light-driven method was developed to achieve self-oscillating motion under optical stimulation (Fig. 14e)[316]. This system operates without external circuits or controllers, relying on continuous light exposure to induce non-equilibrium dynamics and autonomous oscillation. Optical stimulation is provided by an 808 nm near-infrared laser, with embedded graphene fillers in the polymer matrix facilitating efficient photothermal conversion. Moreover, the SWFA utilizes a bimorph structure, enabling rotational, tilting, and vertical vibration modes of oscillation. This self-sustained motion capability demonstrates potential for various applications in autonomous systems. Further development directions include tuning the response temperature of the polymer matrix, improving photothermal efficiency, and implementing cooperative motion using multiple actuator arrays.

Liu et al. demonstrated a water/light dual-responsive fiber actuator using hollow hydrogel fibers loaded with reduced graphene oxide (rGO@HHF)[317]. This actuator responds dynamically to both humidity and light stimuli, expanding upon moisture absorption and contracting through light-induced water evaporation. This water/light dual-driven fiber actuator is composed of a porous hydrogel made from polyvinyl alcohol (PVA) and poly(acrylic acid) (PAA) with a double-network structure that offers high mechanical strength and elasticity. The hollow structure in the core enhances water diffusion, resulting in faster response times and larger actuation. Furthermore, the rGO component ensures high photothermal conversion efficiency, facilitating localized heating and moisture evaporation upon light exposure. Based on this actuating performance, a self-desalination process, triggered by sunlight-induced repetitive contraction-extension behavior, was implemented. This process is characterized by its ability to continuously prevent salt buildup on the fiber surface. Upon light exposure, water evaporates from the fiber, causing a temporary accumulation of salt on its surface. When the fiber re-elongates and is re-immersed in saline water, the accumulated salt dissolves back into the solution. Through this mechanism, a stable and sustained evaporation-desalination cycle can be maintained. Comparative tests showed that untwisted rGO@HHFs accumulated salt after evaporation, whereas double-twisted fibers did not (Fig. 14f, g). The proposed water/light dual-responsive fiber actuator significantly improves system reliability and reusability, making rGO@HHFs a promising platform for water-harvesting applications.

Current challenges in fiber-based actuators include achieving reliable actuation cycles, high output and precision, and stable operation under extreme conditions. Addressing these issues requires the development of durable materials and advanced system architectures for precise control. Moreover, integrating sensing and actuation functionalities within a single fiber is essential for the development of intelligent and autonomous smart fiber systems.

Therapeutic stimulation

Electrical stimulation is a technique that induces physiological responses such as neural and muscle activation by delivering electrical signals to biological tissues[318,319]. It has been applied in a wide range of medical fields including neuromodulation[320–323], muscle rehabilitation[318,324–327], pain management[328–330], cardiac pacing[331–333], deep brain stimulation[323,334,335], and disease treatment[336–339]. This technology modulates the membrane potential of neural or muscle cells to elicit targeted responses and has proven particularly effective in promoting neural recovery and functional restoration[336,340]. Early devices were primarily rigid metal-based surface electrodes attached to the skin. However, with advances in materials and device design, electrical stimulation systems have evolved into implantable electrodes and high-resolution microelectrode arrays. Despite these improvements, limitations still remain such as insufficient mechanical flexibility, reduced biocompatibility in long-term use, unstable electrode-target interfaces, and the complex surgical procedures for implantable applications.

To overcome these challenges, fiber-based electrodes have emerged as a promising alternative. Their flexible and lightweight fiber structure conforms naturally to the curvature of skin or internal organs, offering improved comfort, long-term stability, and minimal mechanical mismatch. Moreover, fiber electrodes can be integrated into wearable or implantable systems through weaving, embroidery, or suturing, facilitating versatile biomedical applications. These features make fiber-based electrical stimulation a strong candidate for next-generation personalized bioelectronic therapies.

In response to these research trends, a flexible multimodal fiber probe integrating both optical stimulation and neural signal recording within a single fiber has been developed (Fig. 15a)[341]. The fiber incorporates metal electrodes for electrophysiological monitoring and a double-clad optical waveguide for light delivery. In addition, the entire system was fabricated via thermal drawing to enable meter-scale production. Optical stimulation is based on optogenetic techniques, with the waveguide efficiently transmitting 473 nm blue light deep into brain tissue. This light activates neurons expressing light-sensitive proteins such as channelrhodopsin-2 (ChR2). Upon illumination, ChR2 opens ion channels in the cell membrane, allowing cation influx and triggering membrane depolarization, which in turn induces neural activation. Based on this mechanism, the fiber-based stimulator enables high-resolution and highly selective optical stimulation of genetically targeted neurons, in contrast to conventional non-specific electrical stimulation. The recorded neural signals exhibited a signal-to-noise ratio (SNR) of 30 dB and stable long-term performance for over 10 weeks, indicating superior biocompatibility and signal stability compared to traditional rigid probes (Fig. 15b).

Another study reported the development of a multifunctional fiber integrating optical stimulation, microfluidic drug delivery,

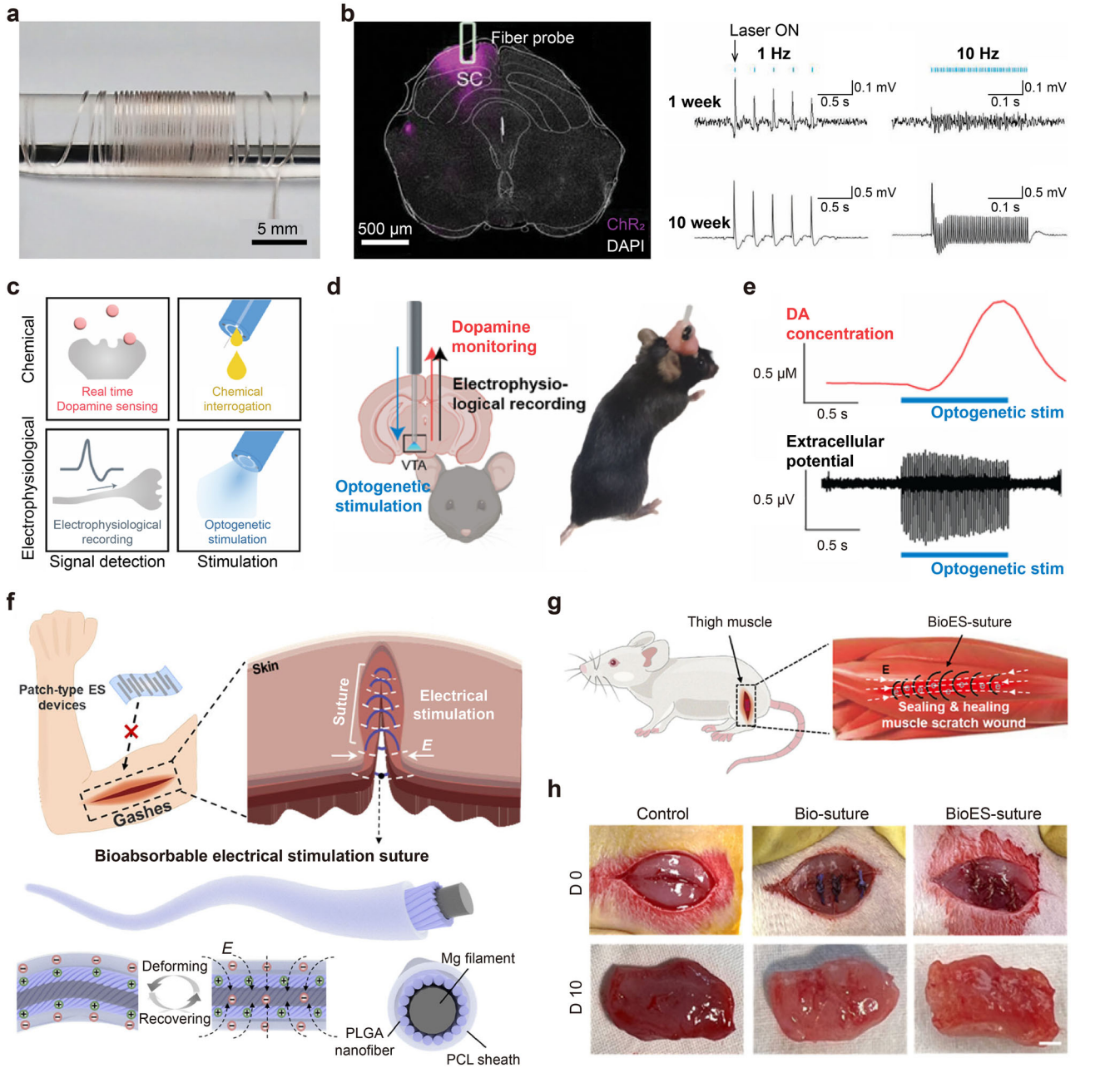

Fig. 15 | Therapeutic stimulation. a Photographic image of the drawn multimodal fiber probe wrapped around a PC rod. **b** Confocal image of a coronal section across the superior colliculus (SC) three weeks after viral transfection, and electrophysiological recording period from 1 to 10 weeks post-implantation. (ChR2: Channelrhodopsin-2; DAPI: 4',6-diamidino-2-phenylindole) **a**, **b** Reprinted with permission[341]. Copyright 2020, WILEY-VCH Verlag GmbH & Co. KgaA, Weinheim. **c** Photographic images of chemical delivery and optical delivery through the multifunctional fiber for synaptic probing. **d** Schematic illustration of the implantation of the multifunctional fiber for synaptic probing and real image of a mouse implanted with a synaptic probing fiber. (VTA: Ventral tegmental area) **e** Representative dopamine (DA) signals (top) and extracellular potential signals (bottom) under optogenetic stimulations (50 Hz, 50 pulses, 4 ms pulse width, 63.6 mW/mm^2 optical power). Phasic dopamine release correlated with laser pulses was observed. **c**–**e** Reprinted with permission[342]. Copyright 2024, American Chemical Society. **f** The tissue recovery process with bioabsorbable electrical stimulation (ES) suture and structure of the bioabsorbable electrical stimulation suture. (PLGA: Poly(lactic-co-glycolic acid; PCL: Polycaprolactone). **g** Schematic illustration showing a mouse model sutured with the bioabsorbable electrical stimulation suture. **h** Optical images of wound areas after 10 days of recovery in each group. The control group muscles appeared abnormally blood-red, indicative of severe tissue infection. **f**–**h** Reprinted with permission[343]. Copyright 2024, Springer Nature.

electrophysiological recording, and neurotransmitter sensing in a single fiber platform (Fig. 15c)[342]. Concretely, optical stimulation enables neuron activation via a waveguide delivering light deep into the brain (Table 11). The microfluidic channel allows localized delivery of chemical agents for neuromodulation. Neurotransmitter sensing is achieved through fast-scan cyclic voltammetry (FSCV), which permits real-time detection of signaling molecules such as dopamine with high temporal resolution. This multimodal platform expands the range of physiological interactions that can be investigated compared to previous systems, enabling detailed analysis at the synaptic level. On the basis of these features, the multifunctional fiber probe successfully demonstrated in vivo frequency-dependent dopamine release induced by optical stimulation, pharmacologically responsive dopamine sensing, and precise recording of spontaneous neural signals (Fig. 15d, e). These results verify the strong potential of the multifunctional fiber

Table 11 | Performance comparison of fiber-based stimulators

No.	Stimulation waveform	Impedance @ 1 kHz	Stimulation condition			
			Amplitude	Pulse width	Frequency	Duration
1[341]	Pulse	22.71 MΩ·μm^2	2.2 mV (Voltage)	5 ms	1–20 Hz	10 min
2[342]	Pulse	126.9 kΩ	63.6 mW/mm^2 (Optical power)	4 ms	10–50 Hz	1 s
3[343]	Custom wave	-	100 mV/mm (Electric field)	-	-	1 h

probe for applications in neural circuit mapping, drug response monitoring, and precise neuromodulation. Future work will focus on the development of wireless optoelectronic interfaces for power-free operation is a critical direction for achieving fully autonomous implantable neural platforms.

In contrast to the fiber systems described earlier, which integrate multiple components into a single fiber, Fig. 15f illustrates a device in which a single component simultaneously performs two distinct functions[343]. This device serves both as an electrical stimulator and a surgical suture, promoting wound healing by providing physical closure of ruptured tissues while delivering electrical signals. This dual functionality enables direct fixation at the target site without the need for additional securing mechanisms, simplifying implantation compared to conventional electrode systems. Additionally, the direct suture-based fixation also enhances stimulation accuracy and minimizes contact impedance between electrode and tissue, maintaining the stimulation efficiency. The electrical stimulation mechanism is based on a triboelectric effect generated by friction between two biodegradable polymer interfaces. The device features a multilayer core-shell structure composed of polycaprolactone (PCL) and poly(lactic-co-glycolic acid) (PLGA), with a magnesium (Mg) filament embedded as a conductive pathway. Therefore, following charge generation through friction, an electric field is induced by electrostatic induction, enabling stimulation of surrounding tissues. Consequently, as this self-powered system is driven solely by biomechanical movements such as muscle contractions, it requires no external circuitry or power supply (Fig. 15g, h). However, since stimulation was triggered randomly by spontaneous mouse movements, further quantification is needed to assess the therapeutic efficacy. A key advantage of this stimulator is its complete biodegradability, which eliminates concerns related to long-term foreign body presence and the need for surgical removal. This makes it particularly suitable for short-term electrical therapies following surgery or in cases where re-implantation is undesirable.

Recent efforts are exploring the integration of fiber-based electrical stimulation systems with neuroprosthetic and AI-assisted feedback control. These systems not only allow for personalized therapy but also offer high clinical applicability by providing closed-loop control over stimulation intensity, frequency, and timing. Future challenges include expanding adaptability to other physiological systems such as cardiovascular and endocrine networks, developing multimodal stimulation, ensuring long-term biocompatibility and immune evasion, and refining fiber electrode design for high-resolution stimulation and recording.

Conclusion and perspectives

This Review discusses recent progress and advancement directions in fiber-based electronic devices, with a particular focus on fiber-based sensing technologies, energy harvesting and storage, and active electronic components. Although these components have largely evolved in parallel, their true potential is unlocked through seamless integration into cohesive, multifunctional systems. For example, continuous and reliable sensing capability necessitates a stable energy supply, with the importance of high-performance fiber-based energy storage modules. To further reduce reliance on external power sources and enhance operational longevity, the incorporation of fiber-compatible energy harvesters capable of transducing biomechanical or environmental stimuli into electrical energy is essential. Beyond energy management, the combination of sensing components with output units, such as fiber-based displays, actuators, or electrical stimulators, enables systems capable of autonomously processing and responding to sensory input. These closed-loop systems, in which sensing, energy, and actuation are co-embedded within the fiber platform, offer significant promise for next-generation wearable electronics, implantable therapeutics, smart textiles, human-machine interaction, and personalized health monitoring. Despite notable progress in fiber-based electronics, several challenges remain in realizing their practical applications across diverse fields.

First, ensuring long-term mechanical durability and reliable performance under dynamic loading conditions is challenging (Fig. 16). FEDs are generally designed to operate under both static and dynamic conditions, including wearable and implantable applications involving body motion and mechanical movement in industrial and robotic systems. In these dynamic environments, FEDs are particularly susceptible to mechanical stimuli such as repeated bending, stretching, and twisting, which may act simultaneously in practical scenarios. Changes in the external environment can affect the conductivity, sensitivity, and interfacial stability of the device. Stability against environmental factors such as humidity, temperature, and chemical exposure is essential for the long-term practical use of FEDs. High temperatures can alter material properties or weaken interfacial adhesion, while high humidity or oxygen levels may induce oxidation or degradation of conductive elements. Notably, such environmental instabilities can also compromise biocompatibility, as the release of degraded byproducts or reactive species may trigger skin irritation, allergic responses, or immune reactions upon prolonged contact with biological tissues. Therefore, ensuring both environmental and biological stability is critical for the safe and reliable operation of FEDs. These environmental factors can degrade the reliability not only of individual devices but also of the entire system. Therefore, ensuring environmental stability to maintain consistent performance under diverse operating conditions is essential. Addressing these challenges requires the implementation of effective material and structural strategies. For example, incorporating elastomers or nanocomposites with high mechanical durability as matrix materials or additives can enhance the overall robustness of the system. In addition, introducing complementary structural layers that suppress crack propagation by bridging interfacial gaps can further improve mechanical integrity. Moreover, the use of multifunctional layered architectures-where each layer is specifically engineered to withstand different environmental stressors such as humidity, temperature, or chemical exposure-offers a promising route toward achieving long-term operational stability.

Furthermore, achieving multi-functionality of the fiber electronic systems and wireless platform requires strategies to minimize signal interference and optimize system design (Fig. 16). To support complex functionalities, multiple fiber sensors and devices are often integrated together or densely arranged into a single textile system through conventional textile processes such as weaving techniques. However, in such high-density configurations, electromagnetic interference and electrical crosstalk frequently occur, which can significantly degrade signal accuracy, selectivity, and resolution. To mitigate these issues, the development and integration of soft electromagnetic shielding layers that are mechanically compliant and compatible with fiber-based architectures is essential. In particular, such shielding structures should not only block external interference but also enable selective transmission or reception of target signals, thereby enhancing the signal-to-noise ratio and ensuring accurate sensing in complex electromagnetic environments. Moreover, complementary approaches such as frequency/time-division multiplexing and signal deconvolution algorithms can further enhance signal integrity in multi-channel environments, enabling stable operation of high-density fiber systems. Recently, machine learning techniques have also been actively applied to improve

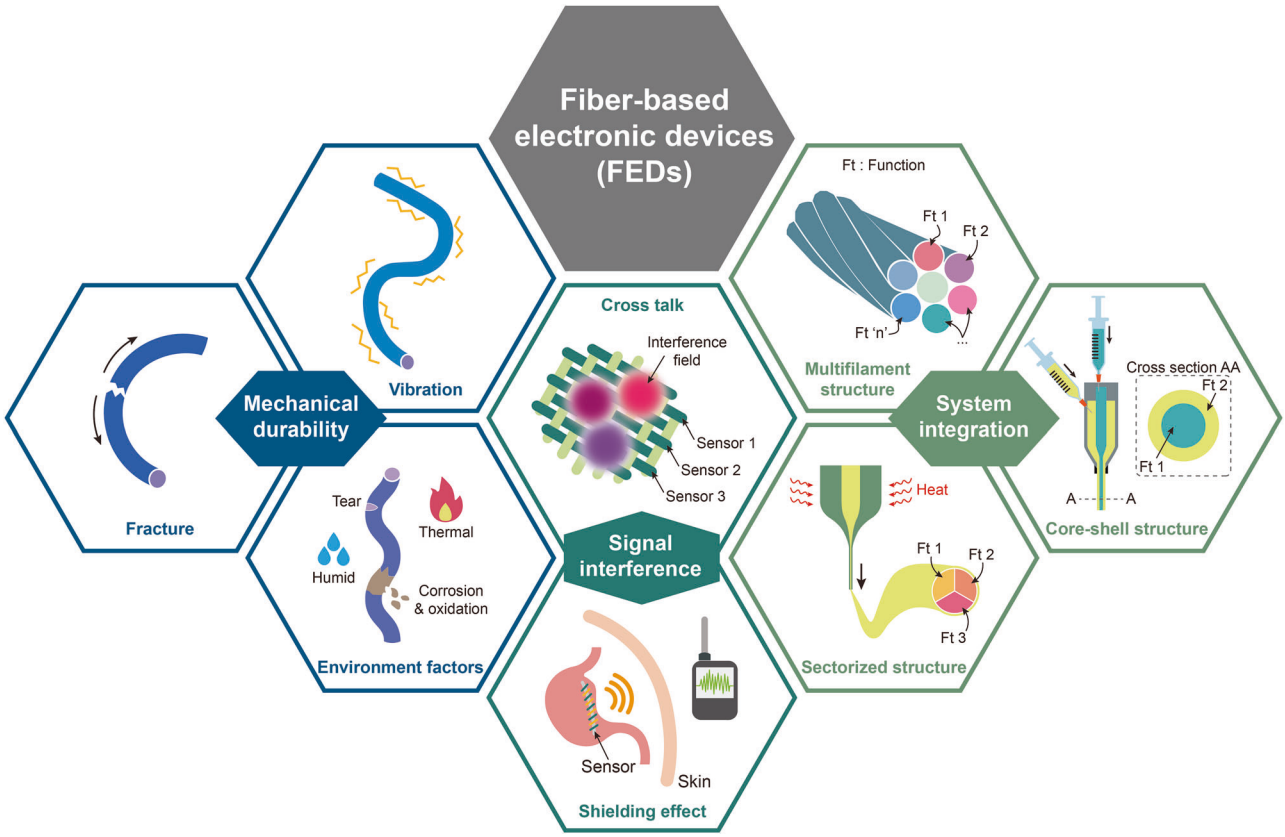

Fig. 16 | Schematic illustration of the future challenges in fiber-based electronic devices, including mechanical durability, signal interference, and system integration.

signal interpretation and noise suppression. For example, convolutional neural networks have been used to classify force distributions and suppress electromagnetic artifacts, while multilayer perceptrons have demonstrated high accuracy in decoding deformation patterns and signal variations. These circuit and software level signal reconstruction strategies play a critical role in maintaining precise control and high resolution data interpretation, even under signal distortion caused by environmental obstacles and biological interfaces such as human skin and organs. By compensating for signal attenuation, scattering, and interference, these approaches contribute significantly to the reliable operation of next-generation fiber-based integrated systems in real-world applications.

Finally, for fiber-based electronic systems that integrate sensors, actuators, and energy modules, the development of robust integration strategies is essential (Fig. 16). Even though individual fiber-based devices demonstrate excellent functional performance, they cannot be assembled into a stable and fully operational system without advanced integration technologies at the system level. Recent advances, including techniques for producing bundled fibers by twisting various functional fibers together, thermal drawing methods for fabricating multifunctional fibers using diverse materials, and multifunctional fiber technologies based on core-shell structures, have shown promising progress in terms of system integration. However, existing methods remain inadequate to realize seamless integration into a unified, reliable, and multifunctional architecture. Concretely, a sectorized structure via thermal drawing approach requires the use of materials with appropriate thermal durability, which limits material selection. In addition, stress relaxation at the interfaces between different materials must be considered. In the case of coaxial extrusion for core-shell structures, the selected materials must exhibit optimized viscosity to enable co-flow with other constituent layers during the extrusion process. In multifilament structures, precise alignment between individual filaments is critical to achieve the intended structural or functional performance.

Furthermore, not only developing fabrication method of multifunctional fibers, but also it should have application flexibility depending on where the device will be applied. In short, various combinations, among sensor, energy generator, energy storage, display, actuator, and stimulator, must be available for specific purposes. To fully utilize this transformable characteristic and prevent performance degradation caused by poor interconnection, it is necessary to enhance the interfacial stability between functional components and improve wiring technologies that ensure stable integration system. In addition to mechanical and electrical interconnection, another essential aspect of fully integrated fiber-based electronic systems is the inclusion of reliable energy storage modules. A fully autonomous fiber-based platform must be supported by a sufficient energy supply to maintain continuous operation. However, current fiber-based energy storage technologies still fall short of meeting this demand, primarily due to their inherently limited volume, which constrains the overall energy storage capacity. This leads to these systems often suffer from intermittent functionality and unstable performance, particularly during prolonged operation. To overcome this limitation, future efforts should focus on the development of high energy density materials specifically tailored for fiber geometries, as well as structural designs that minimize energy loss and support efficient energy retention within the system.

FEDs offer a structural alternative to planar devices, with advantages in conformability and multifunctional integration. This unique advantage has expanded their applicability across wearable, implantable, robotic, and industrial systems. Ultimately, to further advance the next-generation soft systems, a strategy that minimizes system complexity and maximizes functional density by integrating various functions into a single fiber is required. This integration strategy will minimize overall system volume and weight while enabling the development of fully self-powered and autonomous fiber electronics. It is hoped that the technical perspectives and

application strategies outlined in this review will provide a foundation for advancing fiber electronics toward practical deployment and intelligent system integration.

Data availability

No datasets were generated or analysed during the current study.

Code availability

All codes that support the findings of this study are available from the corresponding authors upon reasonable request.

Received: 9 May 2025; Accepted: 24 July 2025;
Published online: 09 August 2025

References

1. Zhang, T. et al. Flexible electronics for cardiovascular healthcare monitoring. *Innovation* **4**, 100485 (2023).
2. Hu, L. et al. Smart electronics based on 2D materials for wireless healthcare monitoring. *Appl. Phys. Rev.* **9**, 041308 (2022).
3. Wang, X. et al. Biocompatible and breathable healthcare electronics with sensing performances and photothermal antibacterial effect for motion-detecting. *npj Flex. Electron.* **6**, 95 (2022).
4. Li, Z., Tian, X., Qiu, C.-W. & Ho, J. S. Metasurfaces for bioelectronics and healthcare. *Nat. Electron.* **4**, 382–391 (2021).
5. Libanori, A., Chen, G., Zhao, X., Zhou, Y. & Chen, J. Smart textiles for personalized healthcare. *Nat. Electron.* **5**, 142–156 (2022).
6. Islam, F. B., Lee, J. M. & Kim, D. S. Smart factory floor safety monitoring using UWB sensor. *IET Sci. Meas. Technol.* **16**, 412–425 (2022).
7. Javaid, M., Haleem, A., Singh, R. P., Rab, S. & Suman, R. Significance of sensors for industry 4.0: roles, capabilities, and applications. *Sens. Int.* **2**, 100110 (2021).
8. Jiang, J., Wang, H., Mu, X. & Guan, S. Logistics industry monitoring system based on wireless sensor network platform. *Comput. Commun.* **155**, 58–65 (2020).
9. Jiang, Y., Yin, S., Dong, J. & Kaynak, O. A review on soft sensors for monitoring, control, and optimization of industrial processes. *IEEE Sens. J.* **21**, 12868–12881 (2021).
10. Zhang, C., Zhu, P., Lin, Y., Jiao, Z. & Zou, J. Modular soft robotics: modular units, connection mechanisms, and applications. *Adv. Intell. Syst.* **2**, 1900166 (2020).
11. Horne, J., McLoughlin, L., Bury, E., Koh, A. S. & Wujcik, E. K. Interfacial phenomena of advanced composite materials toward wearable platforms for biological and environmental monitoring sensors, armor, and soft robotics. *Adv. Mater. Interfaces* **7**, 1901851 (2020).
12. Mishra, R. K. et al. Wearable flexible and stretchable glove biosensor for on-site detection of organophosphorus chemical threats. *ACS Sens* **2**, 553–561 (2017).
13. Hussain, M., Zahra, H., Abbas, S. M. & Zhu, Y. Flexible dielectric materials: potential and applications in antennas and RF sensors. *Adv. Electron. Mater.* **10**, 2400240 (2024).
14. Conroy, B. et al. Real-time infection prediction with wearable physiological monitoring and AI to aid military workforce readiness during COVID-19. *Sci. Rep.* **12**, 3797 (2022).
15. Zou, Y. et al. High-temperature flexible WSe(2) photodetectors with ultrahigh photoresponsivity. *Nat. Commun.* **13**, 4372 (2022).
16. Zou, R. et al. Self-powered and self-sensing wearable devices from a comfort perspective. *Device* **2**, 100466 (2024).
17. Lu, K., Karlsson, J., Dahlman, A. S., Sjoqvist, B. A. & Candefjord, S. Detecting driver sleepiness using consumer wearable devices in manual and partial automated real-road driving. *IEEE Trans. Intell. Transp. Syst.* **23**, 4801–4810 (2022).
18. Yin, J., Hinchet, R., Shea, H. & Majidi, C. Wearable soft technologies for haptic sensing and feedback. *Adv. Funct. Mater.* **31**, 2007428 (2020).
19. Wei, R. et al. Revolutionizing wearable technology: advanced fabrication techniques for body-conformable electronics. *npj Flex. Electron.* **8**, 83 (2024).
20. Heng, W., Solomon, S. & Gao, W. Flexible electronics and devices as human-machine interfaces for medical robotics. *Adv. Mater.* **34**, e2107902 (2022).
21. Zhang, J. H. et al. Versatile self-assembled electrospun micropyramid arrays for high-performance on-skin devices with minimal sensory interference. *Nat. Commun.* **13**, 5839 (2022).
22. Liu, S. et al. Conformability of flexible sheets on spherical surfaces. *Sci. Adv.* **9**, eadf2709 (2023).
23. Rich, S. I., Lee, S., Fukuda, K. & Someya, T. Developing the nondevelopable: creating curved-surface electronics from nonstretchable devices. *Adv. Mater.* **34**, e2106683 (2022).
24. Wu, R. et al. Silk composite electronic textile sensor for high space precision 2D combo temperature-pressure sensing. *Small* **15**, e1901558 (2019).
25. Kim, J. et al. Progresses and perspectives of 1D soft sensing devices for healthcare applications. *Adv. Funct. Mater.* **34**, 2406651 (2024).
26. Zhang, G., Singh, R., Zhang, B., Li, G. & Kumar, S. Optical fiber-based wearable sensors for remote health monitoring [invited]. *Adv. Sens. Res.* **3**, 2400082 (2024).
27. Yang, Z. et al. Conductive and elastic 3D helical fibers for use in washable and wearable electronics. *Adv. Mater.* **32**, e1907495 (2020).
28. Liu, X. et al. Recent progress on smart fiber and textile based wearable strain sensors: materials, fabrications and applications. *Adv. Fiber Mater.* **4**, 361–389 (2022).
29. Won, C. et al. Ultrasensitive and stretchable conductive fibers using percolated Pd nanoparticle networks for multisensing wearable electronics: crack-based strain and H(2) sensors. *ACS Appl Mater. Interfaces* **12**, 45243–45253 (2020).
30. Zou, K. et al. A highly selective implantable electrochemical fiber sensor for real-time monitoring of blood homovanillic acid. *ACS Nano* **18**, 7485–7495 (2024).
31. Lee, J. et al. Stretchable and suturable fibre sensors for wireless monitoring of connective tissue strain. *Nat. Electron.* **4**, 291–301 (2021).
32. Rao, Z. et al. Soft electronics for the skin: from health monitors to human–machine interfaces. *Adv. Mater. Technol.* **5**, 2000233 (2020).
33. Kim, H. et al. Inherently integrated microfiber-based flexible proprioceptive sensor for feedback-controlled soft actuators. *npj Flex. Electron.* **8**, 15 (2024).
34. Li, T. et al. An artificial intelligence-motivated skin-like optical fiber tactile sensor. *Adv. Intell. Syst.* **5**, 2200460 (2023).
35. Yu, Y. et al. All-printed soft human-machine interface for robotic physicochemical sensing. *Sci. Robot.* **7**, eabn0495 (2022).
36. Ning, C., Zheng, G. & Dong, K. Emerging self-powered autonomous sensing triboelectric fibers toward future wearable human-computer interaction devices. *Adv. Sens. Res.* **2**, 2200044 (2023).
37. Ren, Z. et al. Energy harvesting from breeze wind (0.7–6ms−1) using ultra-stretchable triboelectric nanogenerator. *Adv. Energy Mater.* **10**, 2001770 (2020).
38. Gu, J. et al. Extremely robust and multifunctional nanocomposite fibers for strain-unperturbed textile electronics. *Adv. Mater.* **35**, e2209527 (2023).
39. Zhu, S. et al. Multi-functional and highly conductive textiles with ultra-high durability through 'green' fabrication process. *Chem. Eng. J.* **406**, 127140 (2021).
40. Wang, L. et al. Application challenges in fiber and textile electronics. *Adv. Mater.* **32**, e1901971 (2020).
41. Liu, Z. et al. Functionalized fiber-based strain sensors: pathway to next-generation wearable electronics. *Nanomicro Lett.* **14**, 61 (2022).
42. Zhang, C., Ouyang, W., Zhang, L. & Li, D. A dual-mode fiber-shaped flexible capacitive strain sensor fabricated by direct ink writing

technology for wearable and implantable health monitoring applications. *Microsyst. Nanoeng.* **9**, 158 (2023).
43. Hwang, C. et al. Highly flexible electrodes based on nano/micro-fiber for flexible lithium metal batteries. *Adv. Funct. Mater.* **34**, 2404649 (2024).
44. Zhang, H. et al. Recent progress of fiber-based transistors: materials, structures and applications. *Front Optoelectron* **15**, 2 (2022).
45. Fakharuddin, A. et al. Fiber-shaped electronic devices. *Adv. Energy Mater.* **11**, 2101443 (2021).
46. Huynh, T. P. & Haick, H. Autonomous flexible sensors for health monitoring. *Adv. Mater.* **30**, e1802337 (2018).
47. Jang, Y. W. et al. Autonomous artificial olfactory sensor systems with homeostasis recovery via a seamless neuromorphic architecture. *Adv. Mater.* **36**, e2400614 (2024).
48. Weng, W. et al. A route toward smart system integration: from fiber design to device construction. *Adv. Mater.* **32**, e1902301 (2020).
49. Gao, Z. et al. Advances in wearable strain sensors based on electrospun fibers. *Adv. Funct. Mater.* **33**, 4 (2023).
50. Zhi, Y. et al. Pressure sensors based on densely structured graphene fibers for motion monitoring. *Adv. Fiber Mater.* **7**, 541–553 (2024).
51. Li, Z. et al. Fiber-junction design for directional bending sensors. *npj Flex. Electron.* **5**, 2214265 (2021).
52. Li, M. et al. Organic/inorganic hybrid ionogel fiber with synergistically enhanced mechanical and ionic thermoelectric performances. *Adv. Funct. Mater.* **35**, 2415856 (2024).
53. On, S. Y., Park, S. Y., Chung, Y. S. & Kim, S. S. Effects of microwave-assisted cross-linking on the creep resistance and sensing accuracy of a coaxial-structured fiber strain sensor. *Adv. Mater. Technol*. **8** (2022).
54. Sarabia-Riquelme, R. et al. Highly conductive n-type polymer fibers from the wet-spinning of n-doped PBDF and their application in thermoelectric textiles. *Adv. Funct. Mater.* **34**, 2311379 (2023).
55. Yu, S. et al. A biodegradable fiber calcium ion sensor by covalently bonding ionophores on bioinert nanoparticles. *Adv. Health Mater.* **13**, e2400675 (2024).
56. Wang, J. et al. A fiber sensor for long-term monitoring of extracellular potassium ion fluctuations in chronic neuropsychiatric diseases. *Adv. Mater.* **36**, e2309862 (2024).
57. Tang, C. et al. A soft-fiber bioelectronic device with axon-like architecture enables reliable neural recording in vivo under vigorous activities. *Adv. Mater.* **36**, e2407874 (2024).
58. Wang, K. et al. High-performance graphene-fiber-based neural recording microelectrodes. *Adv. Mater.* **31**, e1805867 (2019).
59. Li, T. et al. Bioinspired stretchable fiber-based sensor toward intelligent human-machine interactions. *ACS Appl. Mater. Interfaces* **14**, 22666–22677 (2022).
60. Wang, M. et al. Gesture recognition using a bioinspired learning architecture that integrates visual data with somatosensory data from stretchable sensors. *Nat. Electron.* **3**, 563–570 (2020).
61. Loke, G. et al. Digital electronics in fibres enable fabric-based machine-learning inference. *Nat. Commun.* **12**, 3317 (2021).
62. Luo, Z. et al. Advances in fiber-based wearable sensors with machine learning. *Adv. Dev. Instrum*. **5** (2024).
63. Araromi, O. A. et al. Ultra-sensitive and resilient compliant strain gauges for soft machines. *Nature* **587**, 219–224 (2020).
64. Liu, W. et al. Highly flexible and multifunctional CNTs/TPU fiber strain sensor formed in one-step via wet spinning. *J. Alloy. Comp.* **948**, 169641 (2023).
65. Ning, C. et al. Helical fiber strain sensors based on triboelectric nanogenerators for self-powered human respiratory monitoring. *ACS Nano* **16**, 2811–2821 (2022).
66. Sun, H. et al. An ultrasensitive and stretchable strain sensor based on a microcrack structure for motion monitoring. *Microsyst. Nanoeng.* **8**, 111 (2022).
67. Tang, J., Zou, Y., Liu, C. & Lv, Y. Liquid metal fiber-based high-sensitivity strain and pressure sensors enhanced by porous structure. *ACS Appl. Electron. Mater.* **6**, 7512–7521 (2024).
68. Ma, D. et al. Skin-core-fiber-based fabric integrated with pressure sensing and deep learning for posture recognition. *Nano Energy* **132**, 110376 (2024).
69. Lan, L., Zhao, F., Yao, Y., Ping, J. & Ying, Y. One-step and spontaneous in situ growth of popcorn-like nanostructures on stretchable double-twisted fiber for ultrasensitive textile pressure sensor. *ACS Appl. Mater. Interfaces* **12**, 10689–10696 (2020).
70. Kim, S. W. et al. Mechanically robust and linearly sensitive soft piezoresistive pressure sensor for a wearable human-robot interaction system. *ACS Nano* **18**, 3151–3160 (2024).
71. Li, J. et al. Thin, soft, wearable system for continuous wireless monitoring of artery blood pressure. *Nat. Commun.* **14**, 5009 (2023).
72. Lee, D. H. et al. Bending sensor based on controlled microcracking regions for application toward wearable electronics and robotics. *ACS Appl. Mater. Interfaces* **14**, 31312–31320 (2022).
73. Li, W. et al. Core–sheath fiber-based wearable strain sensor with high stretchability and sensitivity for detecting human motion. *Adv. Electron. Mater.* **7**, 2000865 (2020).
74. Li, C. et al. Sensing of joint and spinal bending or stretching via a retractable and wearable badge reel. *Nat. Commun.* **12**, 2950 (2021).
75. Wan, X. et al. All-textile piezoelectric nanogenerator based on 3D knitted fabric electrode for wearable applications. *ACS Sens* **9**, 2989–2998 (2024).
76. Kato, Y., Fukuda, K., Someya, T. & Yokota, T. An ultra-flexible temperature-insensitive strain sensor. *J. Mater. Chem. C.* **11**, 14070–14078 (2023).
77. Modes, V., Ortmaier, T. & Burgner-Kahrs, J. Shape sensing based on longitudinal strain measurements considering elongation, bending, and twisting. *IEEE Sens. J.* **21**, 6712–6723 (2021).
78. Cheng, Y., Wang, R., Sun, J. & Gao, L. A stretchable and highly sensitive graphene-based fiber for sensing tensile strain, bending, and torsion. *Adv. Mater.* **27**, 7365–7371 (2015).
79. Cooper, C. B. et al. Stretchable capacitive sensors of torsion, strain, and touch using double helix liquid metal fibers. *Adv. Funct. Mater.* **27**, 1605630 (2017).
80. Qaiser, N. et al. A robust wearable point-of-care CNT-based strain sensor for wirelessly monitoring throat-related illnesses. *Adv. Funct. Mater.* **31**, 2103375 (2021).
81. On, S. Y., Park, S. & Kim, S. S. Preparation and characterization of hybrid structured MWCNT/UHMWPE fiber sensors for strain sensing and load bearing of composite structures. *Adv. Mater. Technol.* **4**, 1900807 (2019).
82. Nela, L., Tang, J., Cao, Q., Tulevski, G. & Han, S. J. Large-area high-performance flexible pressure sensor with carbon nanotube active matrix for electronic skin. *Nano Lett.* **18**, 2054–2059 (2018).
83. Cao, M. et al. Wearable piezoresistive pressure sensors based on 3D graphene. *Chem. Eng. J*. **406** (2021).
84. Li, K., Yang, W., Yi, M. & Shen, Z. Graphene-based pressure sensor and strain sensor for detecting human activities. *Smart Mater. Struct*. **30** (2021).
85. Jiang, X. et al. Highly compressible and sensitive pressure sensor under large strain based on 3d porous reduced graphene oxide fiber fabrics in wide compression strains. *ACS Appl. Mater. Interfaces* **11**, 37051–37059 (2019).
86. Xie, Y. et al. 3D MXene-based flexible network for high-performance pressure sensor with a wide temperature range. *Adv. Sci.* **10**, e2205303 (2023).
87. Fu, X. et al. Knitted Ti(3)C(2)T(x) MXene based fiber strain sensor for human-computer interaction. *J. Colloid Interface Sci.* **604**, 643–649 (2021).
88. Seyedin, S. et al. MXene composite and coaxial fibers with high stretchability and conductivity for wearable strain sensing textiles. *Adv. Funct. Mater.* **30**, 1910504 (2020).
89. Zhu, W.-B. et al. Ti3C2Tx MXene/Bamboo Fiber/PDMS pressure sensor with simultaneous ultrawide linear sensing range, superb

environmental stability, and excellent biocompatibility. *ACS Sustain. Chem. Eng.* **10**, 3546–3556 (2022).
90. Liu, L. et al. Preparation and property research of strain sensor based on PDMS and silver nanomaterials. *J. Sens.* **2017**, 1–8 (2017).
91. Cao, Y., Lai, T., Teng, F., Liu, C. & Li, A. Highly stretchable and sensitive strain sensor based on silver nanowires/carbon nanotubes on hair band for human motion detection. *Prog. Nat. Sci. Mater. Int.* **31**, 379–386 (2021).
92. Zhang, X. et al. Silver nanowire/silver/poly(dimethylsiloxane) as strain sensors for motion monitoring. *ACS Appl. Nano Mater.* **5**, 15797–15807 (2022).
93. Wu, Y. et al. Cellulose nanofibers/PEDOT:PSS conductive aerogel for pressure sensing prepared by a facile freeze-drying method. *ACS Appl. Polym. Mater.* **5**, 3938–3948 (2023).
94. Khedewy, A. T., Saleh, D. I. & Shaker, A. On the effect of fibre orientation and MWCNTs on the strain-sensing performance of TPU/PANI electrospun nanofibres. *Polym. Adv. Technol.* **35**, e6639 (2024).
95. Wei, J. A. et al. Flexible piezoresistive sensors based on ppy granule-anchored multilayer fibrous membranes with a wide operating range and high sensitivity. *ACS Appl. Mater. Interfaces* **16**, 19421–19431 (2024).
96. Shi, W. et al. High-sensitivity and extreme environment-resistant sensors based on PEDOT:PSS@PVA hydrogel fibers for physiological monitoring. *ACS Appl Mater. Interfaces* **14**, 35114–35125 (2022).
97. Liu, H. et al. 3D printed flexible strain sensors: from printing to devices and signals. *Adv. Mater.* **33**, e2004782 (2021).
98. Chen, T. et al. Piezoresistive sensor containing lamellar MXene-plant fiber sponge obtained with aqueous MXene ink. *ACS Appl Mater. Interfaces* **14**, 51361–51372 (2022).
99. Lee, J. et al. Highly sensitive multifilament fiber strain sensors with ultrabroad sensing range for textile electronics. *ACS Nano* **12**, 4259–4268 (2018).
100. Yang, C. et al. In situ polymerized MXene/polypyrrole/hydroxyethyl cellulose-based flexible strain sensor enabled by machine learning for handwriting recognition. *ACS Appl. Mater. Interfaces* **15**, 5811–5821 (2023).
101. Cai, Y. et al. A broad range and piezoresistive flexible pressure sensor based on carbon nanotube network dip-coated porous elastomer sponge. *RSC Adv.* **12**, 34117–34125 (2022).
102. Wang, J. et al. Dip-coated conductive polyurethane fibers composited with liquid metal particles and multiwall carbon nanotubes for multifunctional applications. *ACS Appl. Nano Mater.* **8**, 265–278 (2024).
103. Shen, J. et al. Design intelligent pressure sensing devices and system integrated with conductor-coated porous composites. *Adv. Sens. Res.* **2**, 2200091 (2023).
104. Tseng, S.-F., Huang, J.-W., Lee, C.-C. & Kuo, C.-C. Highly sensitive and flexible strain sensors based on electroplating copper/laser-induced graphene composites. *J. Alloys. Comp.* **1022**, 179928 (2025).
105. Kim, T. et al. Wearable sensors and supercapacitors using electroplated-Ni/ZnO antibacterial fabric. *J. Mater. Sci. Technol.* **100**, 254–264 (2022).
106. Wu, X. et al. Ultra-robust and sensitive flexible strain sensor for real-time and wearable sign language translation. *Adv. Funct. Mater.* **33**, 2303504 (2023).
107. Cheng, X., Cai, J., Xu, J. & Gong, D. High-performance strain sensors based on Au/graphene composite films with hierarchical cracks for wide linear-range motion monitoring. *ACS Appl Mater. Interfaces* **14**, 39230–39239 (2022).
108. Yan, Y. et al. A highly sensitive and stretchable strain sensor based on nested wrinkle microstructures. *J. Electron. Mater.* **54**, 1739–1747 (2025).
109. Ji, J. et al. High sensitivity and a wide sensing range flexible strain sensor based on the V-groove/wrinkles hierarchical array. *ACS Appl. Mater. Interfaces* **14**, 24059–24066 (2022).
110. Li, Y., Peng, H., Peng, Y., Zhou, J. & Zhang, J. Thermoplastic and electrically conductive fibers for highly stretchable and sensitive strain sensors. *ACS Appl. Polym. Mater.* **4**, 8795–8802 (2022).
111. Farid, M. I., Wu, W., Li, G., Zhang, F. & Zhu, X. High-performance 3D printed thermoplastic polyurethane composite resistive flexible strain sensor. *J. Appl. Polym. Sci*. **142** (2025).
112. Zhong, J. et al. Continuous fabrication of core-sheath fiber for strain sensing and self-powered application. *Nano Energy* **118** (2023).
113. Pang, Y.-N. et al. Singlemode-multimode-singlemode optical fiber sensor for accurate blood pressure monitoring. *J. Lightwave Technol.* **40**, 4443–4450 (2022).
114. Boutry, C. M. et al. Biodegradable and flexible arterial-pulse sensor for the wireless monitoring of blood flow. *Nat. Biomed. Eng.* **3**, 47–57 (2019).
115. Chen, S. et al. Noncontact heartbeat and respiration monitoring based on a hollow microstructured self-powered pressure sensor. *ACS Appl. Mater. Interfaces* **10**, 3660–3667 (2018).
116. Li, T. et al. Flexible optical fiber-based smart textile sensor for human–machine interaction. *IEEE Sens. J.* **22**, 19336–19345 (2022).
117. Amit, M., Chukoskie, L., Skalsky, A. J., Garudadri, H. & Ng, T. N. Flexible pressure sensors for objective assessment of motor disorders. *Adv. Funct. Mater.* **30**, 1905241 (2019).
118. Luo, Y. et al. Learning human–environment interactions using conformal tactile textiles. *Nat. Electron.* **4**, 193–201 (2021).
119. Wang, J. et al. Ultra-fine self-powered interactive fiber electronics for smart clothing. *Nano Energy* **107**, 108171 (2023).
120. Cheng, A. J. et al. Recent advances of capacitive sensors: materials, microstructure designs, applications, and opportunities. *Adv. Mater. Technol.* **8**, 2201959 (2023).
121. Mathew, S. & Chintagumpala, K. A review of recent progress in flexible capacitance pressure sensors: materials design, printing methods, and applications. *Adv. Compos. Hybrid. Mater.* **8**, 236 (2025).
122. Lee, J. et al. Conductive fiber-based ultrasensitive textile pressure sensor for wearable electronics. *Adv. Mater.* **27**, 2433–2439 (2015).
123. Qu, X. et al. Highly sensitive fiber pressure sensors over a wide pressure range enabled by resistive-capacitive hybrid response. *ACS Nano* **17**, 14904–14915 (2023).
124. Wang, K. et al. An ultrahigh-strength braided smart yarn for wearable individual sensing and protection. *Adv. Fiber Mater.* **6**, 786–797 (2024).
125. Zhou, B. et al. Large-area knittable, wash-durable, and healable smart fibers for dual-modal sensing applications. *Adv. Funct. Mater.* **34**, 2404064 (2024).
126. Wang, X. Q. et al. Macromolecule conformational shaping for extreme mechanical programming of polymorphic hydrogel fibers. *Nat. Commun.* **13**, 3369 (2022).
127. Lin, S. et al. An ultralight, flexible, and biocompatible all-fiber motion sensor for artificial intelligence wearable electronics. *npj Flexi. Electron.* **6**, 27 (2022).
128. Sun, T. et al. Artificial intelligence meets flexible sensors: emerging smart flexible sensing systems driven by machine learning and artificial synapses. *Nanomicro Lett.* **16**, 14 (2023).
129. Jiang, Y., Sadeqi, A., Miller, E. L. & Sonkusale, S. Head motion classification using thread-based sensor and machine learning algorithm. *Sci. Rep.* **11**, 2646 (2021).
130. Duan, S. et al. Machine-learned, waterproof MXene fiber-based glove platform for underwater interactivities. *Nano Energy* **91**, 106650 (2022).
131. Chen, Y. et al. Biomimetic artificial neuromuscular fiber bundles with built-in adaptive feedback. *Matter* **8**, 101904 (2025).

132. Zheng, Y. et al. Unlocking intrinsic conductive dynamics of ionogel microneedle arrays as wearable electronics for intelligent fire safety. *Adv. Fiber Mater.* **6**, 195–213 (2023).
133. Jiang, Q. et al. Durable and wearable self-powered temperature sensor based on self-healing thermoelectric fiber by coaxial wet spinning strategy for fire safety of firefighting clothing. *Adv. Fiber Mater.* **6**, 1387–1401 (2024).
134. Gao, F. L. et al. Multifunctional thermoelectric temperature sensor for noncontact information transfer and tactile sensing in human-machine interaction. *Adv. Funct. Mater*. **34** (2023).
135. Liang, Q. et al. Fiber-based noncontact sensor with stretchability for underwater wearable sensing and VR applications. *ACS Nano* **18**, 600–611 (2024).
136. Peng, Z. et al. Flexible copper-based thermistors fabricated by laser direct writing for low-temperature sensing. *ACS Appl Mater. Interfaces* **16**, 10496–10507 (2024).
137. Trung, T. Q. et al. Freestanding, fiber-based, wearable temperature sensor with tunable thermal index for healthcare monitoring. *Adv. Health Mater.* **7**, e1800074 (2018).
138. Jha, R. K. Non-dispersive infrared gas sensing technology: a review. *IEEE Sens. J.* **22**, 6–15 (2022).
139. Hanosh, O., Ansari, R., Younis, K. & Cetin, A. E. Real-time epileptic seizure detection during sleep using passive infrared sensors. *IEEE Sens. J.* **19**, 6467–6476 (2019).
140. Biswas, S., Shao, Y., Hachisu, T., Nguyen-Dang, T. & Visell, Y. Integrated soft optoelectronics for wearable health monitoring. *Adv. Mater. Technol.* **5**, 2000347 (2020).
141. Yoon, K. et al. Highly stretchable thermoelectric fiber with embedded copper(I) iodide nanoparticles for a multimodal temperature, strain, and pressure sensor in wearable electronics. *Adv. Funct. Mater.* **35**, 2407759 (2024).
142. Fan, W. et al. An antisweat interference and highly sensitive temperature sensor based on poly(3,4-ethylenedioxythiophene)-poly(styrenesulfonate) fiber coated with polyurethane/graphene for real-time monitoring of body temperature. *ACS Nano* **17**, 21073–21082 (2023).
143. Ryu, W. M., Lee, Y., Son, Y., Park, G. & Park, S. Thermally drawn multi-material fibers based on polymer nanocomposite for continuous temperature sensing. *Adv. Fiber Mater.* **5**, 1712–1724 (2023).
144. Mei, W. et al. Operando monitoring of thermal runaway in commercial lithium-ion cells via advanced lab-on-fiber technologies. *Nat. Commun.* **14**, 5251 (2023).
145. Wang, S. et al. Fiber-shaped temperature sensor with high seebeck coefficient for human health and safety monitoring. *ACS Appl Mater. Interfaces* **16**, 69617–69625 (2024).
146. Shrestha, D. et al. Fabrication of flexible glucose sensor based on heterostructure ZnO nanosheets decorated PU/Chitosan-PANI hybrid nanofiber. *Microchem. J.* **197**, 109915 (2024).
147. Zhi, H., Gao, J. & Feng, L. Hydrogel-based gas sensors for NO(2) and NH(3). *ACS Sens* **5**, 772–780 (2020).
148. Hu, C., Wang, L., Liu, S., Sheng, X. & Yin, L. Recent development of implantable chemical sensors utilizing flexible and biodegradable materials for biomedical applications. *ACS Nano* **18**, 3969–3995 (2024).
149. Sempionatto, J. R., Lasalde-Ramirez, J. A., Mahato, K., Wang, J. & Gao, W. Wearable chemical sensors for biomarker discovery in the omics era. *Nat. Rev. Chem.* **6**, 899–915 (2022).
150. Minamiki, T. et al. Flexible organic thin-film transistor immunosensor printed on a one-micron-thick film. *Commun. Mater*. **2** (2021).
151. Duan, H. et al. Wearable electrochemical biosensors for advanced healthcare monitoring. *Adv. Sci.* **12**, e2411433 (2025).
152. Ye, B. F. et al. Colorimetric photonic hydrogel aptasensor for the screening of heavy metal ions. *Nanoscale* **4**, 5998–6003 (2012).
153. Sulthana, S. F. et al. Electrochemical sensors for heavy metal ion detection in aqueous medium: a systematic review. *ACS Omega* **9**, 25493–25512 (2024).
154. Fu, W. et al. Intelligent fibers and textiles for wearable biosensors. *Respons. Mater.* **2**, e20240018 (2024).
155. Zhao, C., Li, X., Wu, Q. & Liu, X. A thread-based wearable sweat nanobiosensor. *Biosens. Bioelectron.* **188**, 113270 (2021).
156. Wang, R., Zhai, Q., An, T., Gong, S. & Cheng, W. Stretchable gold fiber-based wearable textile electrochemical biosensor for lactate monitoring in sweat. *Talanta* **222**, 121484 (2021).
157. Pickar, D. et al. Neuroleptic-induced decrease in plasma homovanillic acid and antipsychotic activity in schizophrenic patients. *Science* **225**, 954–957 (1984).
158. Zhang, Z. J., Peet, M., Ramchand, C. N., Shah, S. & Reynolds, G. P. Plasma homovanillic acid in untreated schizophrenia—relationship with symptomatology and sex. *J. Psychiatr. Res.* **35**, 23–28 (2001).
159. Zhou, J., Li, J., Papaneri, A. B., Kobzar, N. P. & Cui, G. Dopamine neuron challenge test for early detection of Parkinson's disease. *NPJ Parkinsons Dis.* **7**, 116 (2021).
160. McCutcheon, R. A., Krystal, J. H. & Howes, O. D. Dopamine and glutamate in schizophrenia: biology, symptoms and treatment. *World Psychiatry* **19**, 15–33 (2020).
161. Liu, J. et al. Bioresorbable shape-adaptive structures for ultrasonic monitoring of deep-tissue homeostasis. *Science* **383**, 1096–1103 (2024).
162. Kwon, K. et al. An on-skin platform for wireless monitoring of flow rate, cumulative loss and temperature of sweat in real time. *Nat. Electron.* **4**, 302–312 (2021).
163. Dervisevic, M. et al. Wearable microneedle array-based sensor for transdermal monitoring of pH levels in interstitial fluid. *Biosens. Bioelectron.* **222**, 114955 (2023).
164. Sharifuzzaman, M. et al. Smart bandage with integrated multifunctional sensors based on MXene-functionalized porous graphene scaffold for chronic wound care management. *Biosens. Bioelectron.* **169**, 112637 (2020).
165. Min, Y. et al. The pH-sensitive optical fiber integrated CMCS-PA@Fe hydrogels for photothermal therapy and real-time monitoring of infected wounds. *Adv. Funct. Mater.* **33**, 2212803 (2023).
166. Xiao, J., Zhou, Z., Zhong, G., Xu, T. & Zhang, X. Self-sterilizing microneedle sensing patches for machine learning-enabled wound pH visual monitoring. *Adv. Funct. Mater.* **34**, 2315067 (2024).
167. Kim, H. et al. Bioelectronic sutures with electrochemical pH-sensing for long-term monitoring of the wound healing progress. *Adv. Funct. Mater.* **34**, 2402501 (2024).
168. Zhao, Y. et al. Highly stretchable and strain-insensitive fiber-based wearable electrochemical biosensor to monitor glucose in the sweat. *Anal. Chem.* **91**, 6569–6576 (2019).
169. Kim, D. H. et al. Colorimetric dye-loaded nanofiber yarn: eye-readable and weavable gas sensing platform. *ACS Nano* **14**, 16907–16918 (2020).
170. Cha, J. H., Kim, D. H., Choi, S. J., Koo, W. T. & Kim, I. D. Sub-parts-per-million hydrogen sulfide colorimetric sensor: lead acetate anchored nanofibers toward Halitosis diagnosis. *Anal. Chem.* **90**, 8769–8775 (2018).
171. Gonzalez Serrano, V., Lin, E. Z., Godri Pollitt, K. J. & Licina, D. Adequacy of stationary measurements as proxies for residential personal exposure to gaseous and particle air pollutants. *Environ. Res* **231**, 116197 (2023).
172. Shah, A. et al. Determining methane mole fraction at a landfill site using the Figaro Taguchi gas sensor 2611-C00 and wind direction measurements. *Environ. Sci. Atmos.* **4**, 362–386 (2024).
173. Shin, H. et al. Single-atom Pt stabilized on one-dimensional nanostructure support via carbon nitride/SnO(2) heterojunction trapping. *ACS Nano* **14**, 11394–11405 (2020).
174. Wen, S., Zhang, R., Zhao, Y., Xu, X. & Ji, S. Patterning adhesive layers for array electrodes via electrochemically grafted polymers. *ACS Omega* **10**, 3190–3198 (2025).

175. Zhu, M. et al. Flexible electrodes for in vivo and in vitro electrophysiological signal recording. *Adv. Health Mater.* **10**, e2100646 (2021).
176. Song, Y., Min, J. & Gao, W. Wearable and Implantable Electronics: Moving toward Precision Therapy. *ACS Nano* **13**, 12280–12286 (2019).
177. Ray, T. R. et al. Bio-Integrated Wearable Systems: A Comprehensive Review. *Chem. Rev.* **119**, 5461–5533 (2019).
178. Shin, J. H., Choi, J. Y., June, K., Choi, H. & Kim, T. I. Polymeric conductive adhesive-based ultrathin epidermal electrodes for long-term monitoring of electrophysiological signals. *Adv. Mater.* **36**, e2313157 (2024).
179. Chun, K. Y., Seo, S. & Han, C. S. A wearable all-gel multimodal cutaneous sensor enabling simultaneous single-site monitoring of cardiac-related biophysical signals. *Adv. Mater.* **34**, e2110082 (2022).
180. Ji, S. et al. Water-resistant conformal hybrid electrodes for aquatic endurable electrocardiographic monitoring. *Adv. Mater.* **32**, e2001496 (2020).
181. Zhao, X. et al. A reconfigurable and conformal liquid sensor for ambulatory cardiac monitoring. *Nat. Commun.* **15**, 8492 (2024).
182. Lee, G.-H. et al. Rapid meniscus-guided printing of stable semi-solid-state liquid metal microgranular-particle for soft electronics. *Nat. Commun.* **13**, 2643 (2022).
183. Tan, P. et al. Solution-processable, soft, self-adhesive, and conductive polymer composites for soft electronics. *Nat. Commun.* **13**, 358 (2022).
184. Pan, Y. et al. A stretchable and sweat-adhesive 3d graphene eutectogel electrode for EMG monitoring. *ACS Appl. Nano Mater.* **7**, 12064–12071 (2024).
185. Ma, X. et al. Breathable gelatin conductive hydrogels using a template method and reverse use of Hofmeister effect for wearable sensors. *ACS Appl. Polym. Mater.* **6**, 6290–6301 (2024).
186. Lo, L. W. et al. Stretchable sponge electrodes for long-term and motion-artifact-tolerant recording of high-quality electrophysiologic signals. *ACS Nano* **16**, 11792–11801 (2022).
187. Soleimani Dinani, H. et al. Miniaturized wearable biosensors for continuous health monitoring fabricated using the femtosecond laser-induced graphene surface and encapsulated traces and electrodes. *ACS Sens* **10**, 761–772 (2025).
188. Cao, J. et al. Anti-friction gold-based stretchable electronics enabled by interfacial diffusion-induced cohesion. *Nat. Commun.* **15**, 1116 (2024).
189. Imai, A. et al. Flexible thin-film neural electrodes with improved conformability for ECoG measurements and electrical stimulation. *Adv. Mater. Technol*. **8** (2023).
190. Kim, J. et al. Injectable 2D material-based sensor array for minimally invasive neural implants. *Adv. Mater.* **36**, e2400261 (2024).
191. Zhou, N. et al. Permeable and durable liquid-metal fiber mat as implantable physiological electrodes with long-term biocompatibility. *Adv. Mater.* **37**, e2413728 (2025).
192. Coles, L. et al. Origami-inspired soft fluidic actuation for minimally invasive large-area electrocorticography. *Nat. Commun.* **15**, 6290 (2024).
193. Kireev, D. et al. Multipurpose and reusable ultrathin electronic tattoos based on PtSe and PtTe(2). *ACS Nano* **15**, 2800–2811 (2021).
194. Xu, J. et al. Electrooculography and tactile perception collaborative interface for 3D human-machine interaction. *ACS Nano* **16**, 6687–6699 (2022).
195. Xie, L. et al. Ultrasensitive wearable pressure sensors with stress-concentrated tip-array design for long-term bimodal identification. *Adv. Mater.* **36**, e2406235 (2024).
196. Han, Q. et al. Hydrogel nanoarchitectonics of a flexible and self-adhesive electrode for long-term wireless electroencephalogram recording and high-accuracy sustained attention evaluation. *Adv. Mater.* **35**, e2209606 (2023).
197. Shi, Y. et al. Eye tracking and eye expression decoding based on transparent, flexible and ultra-persistent electrostatic interface. *Nat. Commun.* **14**, 3315 (2023).
198. Qin, X. et al. Wearable electrodriven switch actively delivers macromolecular drugs to fundus in non-invasive and controllable manners. *Nat. Commun.* **16**, 33 (2025).
199. Zhu, Y. et al. Lab-on-a-contact lens: recent advances and future opportunities in diagnostics and therapeutics. *Adv. Mater.* **34**, e2108389 (2022).
200. Lim, H. R. et al. Advanced soft materials, sensor integrations, and applications of wearable flexible hybrid electronics in healthcare, energy, and environment. *Adv. Mater.* **32**, e1901924 (2020).
201. Seo, H. et al. Smart contact lenses as wearable ophthalmic devices for disease monitoring and health management. *Chem. Rev.* **123**, 11488–11558 (2023).
202. Pang, J. et al. Applications of graphene in five senses, nervous system, and artificial muscles. *ACS Sens* **8**, 482–514 (2023).
203. Gao, W. & Yu, C. Wearable and implantable devices for healthcare. *Adv. Health Mater.* **10**, e2101548 (2021).
204. Madhvapathy, S. R. et al. Implantable bioelectronics and wearable sensors for kidney health and disease. *Nat. Rev. Nephrol.* **21**, 443–463 (2025).
205. Wang, J. et al. Ultra-small wearable flexible biosensor for continuous sweat analysis. *ACS Sens* **7**, 3102–3107 (2022).
206. Du, T., Zhu, Z., Chen, M., Yan, X. & Li, Y. Functional hydrogel strain sensors for smart electronic devices: strategies and recent progress. *ACS Appl. Electron. Mater.* **8**, 5402–5428 (2024).
207. Kang, T. W., Lee, J., Kwon, Y., Lee, Y. J. & Yeo, W. H. Recent progress in the development of flexible wearable electrodes for electrocardiogram monitoring during exercise. *Adv. NanoBiomed. Res.* **4**, 2300169 (2024).
208. Joutsen, A. et al. ECG signal quality in intermittent long-term dry electrode recordings with controlled motion artifacts. *Sci. Rep.* **14**, 8882 (2024).
209. Xue, H. et al. Hydrogel electrodes with conductive and substrate-adhesive layers for noninvasive long-term EEG acquisition. *Microsyst. Nanoeng.* **9**, 79 (2023).
210. Ding, L. et al. In situ deposition of skin-adhesive liquid metal particles with robust wear resistance for epidermal electronics. *Nano Lett.* **22**, 4482–4490 (2022).
211. Reis Carneiro, M., Majidi, C. & Tavakoli, M. Multi-electrode printed bioelectronic patches for long-term electrophysiological monitoring. *Adv. Funct. Mater.* **32**, 2205956 (2022).
212. Roh, Y. et al. Transient shuttle for a widespread neural probe with minimal perturbation. *npj Flex. Electron.* **8**, 40 (2024).
213. Trotier, A. et al. Micromotion derived fluid shear stress mediates peri-electrode gliosis through mechanosensitive ion channels. *Adv. Sci.* **10**, e2301352 (2023).
214. Taylor, L. W. et al. Washable, sewable, all-carbon electrodes and signal wires for electronic clothing. *Nano Lett.* **21**, 7093–7099 (2021).
215. Wang, W. et al. Imperceptible augmentation of living systems with organic bioelectronic fibres. *Nat. Electron* **7**, 586–597 (2024).
216. Lee, G. H. et al. Conductance stable and mechanically durable bi-layer EGaIn composite-coated stretchable fiber for 1D bioelectronics. *Nat. Commun.* **14**, 4173 (2023).
217. Polikov, V. S., Tresco, P. A. & Reichert, W. M. Response of brain tissue to chronically implanted neural electrodes. *J. Neurosci. Methods* **148**, 1–18 (2005).
218. Winslow, B. D. & Tresco, P. A. Quantitative analysis of the tissue response to chronically implanted microwire electrodes in rat cortex. *Biomaterials* **31**, 1558–1567 (2010).
219. Gregory, B. A. et al. Structural and functional changes of deep layer pyramidal neurons surrounding microelectrode arrays implanted in rat motor cortex. *Acta Biomater.* **168**, 429–439 (2023).

220. Zeng, Q. & Huang, Z. Challenges and opportunities of implantable neural interfaces: from material, electrochemical and biological perspectives. *Adv. Funct. Mater.* **33**, 2301223 (2023).
221. Vitale, F. et al. Fluidic microactuation of flexible electrodes for neural recording. *Nano Lett.* **18**, 326–335 (2018).
222. Ali, I. et al. Advances in smart photovoltaic textiles. *ACS Nano* **18**, 3871–3915 (2024).
223. Gong, W. et al. Continuous and scalable manufacture of amphibious energy yarns and textiles. *Nat. Commun.* **10**, 868 (2019).
224. Park, J. et al. Bio-physicochemical dual energy harvesting fabrics for self-sustainable smart electronic suits. *Adv. Energy Mater.* **13** (2023).
225. Jian, Z. et al. Flexible diamond fibers for high-energy-density zinc-ion supercapacitors. *Adv. Energy Mater.* **10**, 2002202 (2020).
226. Han, D. et al. A self-regulated interface toward highly reversible aqueous zinc batteries. *Adv. Energy Mater.* **12**, 2102982 (2022).
227. Zhao, Y. et al. Injectable fiber batteries for all-region power supply in vivo. *J. Mater. Chem. A* **9**, 1463–1470 (2021).
228. Wang, L. et al. Wearable bending wireless sensing with autonomous wake-up by piezoelectric and triboelectric hybrid nanogenerator. *Nano Energy* **112** (2023).
229. Niu, Z. et al. Electrospun cellulose nanocrystals reinforced flexible sensing paper for triboelectric energy harvesting and dynamic self-powered tactile perception. *Small* **20**, e2307810 (2024).
230. Huang, L. et al. Fiber-based energy conversion devices for human-body energy harvesting. *Adv. Mater.* **32**, e1902034 (2020).
231. Dong, C. et al. High-efficiency super-elastic liquid metal based triboelectric fibers and textiles. *Nat. Commun.* **11**, 3537 (2020).
232. Duan, E., Jaseem, S. A., Kim, J. Y., Dickey, M. D. & Bryant, M. Strain amplification via helically braided fiber reinforced sleeve for soft material energy harvesting. *Adv. Mater. Technol.* **10**, 2402033 (2025).
233. Ye, C., Dong, S., Ren, J. & Ling, S. Ultrastable and high-performance silk energy harvesting textiles. *Nanomicro Lett.* **12**, 12 (2019).
234. Xue, L. et al. A novel strategy to fabricate core-sheath structure piezoelectric yarns for wearable energy harvesters. *Adv. Fiber Mater.* **3**, 239–250 (2021).
235. Feng, Z. et al. Waterproof iontronic yarn for highly sensitive biomechanical strain monitoring in wearable electronics. *Adv. Fiber Mater.* **6**, 925–935 (2024).
236. Feng, Z. et al. Scalable, washable and lightweight triboelectric-energy-generating fibers by the thermal drawing process for industrial loom weaving. *Nano Energy* **74**, 104805 (2020).
237. Tong, Y. et al. 3D printed stretchable triboelectric nanogenerator fibers and devices. *Nano Energy* **75**, 104973 (2020).
238. Gong, J. et al. Towards truly wearable energy harvesters with full structural integrity of fiber materials. *Nano Energy* **58**, 365–374 (2019).
239. Dong, L. et al. Deformable textile-structured triboelectric nanogenerator knitted with multifunctional sensing fibers for biomechanical energy harvesting. *Adv. Fiber Mater.* **4**, 1486–1499 (2022).
240. Lan, L., Jiang, C., Yao, Y., Ping, J. & Ying, Y. A stretchable and conductive fiber for multifunctional sensing and energy harvesting. *Nano Energy* **84** (2021).
241. Yin, H. et al. Ultra-high sensitivity anisotropic piezoelectric sensors for structural health monitoring and robotic perception. *Nanomicro Lett.* **17**, 42 (2024).
242. Eun, J. H., Sung, S. M., Kim, M. S., Choi, B. K. & Lee, J. S. Effect of MWCNT content on the mechanical and piezoelectric properties of PVDF nanofibers. *Mater. Des.* **206**, 109785 (2021).
243. Lu, L., Yang, B., Zhai, Y. & Liu, J. Electrospinning core-sheath piezoelectric microfibers for self-powered stitchable sensor. *Nano Energy* **76**, 104966 (2020).
244. Mokhtari, F. et al. Wearable electronic textiles from nanostructured piezoelectric fibers. *Adv. Mater. Technol.* **5**, 1900900 (2020).
245. Xu, J. et al. A textile magnetoelastic patch for self-powered personalized muscle physiotherapy. *Matter* **6**, 2235–2247 (2023).
246. Chen, G. et al. Discovering giant magnetoelasticity in soft matter for electronic textiles. *Matter* **4**, 3725–3740 (2021).
247. Zhao, X. et al. Giant magnetoelastic effect enabled stretchable sensor for self-powered biomonitoring. *ACS Nano* **16**, 6013–6022 (2022).
248. Yu, B. et al. Core-sheath fiber-based triboelectric nanogenerators for energy harvesting and self-powered straight-arm sit-up sensing. *ACS Omega* **8**, 31427–31435 (2023).
249. Seung, W. et al. Nanopatterned textile-based wearable triboelectric nanogenerator. *ACS Nano* **9**, 3501–3509 (2015).
250. Zhou, L. et al. Reconfigurable fiber triboelectric nanogenerator for self-powered defect detection. *ACS Nano* **16**, 7721–7731 (2022).
251. Tao, D. et al. Electro-spun nanofibers-based triboelectric nanogenerators in wearable electronics: status and perspectives. *npj Flex. Electron.* **9**, 4 (2025).
252. Lu, X., Qu, H. & Skorobogatiy, M. Piezoelectric micro- and nanostructured fibers fabricated from thermoplastic nanocomposites using a fiber drawing technique: comparative study and potential applications. *ACS Nano* **11**, 2103–2114 (2017).
253. Wu, S. et al. Cesium lead halide perovskite decorated polyvinylidene fluoride nanofibers for wearable piezoelectric nanogenerator yarns. *ACS Nano* **17**, 1022–1035 (2023).
254. Wang, K., Hou, C., Zhang, Q., Li, Y. & Wang, H. Highly integrated fiber-shaped thermoelectric generators with radially heterogeneous interlayers. *Nano Energy* **95** (2022).
255. Zhang, Y. et al. Novel wearable pyrothermoelectric hybrid generator for solar energy harvesting. *ACS Appl. Mater. Interfaces* **14**, 17330–17339 (2022).
256. Wu, T. et al. High thermoelectric performance and flexibility in rationally treated PEDOT:PSS fiber bundles. *Adv. Fiber Mater.* **6**, 607–618 (2024).
257. Jang, D., Park, K. T., Lee, S.-S. & Kim, H. Highly stretchable three-dimensional thermoelectric fabrics exploiting woven structure deformability and passivation-induced fiber elasticity. *Nano Energy* **97** (2022).
258. Xu, H. et al. Highly integrable thermoelectric fiber. *ACS Appl Mater. Interfaces* **12**, 33297–33304 (2020).
259. He, X. et al. Three-dimensional flexible thermoelectric fabrics for smart wearables. *Nat. Commun.* **16**, 2523 (2025).
260. Ding, T. et al. Scalable thermoelectric fibers for multifunctional textile-electronics. *Nat. Commun.* **11**, 6006 (2020).
261. Qamar, M. Z. et al. Advancement in indoor energy harvesting through flexible perovskite photovoltaics for self- powered IoT applications. *Nano Energy* **129** (2024).
262. Gao, Z. et al. Advanced energy harvesters and energy storage for powering wearable and implantable medical devices. *Adv. Mater.* **36**, e2404492 (2024).
263. Ma, L. et al. Continuous and scalable manufacture of hybridized nano-micro triboelectric yarns for energy harvesting and signal sensing. *ACS Nano* **14**, 4716–4726 (2020).
264. Zhao, X. et al. Soft fibers with magnetoelasticity for wearable electronics. *Nat. Commun.* **12**, 6755 (2021).
265. Bharti, P., De, D., Chellappan, S. & Das, S. K. HuMAn: complex activity recognition with multi-modal multi-positional body sensing. *IEEE Trans. Mob. Comput.* **18**, 857–870 (2019).
266. Hong, J. et al. Advances of triboelectric and piezoelectric nanogenerators toward continuous monitoring and multimodal applications in the new era. *Int. J. Extrem. Manuf.* **7**, 12007 (2024).
267. Qing, X. et al. All-fiber integrated thermoelectrically powered physiological monitoring biosensor. *Adv. Fiber Mater.* **5**, 1025–1036 (2023).
268. Sun, T. et al. Stretchable fabric generates electric power from woven thermoelectric fibers. *Nat. Commun.* **11**, 572 (2020).

269. Qiu, L., He, S., Yang, J., Deng, J. & Peng, H. Fiber-shaped perovskite solar cells with high power conversion efficiency. *Small* **12**, 2419–2424 (2016).
270. Qi, Q. et al. Large-sized high-efficiency fiber perovskite solar cells fabricated by automatic thin-film coating on curved surfaces. *Adv. Fiber Mater.* **5**, 1799–1809 (2023).
271. Song, J. et al. Integrating light diffusion and conversion layers for highly efficient multicolored fiber-dye-sensitized solar cells. *Adv. Mater.* **36**, e2312590 (2024).
272. Liu, K. et al. A self-supported graphene/carbon nanotube hollow fiber for integrated energy conversion and storage. *Nanomicro Lett.* **12**, 64 (2020).
273. Bae, J. et al. Fiber supercapacitors made of nanowire-fiber hybrid structures for wearable/flexible energy storage. *Angew. Chem. Int Ed. Engl.* **50**, 1683–1687 (2011).
274. Zhang, Y. et al. A fiber-shaped aqueous lithium ion battery with high power density. *J. Mater. Chem. A* **4**, 9002–9008 (2016).
275. Manthiram, A. An outlook on lithium ion battery technology. *ACS Cent. Sci.* **3**, 1063–1069 (2017).
276. Gong, X. et al. Extending the calendar life of fiber lithium-ion batteries to 200 days with ultra-high barrier polymer tubes. *Adv. Mater.* **36**, e2409910 (2024).
277. Jiang, H. et al. A low-permeability and flexible polymer tube for long-life fiber lithium-ion batteries. *Adv. Funct. Mater.* **34**, 2408529 (2024).
278. Lu, C. et al. High-performance fibre battery with polymer gel electrolyte. *Nature* **629**, 86–91 (2024).
279. Luo, J. & Zhang, Q. In situ polymer gel electrolyte in boosting scalable fibre lithium battery applications. *Nanomicro Lett.* **16**, 230 (2024).
280. Wang, H., Yan, W. & Zhu, M. Revolutionizing fiber batteries with polymer gel electrolyte: a groundbreaking innovation in wearable energy. *Chem. Synth.* **4**, 57 (2024).
281. Ranjith Kumar, D. et al. Safe and extended operating voltage zinc-ion battery engineered by a gel-polymer/ionic-liquid electrolyte and water molecules pre-intercalated V2O5 cathode. *J. Mol. Liq.* **367**, 120399 (2022).
282. Gond, R., van Ekeren, W., Mogensen, R., Naylor, A. J. & Younesi, R. Non-flammable liquid electrolytes for safe batteries. *Mater. Horiz.* **8**, 2913–2928 (2021).
283. Xia, Z. et al. Manipulating hierarchical orientation of wet-spun hybrid fibers via rheological engineering for Zn-Ion fiber batteries. *Adv. Mater.* **34**, e2203905 (2022).
284. Liu, Y. et al. Alternating current electroluminescence devices: recent advances and functional applications. *Mater. Horiz.* **11**, 5147–5180 (2024).
285. Cho, S., Chang, T., Yu, T. & Lee, C. H. Smart electronic textiles for wearable sensing and display. *Biosensors* **12**, 222 (2022).
286. Peng, C. et al. Recent advances of soft actuators in smart wearable electronic-textile. *Adv. Mater. Technol*. **9** (2024).
287. Sato, Y. & Guo, Y. Shape-memory-alloys enabled actuatable fiber sensors via the preform-to-fiber fabrication. *ACS Appl. Eng. Mater.* **1**, 822–831 (2023).
288. Li, H. et al. Flexible fibrous electrodes for implantable biosensing. *Nanoscale* **17**, 9870–9894 (2025).
289. Zhang, Y. et al. Multifunctional fibers to shape future biomedical devices. *Adv. Funct. Mater.* **29**, 1902834 (2019).
290. Canales, A., Park, S., Kilias, A. & Anikeeva, P. Multifunctional fibers as tools for neuroscience and neuroengineering. *Acc. Chem. Res* **51**, 829–838 (2018).
291. Kim, C. Y. et al. High mobility, low off-current, and flexible fiber-based A-InGaZnO thin-film transistors toward wearable textile OLED displays. *ACS Appl Mater. Interfaces* **16**, 62335–62346 (2024).
292. Song, H. et al. Water stable and matrix addressable OLED fiber textiles for wearable displays with large emission area. *npj Flex. Electron.* **6**, 66 (2022).
293. Ko, K. J., Lee, H. B. & Kang, J. W. Flexible, wearable organic light-emitting fibers based on PEDOT:PSS/Ag-fiber embedded hybrid electrodes for large-area textile lighting. *Adv. Mater. Technol*. **5** (2020).
294. Song, Y. J. et al. Fibertronic organic light-emitting diodes toward fully addressable, environmentally robust, wearable displays. *ACS Nano* **14**, 1133–1140 (2020).
295. Shi, X. et al. Large-area display textiles integrated with functional systems. *Nature* **591**, 240–245 (2021).
296. Li, P. et al. Wearable and interactive multicolored photochromic fiber display. *Light Sci. Appl* **13**, 48 (2024).
297. Mi, H. et al. Electroluminescent fabric woven by ultrastretchable fibers for arbitrarily controllable pattern display. *ACS Appl. Mater. Interfaces* **13**, 11260–11267 (2021).
298. Yang, W. et al. Body-coupled luminescent fibers enable wireless visual sensing of contacting media. *Matter* **7**, 4309–4318 (2024).
299. Choi, H. W. et al. Smart textile lighting/display system with multifunctional fibre devices for large scale smart home and IoT applications. *Nat. Commun.* **13**, 814 (2022).
300. Hu, Z. et al. Deep learning-assisted electro-thermochromic fluorescent fibers for self-adaptive intelligent display in dynamic environments. *Adv. Opt. Mater.* **13**, 2403126 (2025).
301. Yu, Y. et al. Fiber-shaped soft actuators: fabrication, actuation mechanism and application. *Adv. Fiber Mater.* **5**, 868–895 (2023).
302. Xue, E., Liu, L., Wu, W. & Wang, B. Soft fiber/textile actuators: from design strategies to diverse applications. *ACS Nano* **18**, 89–118 (2024).
303. Zhao, H. et al. Wearable sunlight-triggered bimorph textile actuators. *Nano Lett.* **21**, 8126–8134 (2021).
304. Chen, J. et al. High-performance natural melanin/poly(vinyl alcohol-co-ethylene) nanofibers/PA6 fiber for twisted and coiled fiber-based actuator. *Adv. Fiber Mater.* **2**, 64–73 (2020).
305. Xiao, J. et al. Optical fibre taper-enabled waveguide photoactuators. *Nat. Commun.* **13**, 363 (2022).
306. Lee, Y. et al. Magnetically actuated fiber-based soft robots. *Adv. Mater.* **35**, e2301916 (2023).
307. Li, M. et al. Miniature coiled artificial muscle for wireless soft medical devices. *Sci. Adv.* **8**, eabm5616 (2022).
308. Duan, X. et al. Large-scale spinning approach to engineering knittable hydrogel fiber for soft robots. *ACS Nano* **14**, 14929–14938 (2020).
309. Hu, X. et al. Fast large-stroke sheath-driven electrothermal artificial muscles with high power densities. *Adv. Funct. Mater.* **32**, 2200591 (2022).
310. Liao, W. & Yang, Z. The integration of sensing and actuating based on a simple design fiber actuator towards intelligent soft robots. *Adv. Mater. Technol*. **7** (2021).
311. Kanik, M. et al. Strain-programmable fiber-based artificial muscle. *Science* **365**, 145–150 (2019).
312. Kimura, D. et al. Mechanism for anisotropic thermal expansion of polyamide fibers. *Sens. Actuators B Chem.* **344**, 130262 (2021).
313. Wang, Y., Sun, J., Liao, W. & Yang, Z. Liquid crystal elastomer twist fibers toward rotating microengines. *Adv. Mater.* **34**, e2107840 (2022).
314. Cui, B. et al. Pretension-free and self-recoverable coiled artificial muscle fibers with powerful cyclic work capability. *ACS Nano* **17**, 12809–12819 (2023).
315. Noh, S. et al. High performance proprioceptive fiber actuators based on Ag nanoparticles-incorporated hybrid twisted and coiled system. *Small* **20**, e2309429 (2024).
316. Hu, Z., Li, Y. & Lv, J. A. Phototunable self-oscillating system driven by a self-winding fiber actuator. *Nat. Commun.* **12**, 3211 (2021).
317. Liu, H. et al. Programmable water/light dual-responsive hollow hydrogel fiber actuator for efficient desalination with anti-salt accumulation. *Adv. Funct. Mater.* **33**, 2302038 (2023).

318. Zhou, K. et al. Dual electrical stimulation at spinal-muscular interface reconstructs spinal sensorimotor circuits after spinal cord injury. *Nat. Commun.* **15**, 619 (2024).
319. Han, Z. et al. Precise cell type electrical stimulation therapy via force-electric hydrogel microspheres for cartilage healing. *Adv. Mater.* **37**, e2414555 (2025).
320. Yang, M. et al. Highly-stable, injectable, conductive hydrogel for chronic neuromodulation. *Nat. Commun.* **15**, 7993 (2024).
321. Gupta, I. et al. Quantification of clinically applicable stimulation parameters for precision near-organ neuromodulation of human splenic nerves. *Commun. Biol.* **3**, 577 (2020).
322. Liu, Y. et al. Morphing electronics enable neuromodulation in growing tissue. *Nat. Biotechnol.* **38**, 1031–1036 (2020).
323. Violante, I. R. et al. Non-invasive temporal interference electrical stimulation of the human hippocampus. *Nat. Neurosci.* **26**, 1994–2004 (2023).
324. Choe, G. et al. Effect of electrical stimulation on nerve-guided facial nerve regeneration. *ACS Biomater. Sci. Eng.* **9**, 3512–3521 (2023).
325. Wang, J., Wang, H., Thakor, N. V. & Lee, C. Self-powered direct muscle stimulation using a triboelectric nanogenerator (TENG) integrated with a flexible multiple-channel intramuscular electrode. *ACS Nano* **13**, 3589–3599 (2019).
326. Cui, X., Wu, L., Zhang, C. & Li, Z. Implantable self-powered systems for electrical stimulation medical devices. *Adv. Sci.* **12**, e2412044 (2024).
327. Deng, K. et al. Electrical stimulation therapy - dedicated to the perfect plastic repair. *Adv. Sci.* **12**, e2409884 (2024).
328. Jayathilake, N. J., Phan, T. T., Kim, J., Lee, K. P. & Park, J. M. Modulating neuroplasticity for chronic pain relief: noninvasive neuromodulation as a promising approach. *Exp. Mol. Med.* **57**, 501–514 (2025).
329. Widman, A. J. et al. Chronic, battery-free, fully implantable multimodal spinal cord stimulator for pain modulation in small animal models. *Adv. Sci.* **12**, e2415963 (2025).
330. Zulbaran-Rojas, A. et al. Transcutaneous electrical nerve stimulation for fibromyalgia-like syndrome in patients with Long-COVID: a pilot randomized clinical trial. *Sci. Rep.* **14**, 27224 (2024).
331. Liu, Z. et al. A self-powered intracardiac pacemaker in Swine model. *Nat. Commun.* **15**, 507 (2024).
332. Aydemir, U. et al. In situ assembly of an injectable cardiac stimulator. *Nat. Commun.* **15**, 6774 (2024).
333. Zhao, X. et al. Biodegradable piezoelectric implant for wirelessly delivering electrical stimulation to the heart under ultrasound stress. *Adv. Funct. Mater*. (2025).
334. Kwon, Y. W. et al. Implantable soft neural electrodes of liquid metals for deep brain stimulation. *ACS Nano* **19**, 7337–7349 (2025).
335. Burton, A. et al. Wireless, battery-free, and fully implantable electrical neurostimulation in freely moving rodents. *Microsyst. Nanoeng.* **7**, 62 (2021).
336. Zhan, L. et al. Internal wireless electrical stimulation from piezoelectric barium titanate nanoparticles as a new strategy for the treatment of triple-negative breast cancer. *ACS Appl. Mater. Interfaces* **14**, 45032–45041 (2022).
337. Ria, N. et al. Flexible graphene-based neurotechnology for high-precision deep brain mapping and neuromodulation in Parkinsonian rats. *Nat. Commun.* **16**, 2891 (2025).
338. Sun, J., Xie, W., Wu, Y., Li, Z. & Li, Y. Accelerated bone healing via electrical stimulation. *Adv. Sci.* **12**, e2404190 (2024).
339. Zhou, Y. et al. A wearable self-charging electroceutical device for bacteria-infected wound healing. *ACS Nano* **18**, 15681–15694 (2024).
340. Yang, S. B. et al. Rapid and scar free wound repair by using a biologically flexible and conductive dressing under electrical stimulation. *Adv. Funct. Mater.* **34**, 2403724 (2024).
341. Du, M. et al. Flexible fiber probe for efficient neural stimulation and detection. *Adv. Sci.* **7**, 2001410 (2020).
342. Kim, Y. et al. Multifunctional and flexible neural probe with thermally drawn fibers for bidirectional synaptic probing in the brain. *ACS Nano* **18**, 13277–13285 (2024).
343. Sun, Z. et al. A bioabsorbable mechanoelectric fiber as electrical stimulation suture. *Nat. Commun.* **15**, 8462 (2024).
344. Li, J. et al. Stretchable thermoelectric fibers with three-dimensional interconnected porous network for low-grade body heat energy harvesting. *ACS Nano* **17**, 19232–19241 (2023).
345. Sun, F. et al. Soft fiber electronics based on semiconducting polymer. *Chem. Rev.* **123**, 4693–4763 (2023).
346. Jang, Y., Kim, S. M., Spinks, G. M. & Kim, S. J. Carbon nanotube yarn for fiber-shaped electrical sensors, actuators, and energy storage for smart systems. *Adv. Mater.* **32**, e1902670 (2020).
347. Ershad, F., Patel, S. & Yu, C. Wearable bioelectronics fabricated in situ on skins. *Npj Flex. Electron* **7**, 32 (2023).
348. Vidhya, C. M., Maithani, Y. & Singh, J. P. Recent advances and challenges in textile electrodes for wearable biopotential signal monitoring: a comprehensive review. *Biosensors* **13**, 679 (2023).
349. Le, K. et al. Electronic textiles for electrocardiogram monitoring: a review on the structure–property and performance evaluation from fiber to fabric. *Text. Res. J.* **93**, 878–910 (2022).
350. Zhou, Z. et al. Textile-based mechanical sensors: a review. *Materials* **14**, 6073 (2021).

Acknowledgements

This work was supported by the DGIST R&D Program of the Ministry of Science and ICT (2025010373; 25-IRJoint-06). This work was also supported by the National Research Foundation of Korea (NRF) grant funded by the Korea government (MSIT) (No. NRF-2021R1C1C1009271) and by the Korea Medical Device Development Fund grant funded by the Korea government (the Ministry of Science and ICT, the Ministry of Trade, Industry and Energy, the Ministry of Health & Welfare, the Ministry of Food and Drug Safety) (Project Number: 2710002210, RS-2023-00243310). Finally, this work was supported by the Industrial Fundamental Technology Development Program (20018274, Development of gripper system for various production processes and multi-modal flexible tactile sensor system) funded by the Ministry of Trade, Industry & Energy (MOTIE) of Korea.

Author contributions

H.K. and D.K. wrote the original draft of the manuscript and prepared the figures. J.K., Y.L., M.S., J.K., and F.M.B. contributed to writing the following sections in the manuscript: J.K.—mechanical sensors, J.M.—Temperature sensors for health care, Y.L.—Chemical sensors, M.S.—Electrophysiological sensors, F.M.B.—Temperature sensors for thermal protection. In the remaining section, H.K. and D.K. contributed equally to writing paper. The original draft was reviewed by G.H.L., B.L., and W.R.T. J.L. conceptualized, supervised, reviewed, and edited the entire manuscript. All authors participated in scientific discussions. H.K. and D.K. equally contributed to this work as co-first authors.

Competing interests

The authors declare no competing interests.

Additional information

Correspondence and requests for materials should be addressed to Jaehong Lee.